TECHNISCHE UNIVERSITÄT MÜNCHEN

FAKULTÄT CHEMIE

LEHRSTUHL ORGANISCHE CHEMIE II

A CHEMICAL PROBE TO MONITOR THE PARKINSONISM-ASSOCIATED PROTEIN DJ-1 AND TARGET SPECIFICITY OF TRANYLCYPROMINE IN HUMAN CELLS

DISSERTATION ZUR ERLANGUNG DES AKADEMISCHEN GRADES EINES DOKTORS DER NATURWISSENSCHAFTEN VON

JONAS DRECHSEL

MÜNCHEN 2020

TECHNISCHE UNIVERSITÄT MÜNCHEN

FAKULTÄT CHEMIE

LEHRSTUHL ORGANISCHE CHEMIE II

A CHEMICAL PROBE TO MONITOR THE PARKINSONISM-ASSOCIATED PROTEIN DJ-1

AND

TARGET SPECIFICITY OF TRANYLCYPROMINE IN HUMAN CELLS

Jonas Drechsel

Vollständiger Abdruck der von der Fakultät für Chemie der Technischen Universität München zur Erlangung des akademischen Grades eines

Doktors der Naturwissenschaften (Dr. rer. nat.)

genehmigten Dissertation.

Vorsitzender:		Prof. Dr. Franz Hagn
Prüfer der Dissertation:	1.	Prof. Dr. Stephan A. Sieber
	2.	Prof. Dr. Cathleen Zeymer

Die Dissertation wurde am 06.07.2020 bei der Technischen Universität München eingereicht und durch die Fakultät für Chemie am 11.08.2020 angenommen.

Danksagung

Ich möchte hier die Chance ergreifen, um mich bei denjenigen zu bedanken, die diese Arbeit ermöglicht haben. Herrn Professor Stephan Sieber danke ich für die herzliche Aufnahme in seine Arbeitsgruppe. Vielen Dank, für die ausgezeichnete Betreuung und Unterstützung. Besonders aber auch dafür, wissenschaftliche Freiheit und Kreativität zu fördern und wertzuschätzen.

Des Weiteren möchte ich Frau Dr. Silvia Capello und Frau Dr. Christina Kyrousi für die angenehme Zusammenarbeit und ihre Hilfe bei der Fluoreszenzmikroskopie danken.

Herrn Dr. Stephan Hacker danke ich dafür, dass er in unnachahmlicher Weise fachliche Kompetenz und Geselligkeit miteinander verbindet. Seine Anstöße und Ideen waren eine enorme Bereicherung für mich und ich wünsche ihm und seiner jungen Arbeitsgruppe alles erdenklich Gute für die Zukunft!

Patrick Allihn möchte ich dafür danken, all die Jahre erste Anlaufstelle für mich gewesen zu sein. Die besten Kollegen erkennt man daran, dass durch sie sowohl die eigene Arbeit als auch der Feierabend aufgewertet wird! Das gilt nicht zuletzt auch für Robert Macsics; falls es mit der Wissenschaft nichts wird, versuchen wir einfach unser Glück als Autoren der Buchreihe „Random facts with Robs and Johnny“. Außerdem möchte ich Patrick Zanon danken, der mir zum Ende dieser Arbeit liebevoll Asyl in seinem Labor gewährt hat. Es wird wohl ein ungeklärtes Phänomen bleiben, wie jemand auf der einen Seite ein begnadeter Chemiker sein kann, gleichzeitig aber an der Zubereitung eines Spiegeleis scheitert. Angela Weigert-Muñoz und Till Reinhardt danke ich dafür, den harten Kern so wundervoll und mit beeindruckender Ausdauer vervollständigt zu haben. Großen Dank auch an Dr. Stuart Ruddell, der mit seiner enthusiastischen Art eine absolute Bereicherung für die Gruppe ist. Vielen Dank auch an Dr. Dóra Balogh, mit der ich alle Hochs und Tiefs der letzten vier Jahre teilen durfte. Martin Pfanzelt danke ich für die super Zusammenarbeit im Groupjob. MSQ? Läuft! Ich möchte mich bei Dr. Franziska Madl für die anfängliche Betreuung und die Übergabe ihres Projekts bedanken. Außerdem danke ich Dr. Vadim Korotkov für die großartige, synthetische Unterstützung. Carolin Gleißner danke ich für die guten Tipps und Tricks beim Schreiben dieser Arbeit. Thesi, Thomas,

Konstantin, Alexandra, Jan, Didi, Seppi, Lisa, Michael und allen ehemaligen Kolleginnen und Kollegen danke ich für die Unterstützung und die tolle Arbeitsatmosphäre.
Vielen Dank an Mona Wolff Katja Bäuml und Christina Brumer für die herausragende Unterstützung.
Mein größter Dank gilt aber meiner Familie und Ines Hübner, die mich in der gesamten Zeit so liebevoll unterstützt haben. Ich schätze mich glücklich, dass es euch gibt!

Abstract

Studying the interaction of small molecular compounds with proteins is a major part of modern bioorganic and medicinal chemistry. Most marketed drugs target specific proteins to generate their desired biological effect, so understanding the exact mode of action and having detailed information on off-target reactivity and enzymatic metabolism are crucial for any new pharmaceuticals.

The development of activity-based protein profiling (ABPP) that utilizes probes tailored to display the same protein binding behaviour as the studied drug, while allowing late-stage detectability, introduced a new layer of complexity to the field. Combination with high resolution mass spectrometry leads to robust identification of target proteins. This work presents two projects, in which ABPP was successfully used to identify drug-protein interactions.

In the first chapter, natural product-derived aminoepoxycyclohexenones were found to selectively target the human Parkinson disease protein 7 (DJ-1). Detailed enzymatic studies revealed a redox-dependent binding mechanism to the active-site cysteine of DJ-1. Most importantly, ABPP proved to be an excellent tool to monitor changes of the protein's oxidation state in live cells. As DJ-1 plays a major role in cellular oxidative stress response, these findings are of high value in the field of biomarker development.

The second project focused on revealing the off-target reactivity of the marketed monoamine oxidase inhibitor tranylcypromine. The drug proved to have high covalent reactivity towards many proteins. Further ABPP studies also revealed strong accumulation of tranylcypromine in lysosomes, which was additionally confirmed by fluorescence microscopy. This effect was successfully attenuated by the co-administration of lysosomotropic compounds chloroquine and tamoxifen.

Zusammenfassung

Die Erforschung der Wechselwirkung von niedermolekularen Verbindungen und Proteinen ist ein wichtiger Bestandteil der modernen bioorganischen und medizinischen Chemie. Die meisten auf dem Markt erhältlichen Medikamente zielen auf bestimmte Proteine ab, um ihre gewünschte biologische Wirkung zu erzielen. Daher sind das Verständnis der genauen Wirkungsweise und detaillierte Informationen über Nebenreaktionen und den enzymatischen Metabolismus für jedes neue Arzneimittel von entscheidender Bedeutung.

Die Entwicklung des aktivitätsbasierten Protein-Profilings (ABPP), bei der Sonden verwendet werden, die so konzipiert sind, dass sie dasselbe Proteinbindungsverhalten wie das untersuchte Medikament zeigen und gleichzeitig eine Nachweisbarkeit im Verlauf des Experiments ermöglichen, eröffnete neue Möglichkeiten auf diesem Feld. Die Kombination mit hochauflösender Massenspektrometrie führt zu einer robusten Identifizierung von Zielproteinen. In dieser Arbeit werden zwei Projekte vorgestellt, in denen ABPP erfolgreich zur Identifizierung von Molekül-Protein-Interaktionen eingesetzt wurde.

Im ersten Projekt wurde gezeigt, dass von Naturstoffen abgeleitete Aminoepoxy-cyclohexenone selektiv das menschliche Parkinson-Protein 7 (DJ-1) binden. Detaillierte enzymatische Studien zeigten einen Redox-abhängigen Bindungsmechanismus an das Cystein im aktiven Zentrum von DJ-1. Vor allem aber erwies sich ABPP als ausgezeichnetes Instrument zur Darstellung von Änderungen des Oxidationszustandes des Proteins in lebenden Zellen. Da DJ-1 eine wichtige Rolle in der zellulären oxidativen Stressantwort spielt, sind diese Ergebnisse von hohem Wert auf dem Gebiet der Biomarker-Entwicklung.

Das zweite Projekt konzentrierte sich auf die Aufklärung von unerwünschter Reaktivität des vermarkteten Monoaminoxidase-Inhibitors Tranylcypromin. Das Medikament zeigte in hohem Maße kovalente Proteinbindung. Weitere ABPP-Studien zeigten außerdem eine starke Anreicherung von Tranylcypromin in Lysosomen; dies konnte zusätzlich durch Fluoreszenzmikroskopie bestätigt werden. Die Anreicherung wurde durch die

gemeinsame Verabreichung der lysosomotropen Verbindungen Chloroquin und Tamoxifen erfolgreich abgeschwächt.

Introductory remarks

Parts of this thesis have been published in:

Drechsel, J.; Mandl, F. A.; Sieber, S. A. Chemical Probe To Monitor the Parkinsonism-Associated Protein DJ-1 in Live Cells. *ACS chemical biology* **2018**, *13* (8), 2016–2019.

Drechsel, J; Kyrousi, C; Cappello, S; Sieber, S. A. Tranylcypromine Specificity for Monoamine Oxidase is Limited by Promiscuous Protein Labelling and Lysosomal Trapping. *RSC chemical biology*, **2020**, manuscript under revision.

Table of Content

I. Introduction

1. Activity-Based Protein Profiling

In 2017, *Santos et al.* comprehensively mapped molecular targets of FDA-approved drugs.[1] With their approach, they identified a total number of 695 human drug targets, of which 96% proved to be proteins. This explains huge efforts made by pharmaceutical companies and biochemical academia to deepen knowledge in drug-protein-interactions. In an attempt to depict and classify methods available for this purpose, *Schenone et al*. presented three major categories: direct biochemical methods, genetic interaction methods and computational inference methods.[2] Genetic approaches range from screening compounds in libraries of cells bearing single-gene deletions, to sequencing the genome of resistant mutants.[3,4] Computational methods largely rely on information in drug-databases on ligand binding or pattern recognition among a given set of small molecules, but proved to be a valuable addition to the field.[5,6] The most straight forward concept is to incubate a protein sample with the small molecule of interest and directly measure the binding. Advantageously, this can be done under native conditions, meaning the binding between drug and protein target is a result of protein activity. This method was developed in the laboratories of *Cravatt*[7–12] and *Bogyo*[13–16] and is nowadays known as *Activity-Based Protein Profiling* (ABPP) (Figure 1).[17] In these initial studies, small electrophilic compounds, also referred to as ABPP-probes, were used that react covalently with nucleophilic amino acid residues, *e.g.* cysteines or activated serines like is the case in many kinases. When the probe is now equipped with a reporter tag, target proteins can subsequently be identified. In the beginning, reporter tags were directly attached to the molecule of interest, limiting the methodology as many commonly used tags are too polar or bulky to enter cells. Using *Huisgen*-[3+2] azide-alkyne cycloaddition (“click” reaction) for late-stage introduction of the reporter tag overcame this restriction and paved the way for ABPP as one of today’s most widely used target identification tools.[9,18–21]

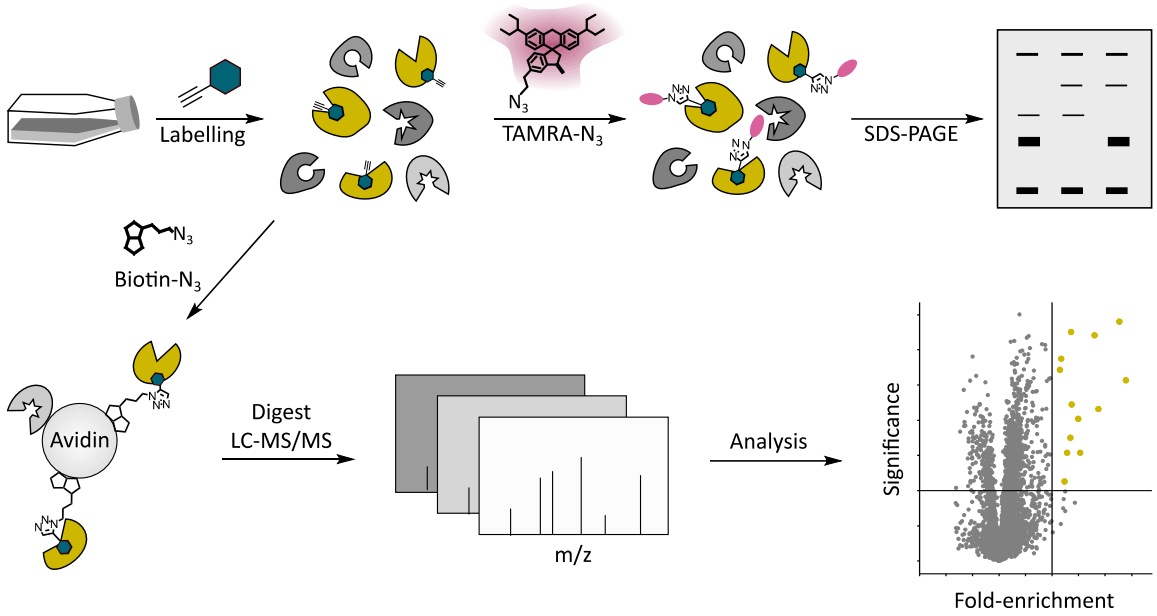

Figure 1: Schematic workflow of an ABPP experiment. After probe treatment, proteins are either conjugated to a fluorescent dye for analytical scale SDS-PAGE or target proteins are enriched *via* an affinity handle and identified by LC-MS/MS analysis.

A suitable reporter tag is dependent on the choice of down-stream experiment planed. A fast and cost-efficient way to qualitatively display protein targets *via* ABPP is the use of fluorescent tags followed by SDS-PAGE. This technique is often used to optimize labelling conditions for specific probes and serves thereby as starting point for many target identification experiments. Subsequently, changing the tag to an affinity handle allows selective enrichment of probe bound proteins and their identification as well as quantification by high resolution mass spectrometry (HR-MS). A prominent example for such an affinity system exploits the strong natural binding between avidin and biotin.[22] Probe-bound proteins are conjugated to biotin, and afterwards extracted from a complex sample by introduction of bead-bound avidin. The ability to quantify enriched proteins adds another layer of complexity to ABPP as it allows ranking of the targets by potency of binding to a specific probe, as well as monitoring differences of said binding under changing conditions. To date, various methods for LC-MS/MS based protein quantification have been developed, and will be discussed in more detail in the following section.

2. MS/MS Target Identification

There are two concepts used in MS-based protein analysis, known as top-down and bottom-up proteomics.[23] The former utilises intact proteins that are directly measured in the spectrometer. This often simplifies sample preparation and minimizes the risk of losing unstable post-translational modifications (PTMs), but various drawbacks including challenging chromatography and difficult spectra interpretation keep top-down approaches a niche method.[24,25] The vast majority of MS-based ABPP experiments is conducted in a bottom-up manner, meaning proteins are digested into peptides during sample preparation (Figure 2).[26–28] As this step leads to high fragmentation of the initial protein sample, the facetious description “shotgun proteomics” was established. To reduce MS-spectra complexity at any given time point during the following MS-detection, peptides are separated by LC prior to measurement. As the mass of a single peptide is not necessarily unique among a digested proteome, a MS/MS approach is needed for unequivocal identification. For this purpose, modern mass spectrometers not only measure the exact mass of a peptide (MS^1-level), but also generate fragmentation spectra

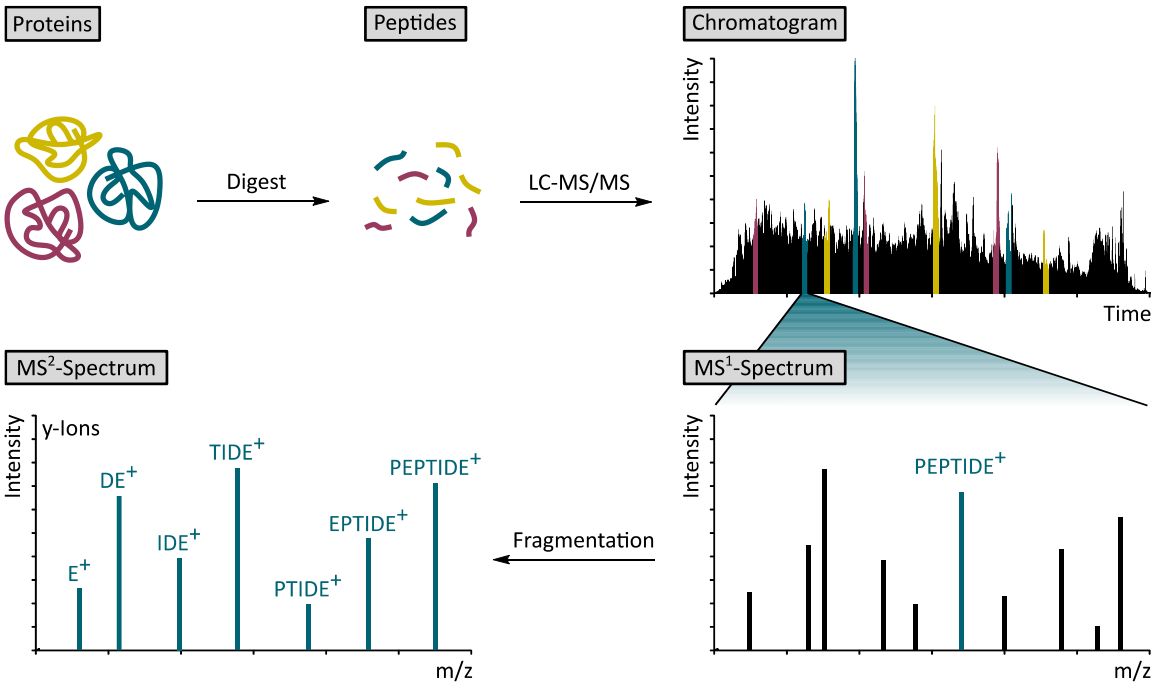

Figure 2: Schematic depiction of MS/MS-based protein identification. After digestion, peptides are separated by HPLC and measured on the mass spectrometer. Most intense peptides on MS^1-level are selected for fragmentation and subjected to MS^2 measurement. By mapping peptide fragments to the organism’s proteome the corresponding proteins can be deduced.[28]

of selected peptide ions (MS^2-level) allowing downstream extraction of the peptide's amino acid sequence by computational methods. By mapping this peptide sequence against the proteome of the analyzed organism, the corresponding proteins can be traced back. To gather all this information in reasonable time, bioinformatics programs were developed that can annotate thousands of peptide spectra within hours.[29–31] At this point, proteins are efficiently identified, yet no statement can be made about the changes between samples. This relative quantification among experiments, *e.g.* drug treated and control cells, is obviously of high interest.

In this matter, several techniques were developed, all having their specific advantages depending on the experimental set-up. The most basic categorization for these strategies is to pigeonhole them by the MS-level used for quantification. The following sections shall give a brief overview on the most important quantification strategies and their field of use.

2.1. Quantification on MS^1-level

Integration of the signal intensity in MS^1-spectra over the elution time from the HPLC column is a reflection for the amount of a peptide per sample. Using these integrated intensities is a straight forward way for protein quantification, yet it can be conducted in numerous ways. Isotopic labelling of samples allows protein ratio calculations within a single MS-run, whereas label-free approaches enable quantification between various runs (Figure 3). Both approaches will be highlighted in this section.

The first possibility to measure proteomic changes, is to isotopically label one set of peptides and compare it to an unlabelled counterpart. These generated "heavy" and "light" proteomes are pooled prior to MS-measurement. When assuming an unaltered chromatographic elution behaviour, peptide pairs with a mass to charge difference that reflects the used label appear on MS^1-level. The ratio between their intensities is then used for quantification. For this to work, there are some requirements an isotopic label needs to fulfil. The label needs to be incorporated or attached with close to 100% efficiency, to allow statistically relevant calculations. Additionally, it needs to be present in every peptide, as unlabelled peptides fail to report ratios, and are therefore lost to quantification. If the label is introduced before protein digestion, choosing a suitable

protease-label-pair does account for this problem. In 2006, *Ong* and *Mann* developed a method called “Stable Isotope Labelling by Amino acids in Cell culture” (SILAC), in which human cells are grown in the presence of isotopically labelled arginine and lysine (Figure 4A).[32] When fully incorporated in the proteome, digestion with trypsin generates only labelled peptides, as the protease cleaves always at the C-terminal site of these two amino acids. The major advantages of SILAC experiments is the very accurate quantification. As the label is introduced at a metabolic level and samples can be pooled very early in the work-flow, the relative protein-ratio between conditions remains unaltered by any downstream processing. However, SILAC is limited to three different conditions per sample (light, medium, heavy), which makes it less attractive for high-throughput approaches.[33] Another drawback of this method is, that it cannot routinely be used for

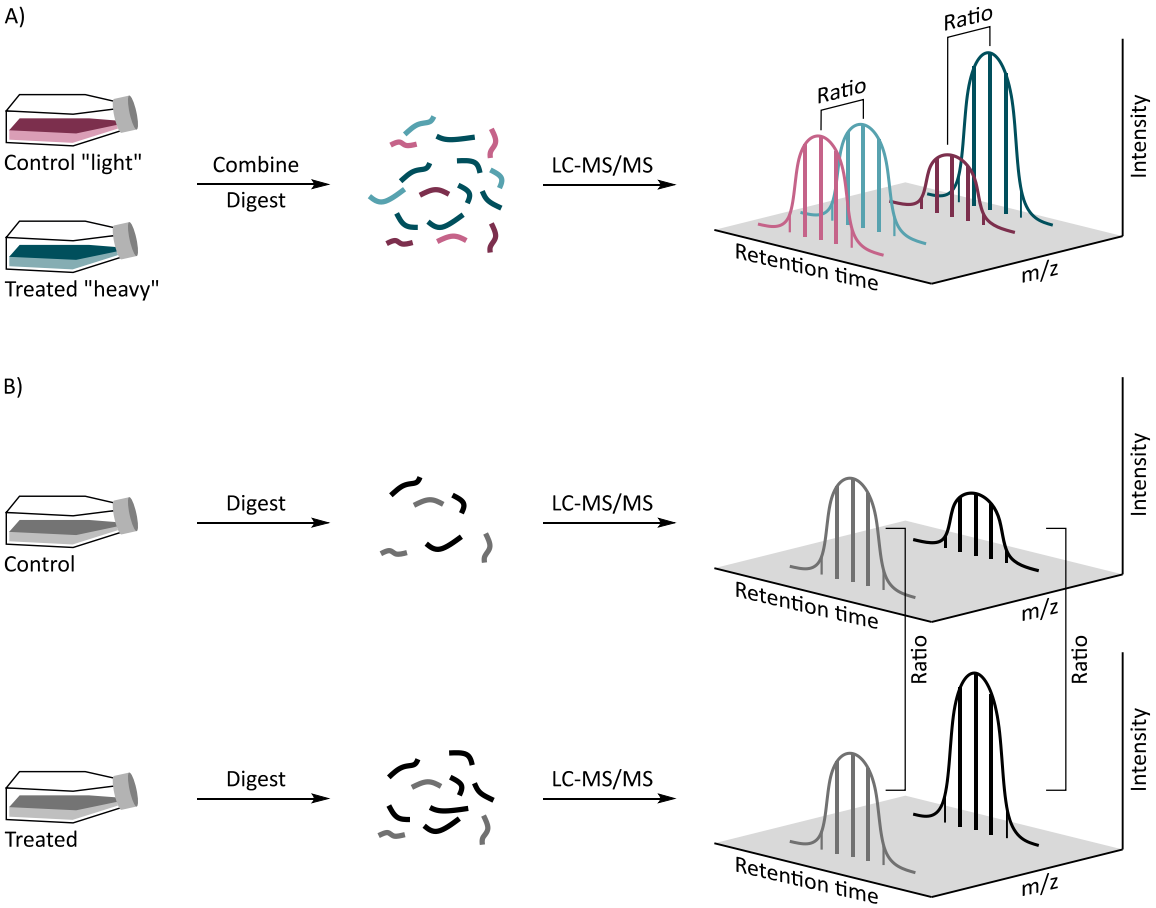

Figure 3: Overview on MS[1]-based quantification principles. A) Quantification of isotopically labelled peptide pairs. Peptide samples are combined and measured in a single LC-MS/MS run. Relative quantification is based on the intensity ratios of peptide pairs. B) Label-free quantification of various samples. Quantification is based on the intensity differences of corresponding peptides in separate LC-MS/MS runs.

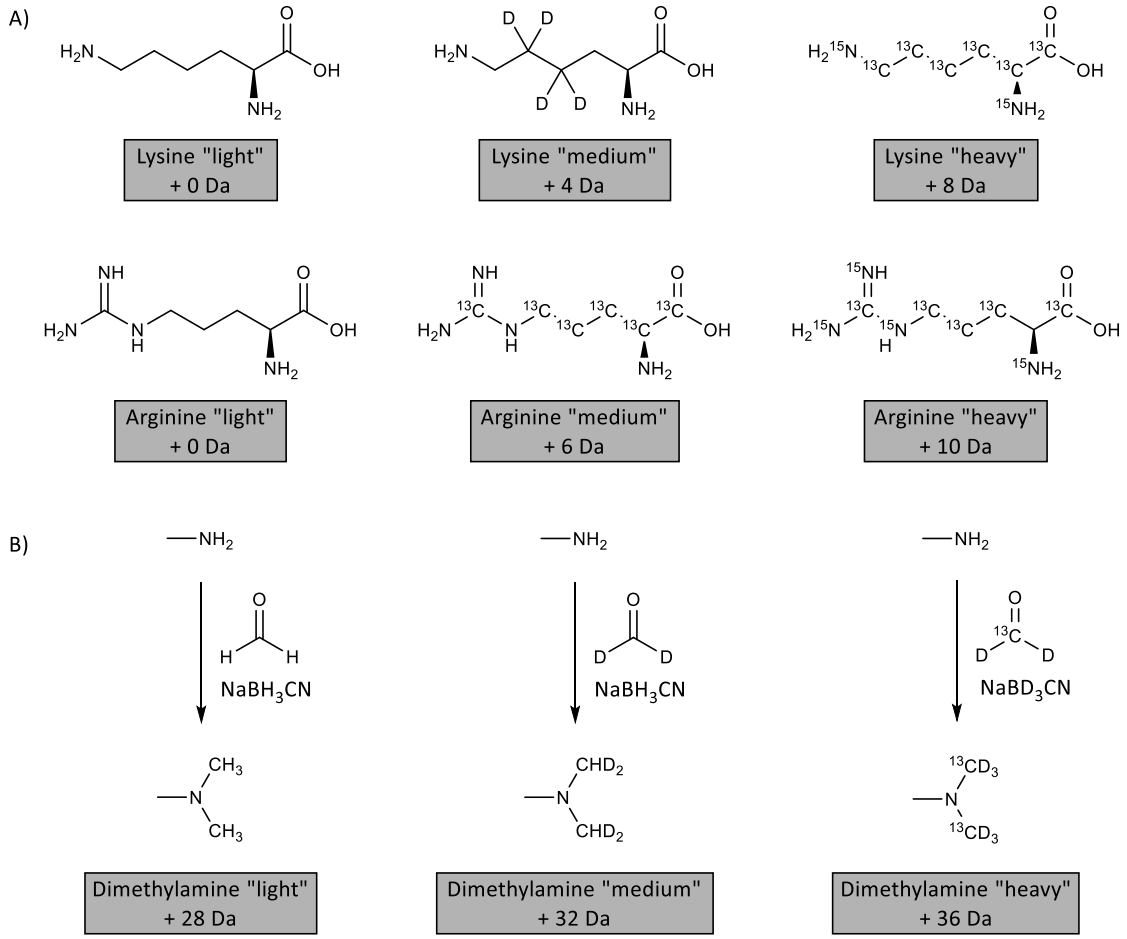

Figure 4: A) Structure of isotopically labelled amino acids lysine and arginine used in SILAC experiments. B) Reductive amination of primary amines performed in DML approaches to generate isotopically labelled dimethylated amines.

proteomic studies in bacteria as their *de novo* synthesis of amino acids makes reproducible incorporation difficult. To overcome this, strategies were developed, that don't rely on the metabolic incorporation of labelled amino acids, but rather introduce the isotopic label after digestion of the proteins. The most common approach is called "DiMethyl Labelling" (DML), in which all primary amines, *i.e.* lysines and N-termini, undergo reductive amination to form isotopically labelled dimethylamines (Figure 4B).[*34,35*] This approach is quick and cost efficient, but requires handling of highly toxic reagents. A drawback, inherent to all methods that measure isotopically labelled samples in one LC-MS/MS run, is signal overlapping, as the amount of peptide signals increases proportional to the number of labels used. To some extent, this can be overcome by fractionation of samples, but at the cost of measurement time.

To reduce both, spectral complexity and additional preparation steps in proteomic workflows, high effort was put into developing label-free techniques.[36] One strategy is based on the concept, to count all MS-spectra that contain a certain peptide and compare these results among runs.[37] This works mostly for less computationally demanding samples, but quickly comes to a limit as sample complexity increases.[36] By developing an algorithm that normalizes MS-runs in a way that accounts for slight variations in sample handling and quantifies peptide profiles in a very efficient manner, *Cox et al.* introduced a technique that is nowadays just referred to as label-free quantification (LFQ).[38] In theory, this allows to compare an indefinite number of conditions. It also gives access to samples that cannot be metabolically labelled, like for example clinical isolates. The computational quantification also allows comparison of samples for which standardized sample handling is challenging, *e.g.* gathered in separate laboratories. The major disadvantage of this technique, is the vast amount of measurement time needed, as every sample needs to be measured individually, compared to the discussed labelled approaches that calculate protein ratios within one MS-run. LFQ also depends stronger on reproducible performance of the HPLC-system because the elution time, among other criteria, is used for peptide identification.

All these methods depend heavily on the quality of the corresponding MS^1-spectra. The signal-to noise ratio affects both sensitivity as well as accuracy of the experiment. As spectral complexity drops significantly after peptide isolation and fragmentation, new techniques that quantify on the MS^2-level were introduced.

2.2. Quantification on MS^2-level

In order to find a way to combine the robustness of isotopic labelling with high-throughput workflows while limiting signal overlap, strategies were developed that allow quantification on the MS^2-level. The two most frequently used systems are called “Tandem Mass Tag” (TMT) and “isobaric Tags for Relative and Absolute Quantitation” (iTRAQ) (Figure 5).[39–43] Both are NHS-ester that react specifically with primary amines and allow late-stage introduction of the tags, making them applicable for *in vivo* samples. Each tag contains an MS-labile bond, in most cases an amide bond, and is introduced at the peptide level. These labelling agents normally consist of three parts: a reporter group, a mass balancer and a leaving group. During MS-fragmentation, this tag is split into two parts, a reporter group that is used for quantification and a mass balancer that remains on the peptide of interest. The main idea behind this method, is to use a set of isobaric tags that all share the same amount of heavy isotopes, but the distribution over reporter group and mass balancer is unique for each tag. After labelling different samples, peptides are pooled and measured in one MS-run. As corresponding peptides from different conditions share the same total mass, they give only one combined signal on MS^1-level.[28] Then, by carefully choosing the right fragmentation energy, the bond between reporter group and mass balancer is broken. As the resulting reporter ions have unique masses for each condition, they give characteristic finger-print peaks in the MS^2-spectra. This not only allows unambiguous differentiation between the tags, but by comparing the intensities of the reporter groups also allows quantification between samples (Figure 6). As of today,

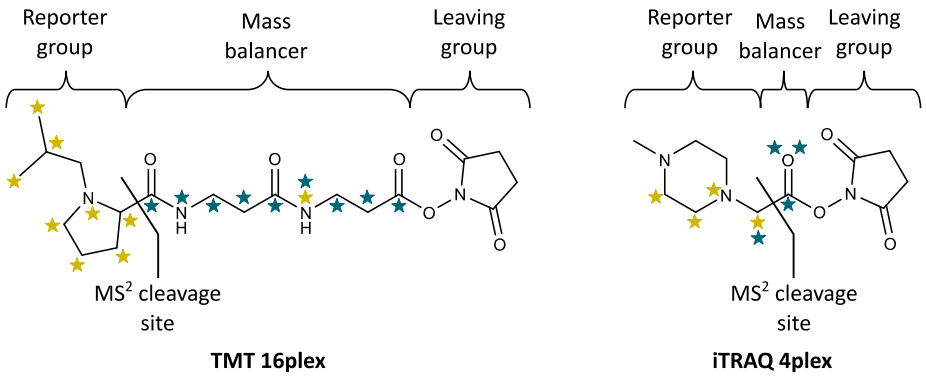

Figure 5: Commonly used TMT and iTRAQ labelling agents used for MS^2-level peptide quantification. Stars indicate heavy isotope positioning for versions with lightest (blue) and heaviest (yellow) reporter group of each set.

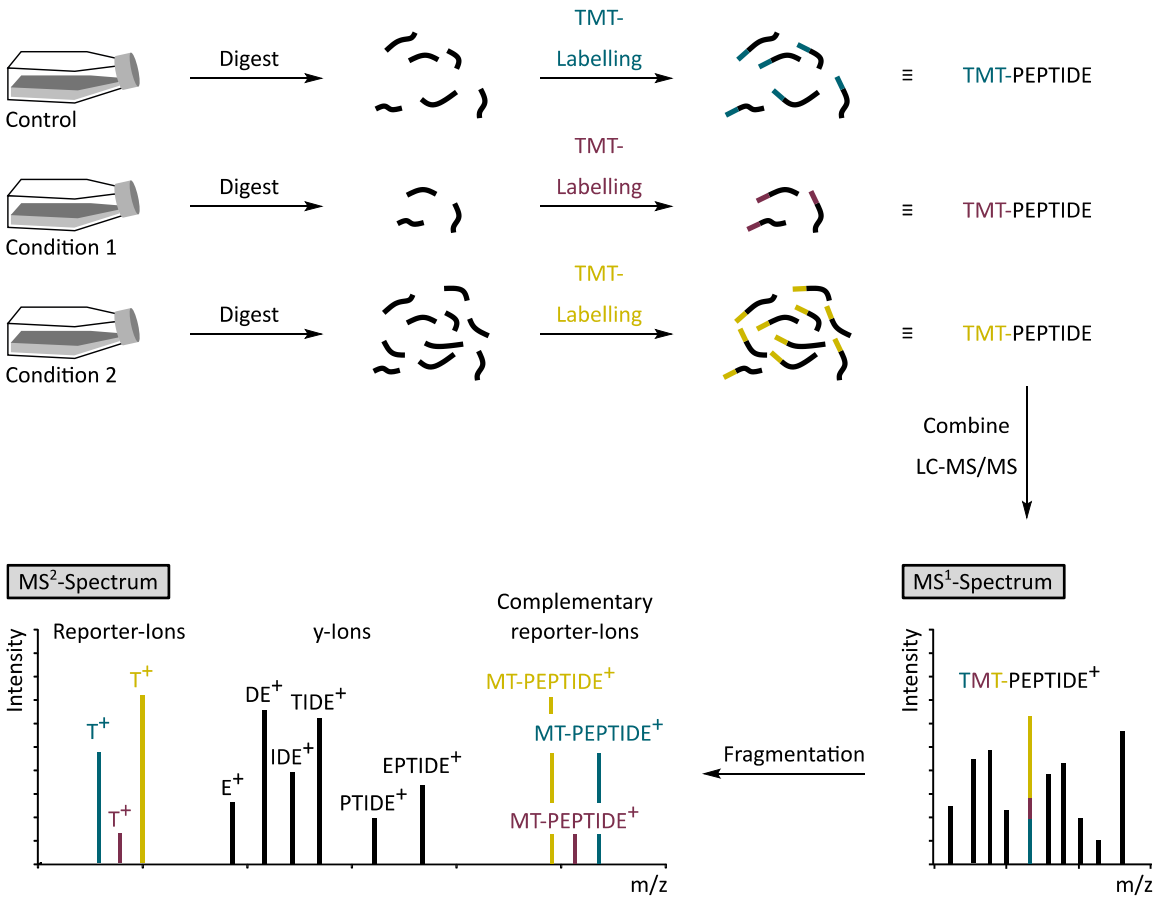

Figure 6: Overview on MS²-based peptide quantification. Each sample is coupled to an MS-labile isobaric labelling agent. Subsequently, samples are pooled and measured in a single LC-MS/MS run. Corresponding peptides give one combined signal on MS¹-level. During fragmentation, the reporter-ions are cleaved off. Their intensity differences are used for peptide quantification.

up to 16plex reagent kits are commercially available. The main advantage of these tags is unquestionably extreme sample-throughput achieved by the mentioned combination of low complex MS¹-spectra with simple quantification on MS²-level. However, there are limitations to this approach due to ratio distortion caused by co-fragmentation of peptides, as the isolation of similarly massed peptides after MS¹-scanning can be rather challenging (Figure 7). Most of the time, the fragmentation chamber will not only be filled with the peptide of interest, but also with co-eluting peptides of similar mass. As no differentiation between the cleaved reporter groups can be made, the intensities will add and give flawed results. This challenge has been tackled both, from a computational as well as experimental side, continuously diminishing this problem.[44–47]

Taking into account all information on the different quantification methods available when conducting MS-based proteomics, the conclusion must be that there is no “one

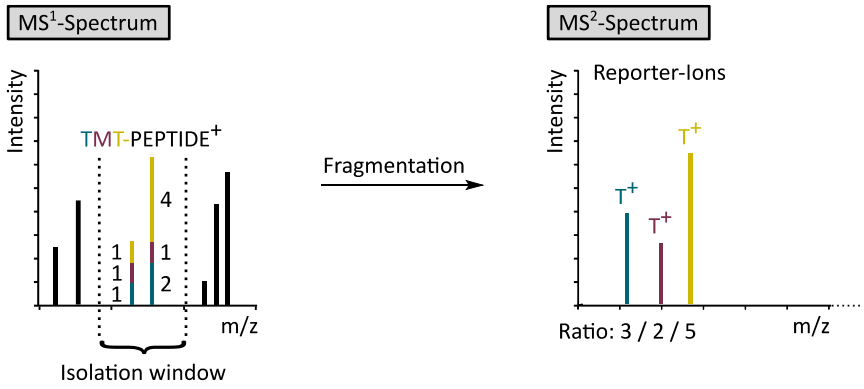

Figure 7: Ratio distortion as major problem of MS^2-based quantification methods. As the isolation window to separate peptides for fragmentation is limited by the technical specifications of the spectrometer, co-isolation of peptides with similar m/z can frequently be observed. Due to the fact that reporter-ions are indistinguishable after fragmentation, their intensities are added, resulting in distorted ratios.

technique serves all" kind of approach. One has to choose the strategy based on the experimental question asked. High ratio accuracy might require isotopic label, whereas routinely comparing diverse samples might justify the use of an LFQ set-up. This thesis includes two separate works, studying small-molecule protein interactions that were based on said decision making.

II. Chemical Probe to Monitor the Parkinsonism-Associated Protein DJ-1 in Live Cells

1. Introduction

With an approximate incidence of 12 to 19 cases per 100,000 per year, Parkinson's disease (PD) is the second-most common neurodegenerative disorder worldwide.[48,49] These numbers depend heavily on the study setting, yet tendencies towards a higher prevalence for men as well as a significant increase of incidents after the age of 60 can be seen throughout.[50,51] Despite being first described in the early 19th century, the cause of PD is still not understood in its whole. Indication is based on various criteria including accumulation of α-synuclein, so called Lewy bodies, and cell degeneration in the substantia nigra.[52–54] The latter is strongly associated with high levels of reactive oxygen species (ROS) within the cells.[55] In the cause of this, the Parkinson disease protein 7 (DJ-1) gained major attention for its putative role in sensing and mediating oxidative stress (Figure 8).[56–58]

DJ-1 contains 189 amino acids and is functional as homo-dimer.[59,60] It is ubiquitously expressed throughout all cell types and tissues including neurons and glia cells in the brain.[61–64] As highly multifunctional protein, DJ-1 takes part in diverse cellular functions such as transcriptional regulation, protease activity and, importantly, in the antioxidative stress reaction.[65–70]

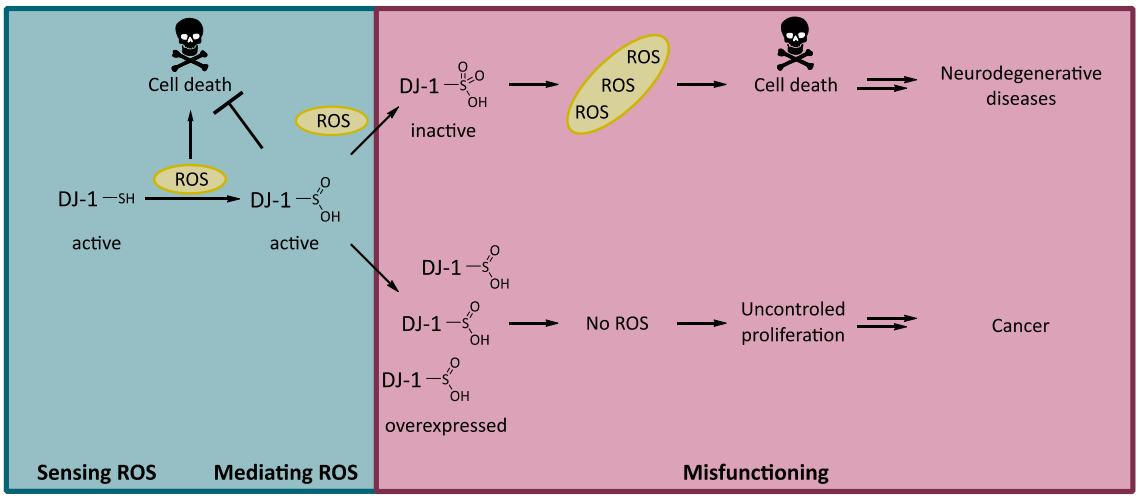

Figure 8: Schematic overview on the ROS-induced activity of DJ-1. Upon oxidation by rising levels of intracellular ROS, DJ-1 acts as ROS mediator to prevent cell death. Extreme levels of ROS were shown to deactivate DJ-1 by over-oxidation to the corresponding sulfonic acid, consequently leading to cell death, and are therefore associated with neurodegenerative diseases. Accordingly, high expression levels of DJ-1 can benefit uncontrolled cell proliferation contributing to cancer development.

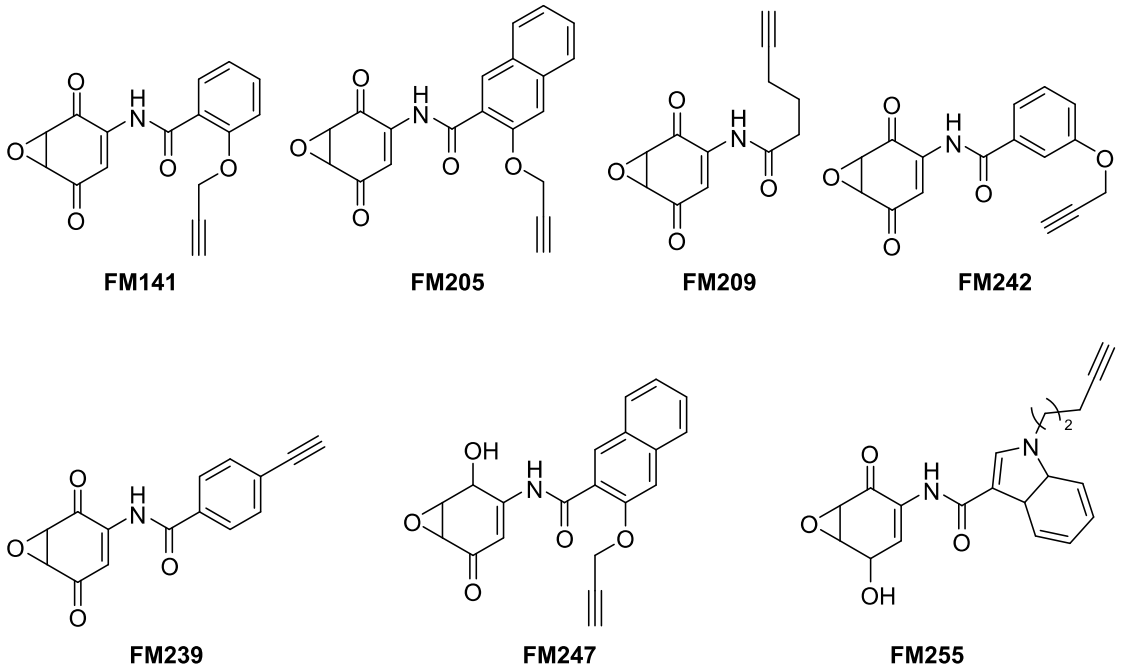

Figure 9: Panel of aminoepoxycyclohexenone and aminoepoxyquinone probes used in this study.

DJ-1 contains a conserved cysteine (C106) that is easily oxidized, allowing for a very efficient way of ROS-detection (Figure 8).[71,72] Upon oxidation to the highly stabilized corresponding sulfinic acid, DJ-1 experiences a conformational change, leading to a variety of ROS-mediating functions including chaperone activity and regulation of gene expression.[71,73–79] In this matter, it was also shown that mutations in the *PARK7* gene that lead to reduced expression or protein activity are associated with early-onset PD, making DJ-1 a possible biomarker for early diagnosis.[80–82] As the treatment and thus the prognosis of PD is dependent on the progression of the disease, fast identification is crucial.[54]

In 2016 *Mandl et al.* reported the antibiotic effect of aminoepoxycyclohexenones (AECHs), a class of structurally diverse natural products.[83] In their work, they synthesized a representative panel of ABPP-probes and control molecules (Figure 9). By chemical proteomics and biochemical validation, they discovered sigma cross-reacting protein 27A (SCRP-27A), a member of the DJ-1 superfamily, as direct target.[84] Based on these results, the following work was initiated to examine the general applicability of AECHs as molecular tools to monitor DJ-1.

2. Results and Discussion

2.1. Esterase Activity Assay

After initial attention had been drawn to DJ-1, a plethora of molecular functions for this protein were discovered, yet many of them are still debated in the scientific community. In 2016 *Vázquez-Mayorga et al.* described a so far unknown esterase activity for DJ-1 that had also been reported for other proteins of this superfamily.[83,85] This activity can be measured in an easy and robust enzyme assay, which monitors the cleavage of the

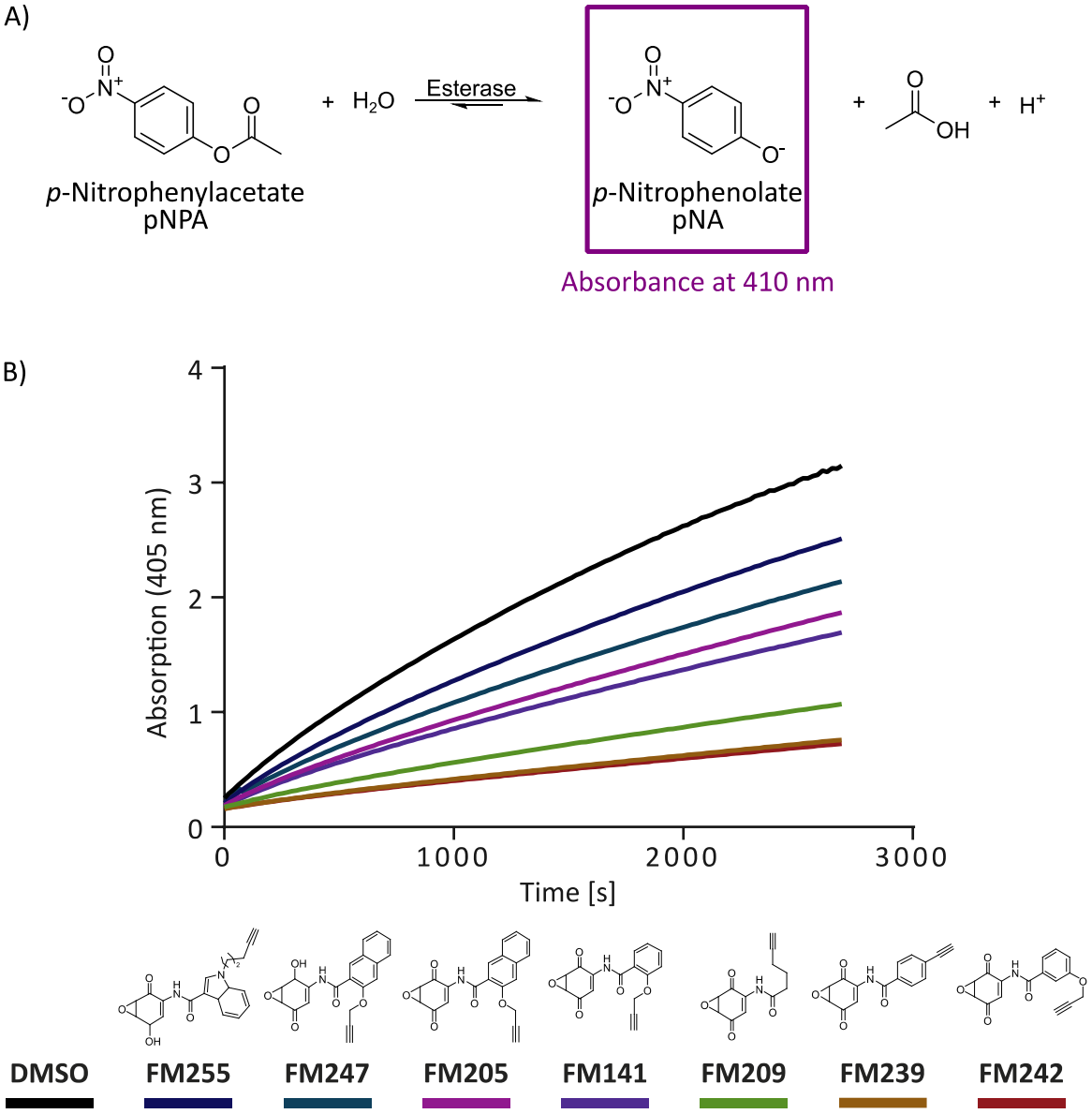

Figure 10: A) Schematic presentation of the enzymatic ester cleavage measured at 410 nm. B) Probe dependent inhibition of recombinant DJ-1 monitored over time *via* esterase assay at 410 nm. The probes show distinguishably different inhibitory profiles.

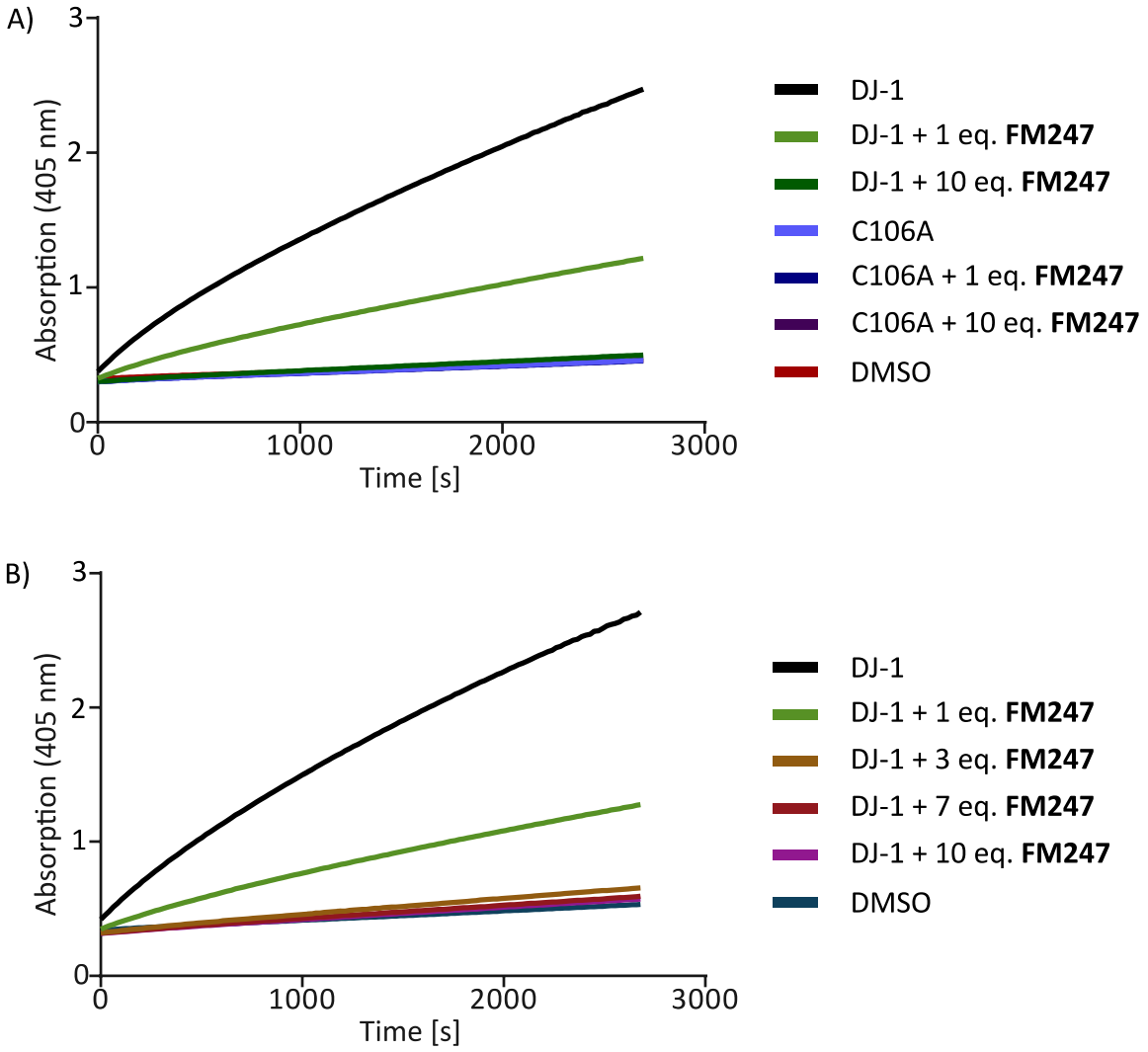

Figure 11: A) The ester cleavage of pNPA by DJ-1 or the C106A point mutant was monitored after preincubation with various equivalents of **FM247**. No esterase activity was detectable for the point mutant. B) The ester cleavage of pNPA by DJ-1 was monitored after preincubation for 30 min with various equivalents of **FM247**. Three equivalents of probe proved to nearly abolish enzymatic activity.

substrate *p*-nitrophenyl acetate (pNPA) to the photometrically detectable product *p*-nitrophenol (pNP) at 405 nm (Figure 10A). As Cys106 is part of the esterase dyad that is essential for substrate turnover, the assay can directly be used to measure modification of this crucial oxidation sensor. *Mandl et al.* demonstrated the inhibition of esterase activity of the bacterial homolog SCRP-27A upon treatment with AECHs through irreversible opening of the epoxide ring by the catalytic cysteine.[83] Following up on these results, a panel of AECHs was tested for their inhibitory potential towards DJ-1. For this, DJ-1 was preincubated with 1 eq. of the corresponding probe for 30 min at RT, and its residual esterase activity subsequently monitored over time (Figure 10B). Out of seven

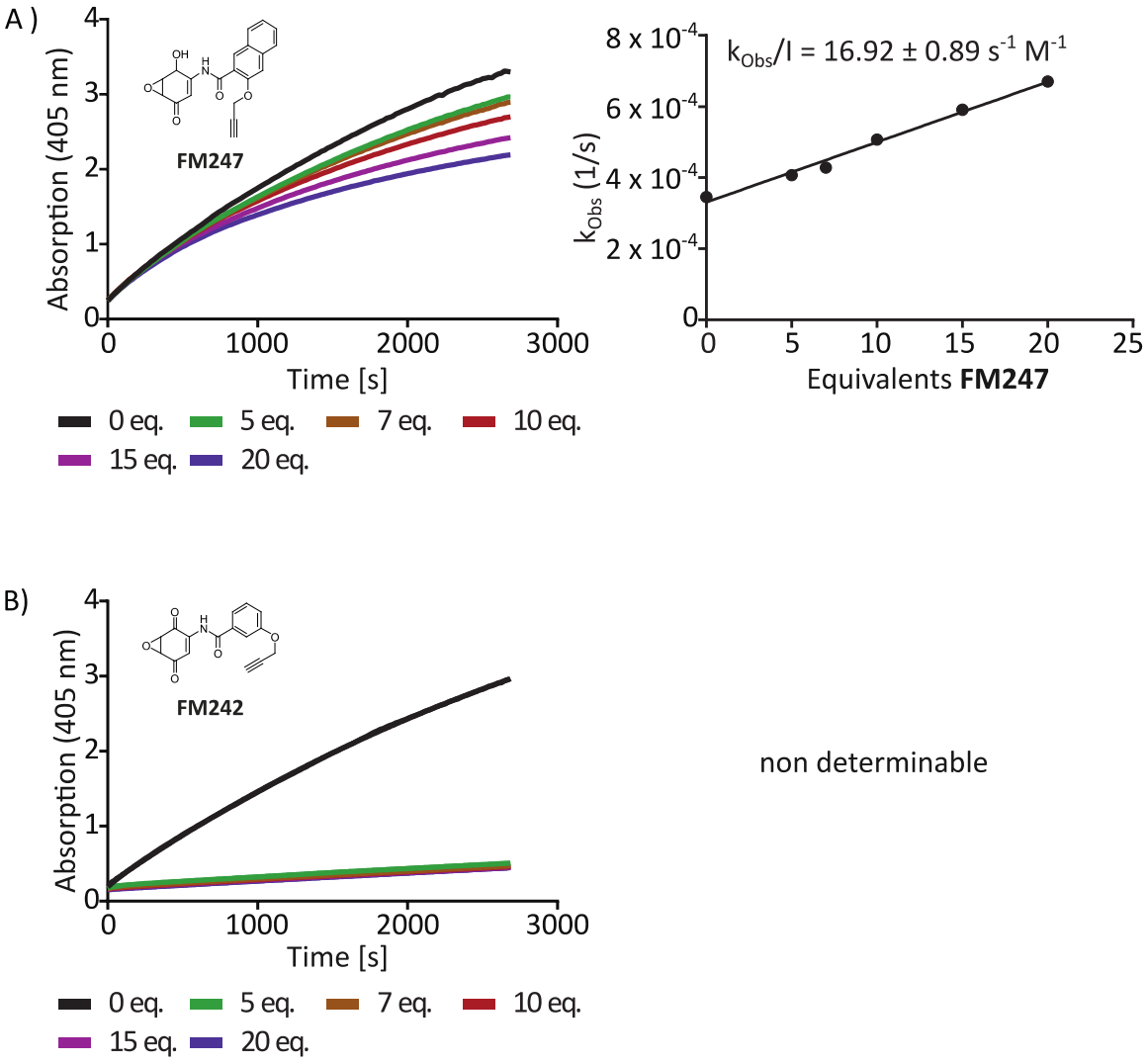

Figure 12: A)) The ester cleavage of pNPA by DJ-1 was attenuated directly upon addition of various equivalents of **FM247**. The obtained K_{Obs} values were plotted against the inhibitor equivalents and subjected to linear fitting yielding K_{Obs}/I values as the slope. B) **FM242** inhibition kinetics were too fast to calculate K_{Obs} values.

tested AECHs, three resulted in strong and four in moderate time-dependent inhibition of DJ-1.

In order to verify the significance of Cys106 for protein activity, a Cys106Ala mutant was generated. As expected, the point mutant did not lead to any substrate conversion (Figure 11A). To exemplarily determine the amount of moderate inhibitor needed for complete protein inhibition, the assay was repeated with varying concentrations of **FM247**. Three equivalents of **FM247** were already sufficient to abolish esterase activity (Figure 11B). Binding kinetics were exemplarily determined for one moderate (**FM247**) and one strong inhibitor (**FM242**), by detecting the residual enzyme activity directly after treatment with

various probe concentrations. While the binding of **FM242** to DJ-1 was too fast for determination of K_{obs}/I values, **FM247** yielded a K_{obs}/I of 16.92 $s^{-1}M^{-1}$ (Figure 12). Combining these results, AECHs proved to be promising tools to target DJ-1 and were therefore used in further validation experiments.

2.2. Intact Protein Mass Spectrometry

Intact protein mass spectrometry (IP-MS) is a very powerful technique to monitor covalent modifications of proteins. Proteins are directly subjected to detection by MS, after which deconvolution of the resulting m/z states retrieves the corresponding protein mass. Modern MS-instruments allow the detection of mass changes < 1 Da, so that even minor protein modifications, *e.g.* oxidation or even deuteration, can be observed.

To expand on the results obtained from the esterase assay, DJ-1 was treated with 10 eq. of either the moderate inhibitor **FM247** or the strong inhibitor **FM242** and measured periodically for 1 h (Figure 13). **FM247** exclusively mono-alkylated DJ-1, while **FM242** double modified the protein significantly. Moreover, **FM242** labelled a mutant protein

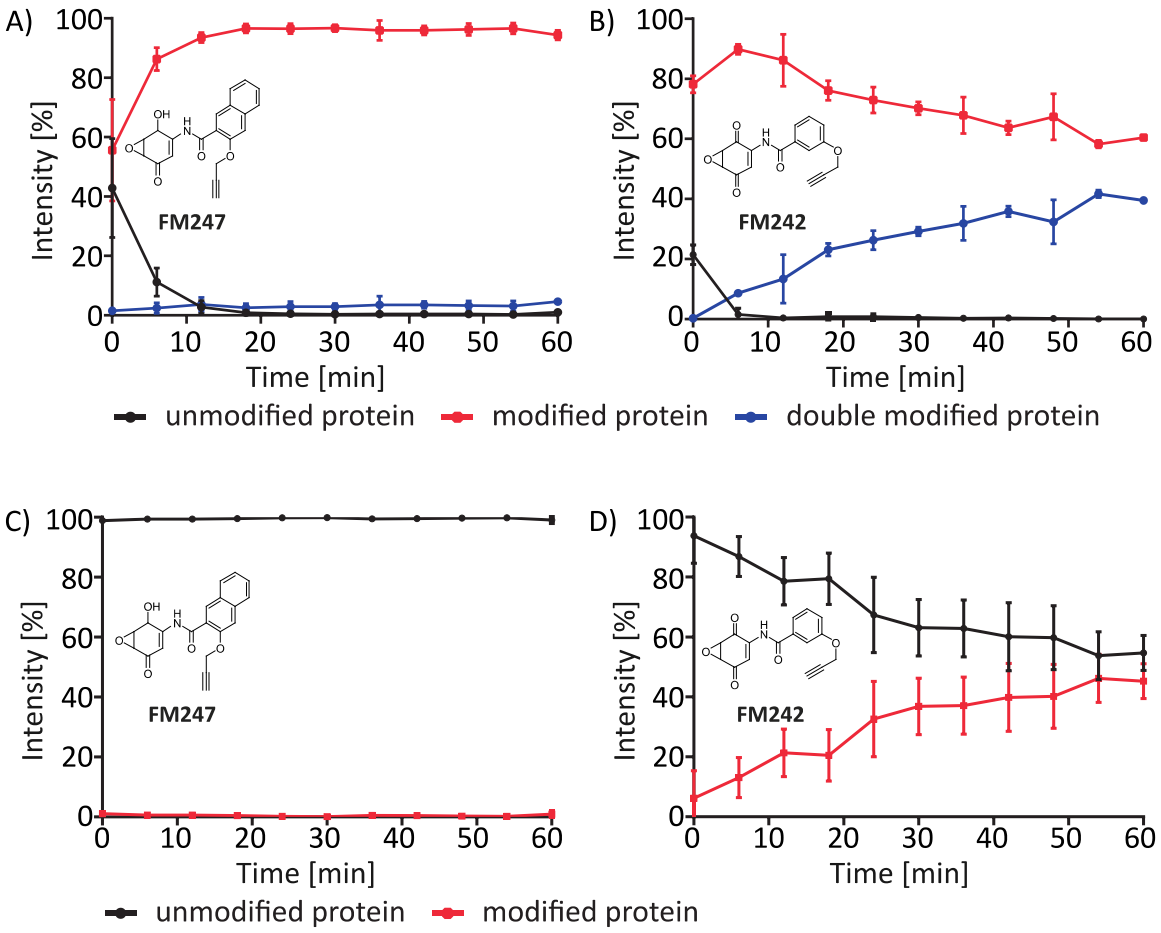

Figure 13: A) The modification of DJ-1 by 10 eq. **FM247** was measured in a time-dependent manner using intact protein MS. **FM247** was able to completely modify DJ-1 without showing significant double modification. B) **FM242**, in contrast, showed about 50% of undesired double modification after 60 min. C) The modification of DJ-1 C106A point mutant by 10 eq. **FM247** was measured in a time-dependent manner using intact protein MS. **FM247** did not show any binding within the observed time-frame. D) **FM242**, in contrast, showed about 50% of undesired modification after 60 min.

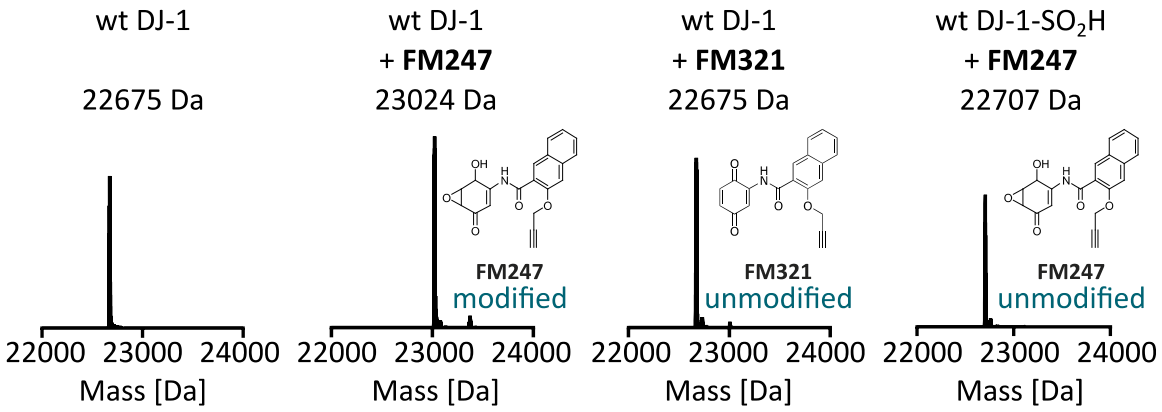

Figure 14: Intact protein MS measurements of DJ-1 labelled with inhibitor **FM247** showed complete conversion of the protein, whereas the inactive, epoxide lacking probe **FM321** did not modify DJ-1. Measurements of oxidized DJ-1-SO_2H incubated with inhibitor **FM247** showed no reaction with the protein.

bearing an active site Cys106Ala mutant making it unsuitable for selective monitoring of the catalytic Cys106; in contrast, **FM247** did not label the mutant and was therefore selected as probe, with the best share of reactivity and selectivity, for further DJ-1 studies. Ideally the AECH scaffold would not only enable specificity for DJ-1, but also provide a direct readout of the thiol oxidation sensor. For this, the binding mode of **FM247** and a close analogue lacking the epoxide ring (**FM321**) were tested (Figure 14). As expected, only the epoxide containing probe was able to react with DJ-1's active site cysteine, speaking for a ring opening by nucleophilic substitution. This theory is further supported by the fact that **FM247** did not modify oxidized DJ-1, as the sulfinic acid is a much weaker nucleophile. This finding enables a direct and specific readout of the reduced state.

2.3. Thermal Shift

When investigating covalent and non-covalent interaction of small molecules and proteins, a widespread method is to determine the proteins' thermal stability.[86] Protein and molecule of interest are combined together with a dye whose fluorescence increases upon protein unfolding, and monitored during gradual temperature increase. The inflection point of the resulting melting curves of this assay represents the melting temperature T_M, which shifts upon changes in protein stability.

Addition of **FM247** destabilized the enzyme as shown by a negative thermal shift in a concentration dependent manner (Figure 15A). No such shift was observed in case of the

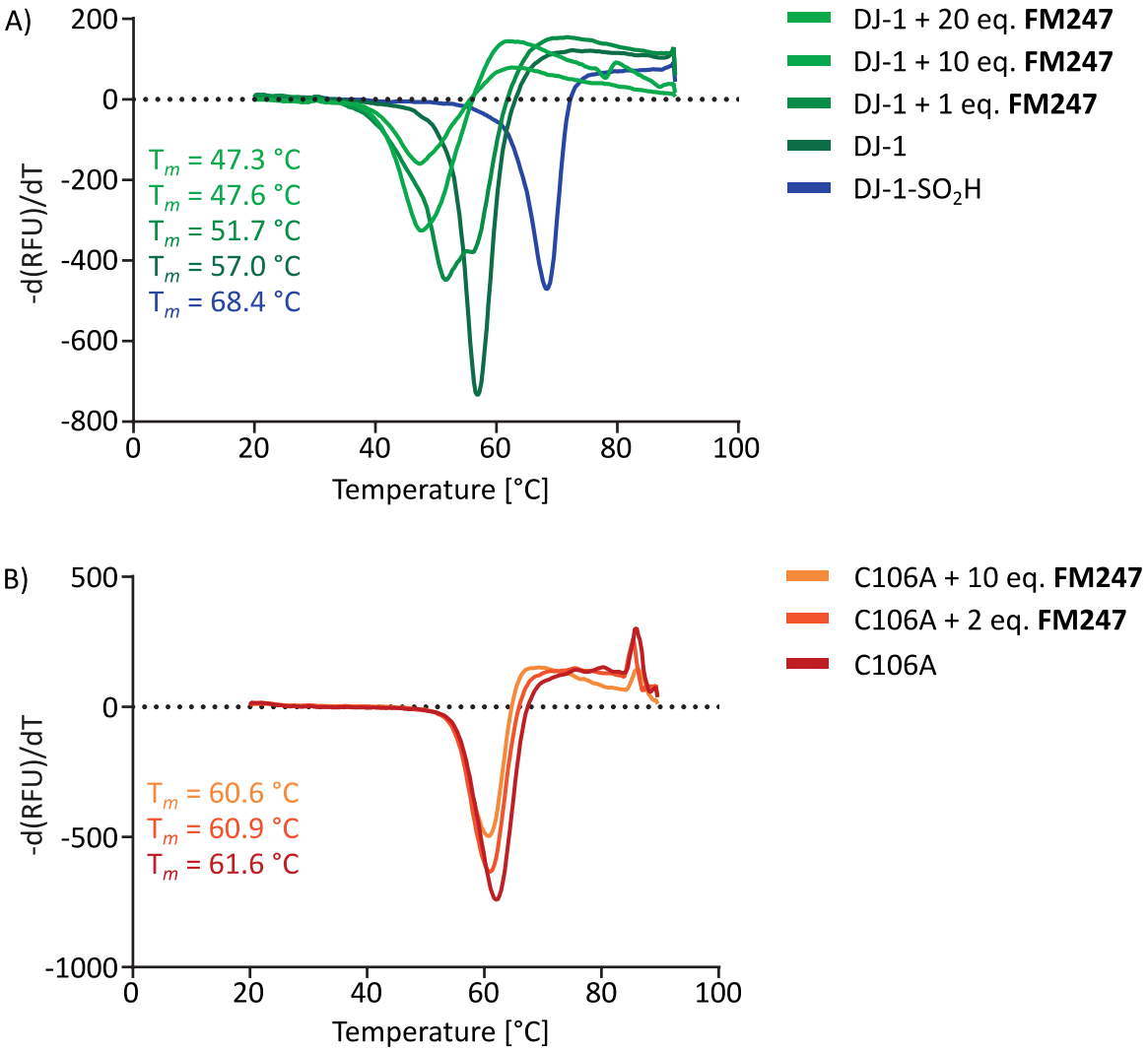

Figure 15: Melting temperatures (T_m) of DJ-1 (A) and the inactive C106A point mutation (B) treated with different concentrations of **FM247** via thermal shift assay. A concentration dependent decrease of T_m for the wild-type but not for the active-site mutation could be observed. Oxidated DJ-1 showed a significant increase in stability.

active site Cys106Ala mutant, further corroborating this binding site (Figure 15B). Interestingly, oxidation of DJ-1 with H_2O_2 to the sulfinic acid resulted in strong enzyme stabilization by 11 °C. This is in line with crystal structure information showing stabilization of oxidized Cys106 via a pronounced H-bond network.[87]

2.4. Site-Identification

As final proof for the site selectivity of **FM247** towards Cys106 of DJ-1, an MS/MS-based approach was used. After incubation of DJ-1 with a three-fold excess of probe, the protein was digested with chymotrypsin and peptides were subjected to MS analysis. Corresponding peptides showed modification by **FM247** with 100% localization probability at Cys106 (Figure 16).

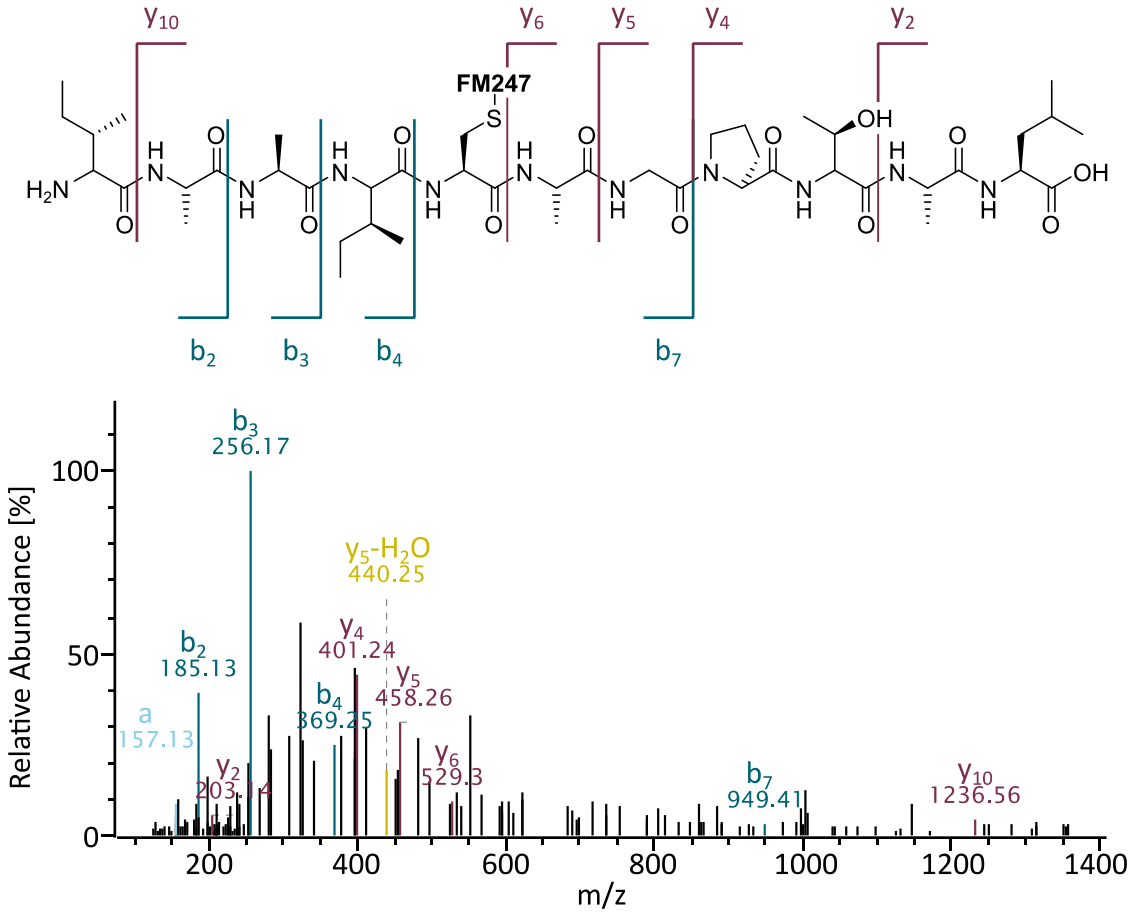

Figure 16: MS^2 spectrum of peptide Ile102-Leu112 modified by **FM247** at position Cys106.

2.5. Gel-based Labelling

After these initial experiments to validate **FM247** binding and inhibiting DJ-1, the next step was to test the probe in a cellular ABPP approach. As **FM247** is equipped with an alkyne handle, it is suitable for labelling proteins in intact cells followed by detection using click chemistry. After incubating the cells with the probe, a fluorophore is attached. Using SDS-PAGE, the proteins are separated by size and the corresponding fluorescence signal measured as degree of probe binding.

Purified DJ-1 could be clearly labelled with 0.1 - 0.3 equivalents of **FM247** (Figure 17). In line with the previous results, the oxidized protein as well as the Cys106Ala point mutant escaped detection, again showing the high selectivity of the probe towards the reduced Cys106.

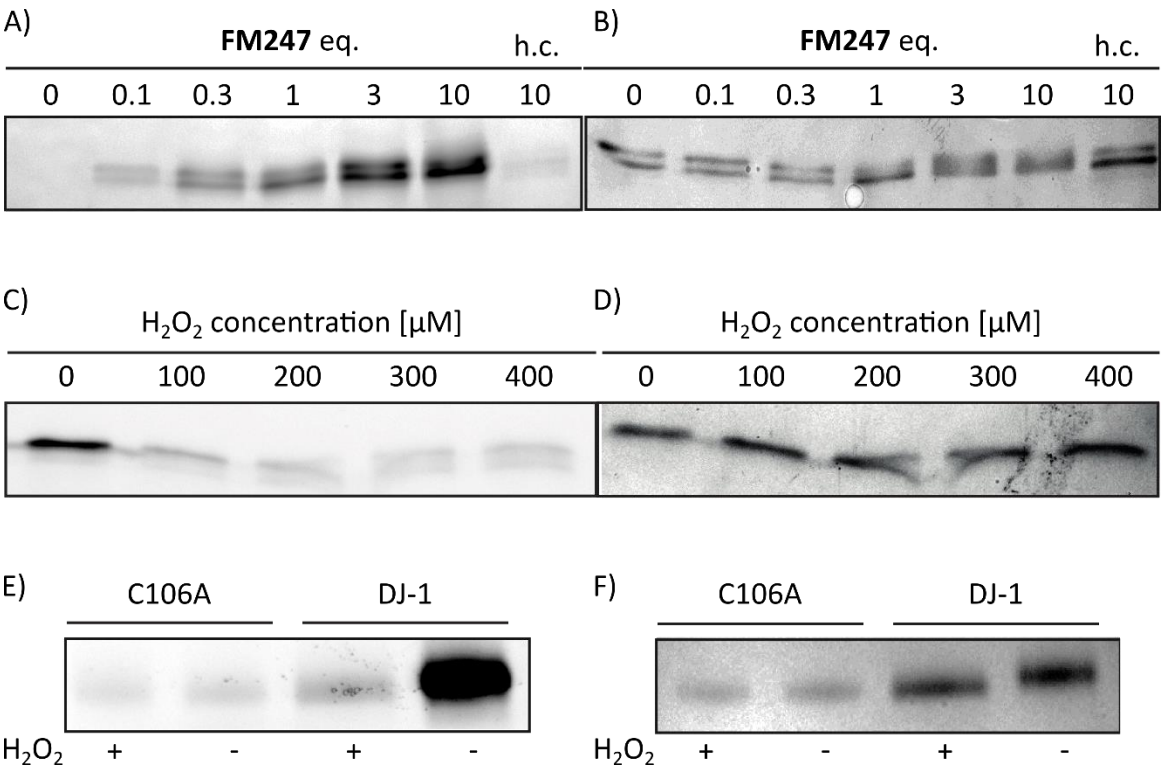

Figure 17: A) Labelling recombinant DJ-1 with various equivalents of **FM247** led to concentration dependent modification of the protein. The heat control (h.c.) resulted in no detectable signal, demonstrating that **FM247** solely binds to the correctly folded protein. B) The coomassie-stained gel proves the same protein concentration in each sample. C) Labelling of recombinant DJ-1 with **FM247** after treating the protein with various concentrations of H_2O_2 showed the oxidation-state dependent binding of the probe. D) The coomassie-stained gel proves the same protein concentration in each sample. E) Labelling of recombinant DJ-1 and the point mutant C106A with **FM247** after treating the protein with 100 µM concentrations of H_2O_2 showed the oxidation-state dependent binding of the probe to the active site cysteine. F) The corresponding coomassie-stained gel shows comparable protein concentrations in each sample pair.

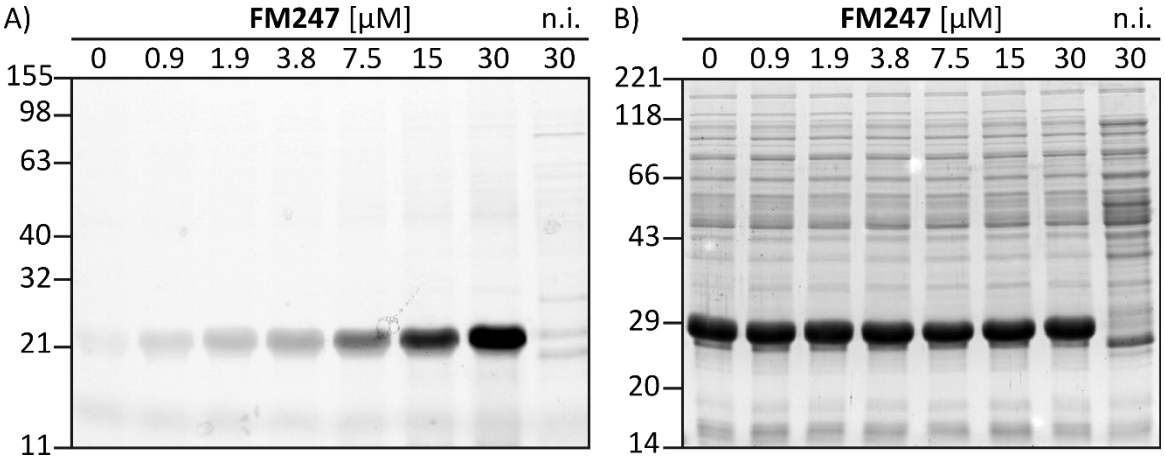

Figure 18: A) Fluorescent SDS gel of DJ-1 labelled with various concentrations of **FM247** in the expression strain Rosetta2. No labelling was observed for the non-induced (n.i.) sample. B) The corresponding coomassie-stained gel proves the same protein concentration in each sample.

In a more complex proteomic set-up, binding of the probe was established in *E. coli* cells expressing DJ-1. Cells were treated with the probe at various concentrations, lysed and conjugated to rhodamine azide (RhN_3). The fluorescent scan of the corresponding gel

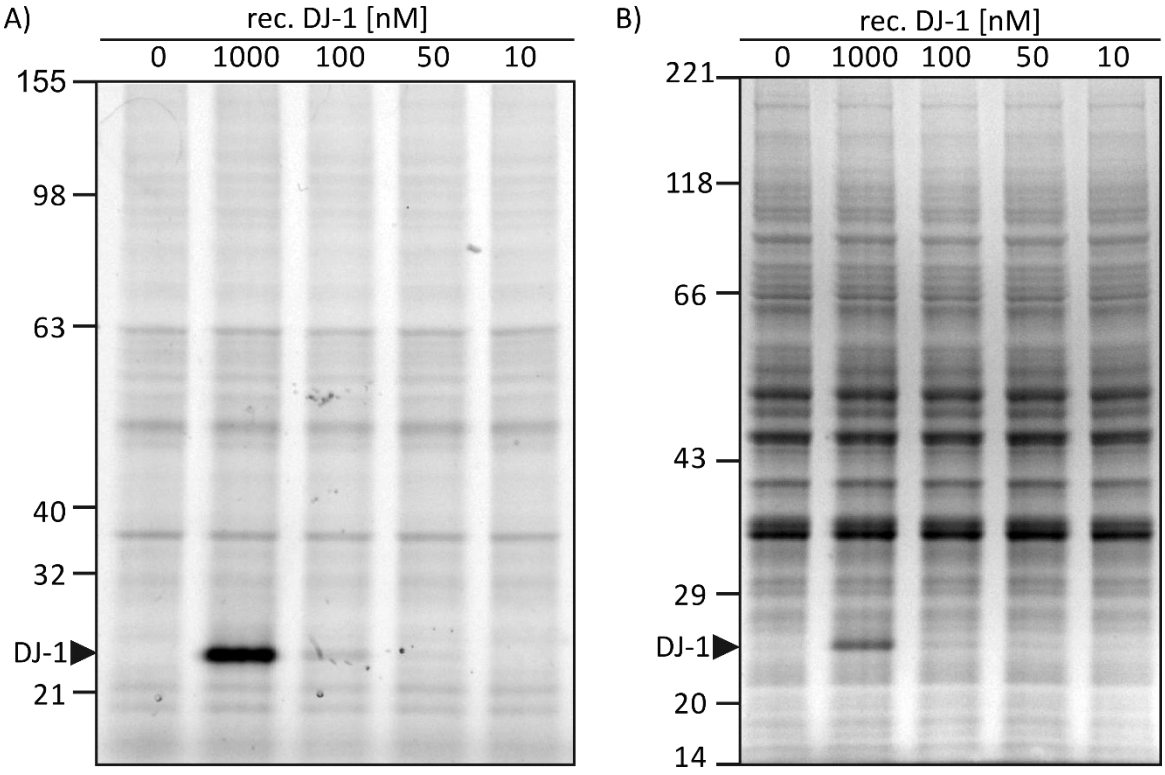

Figure 19: A) Fluorescent SDS gel of various concentrations of recombinant DJ-1 spiked into A549 lysate. Labelling with 10 µM **FM247** showed a detection limit at about 50 nM. B) The corresponding coomassie-stained gel proves the same lysate concentration in each sample.

revealed a strong protein signal at 23 kDa, visible down to 1 µM probe concentration, which was absent in cells lacking DJ-1 expression (Figure 18). Finally, 10 µM **FM247** showed a detection limit of about 50 nM DJ-1 when spiked into A549 cell lysate (Figure 19).

Encouraged by these results, **FM247** was next used in preparative ABPP experiments to validate its use as specific probe to detect DJ-1 in complex proteomic samples.

2.6. Target Identification – SILAC

To get a global overview on the protein targets of **FM247**, a quantitative ABPP workflow was used. The experiments were performed in well characterized HeLa and A549 cells and additionally in SH-SY5Y cells, as they are often used as model system in the study of Parkinsonism-associated pathways. Target identification was performed *via* quantitative and gel-free analysis utilizing a SILAC approach, which has proven to give very precise and reliable ratios between treated and untreated samples. After incubation with either 10 µM **FM247** or DMSO as control, cells were lysed, equal protein amounts of treated and control cells were pooled and subsequently conjugated to biotin azide *via* click chemistry. Biotin labelled proteins were enriched on avidin beads and corresponding peptides were released by tryptic digest for LC-MS/MS analysis. The results of these experiments are shown as volcano plot, which displays the statistical significance of enrichment levels as function of protein enrichment ratios of the individual proteins. Throughout all cell lines DJ-1 clearly showed up as the most prominent hit, which is crucial for a diagnostic use as off-target reactivity would lead to flawed results (Figure 20,A1,A2). For example, its enrichment in HeLa cells is 170-fold over DMSO control and 3.58-fold over the second

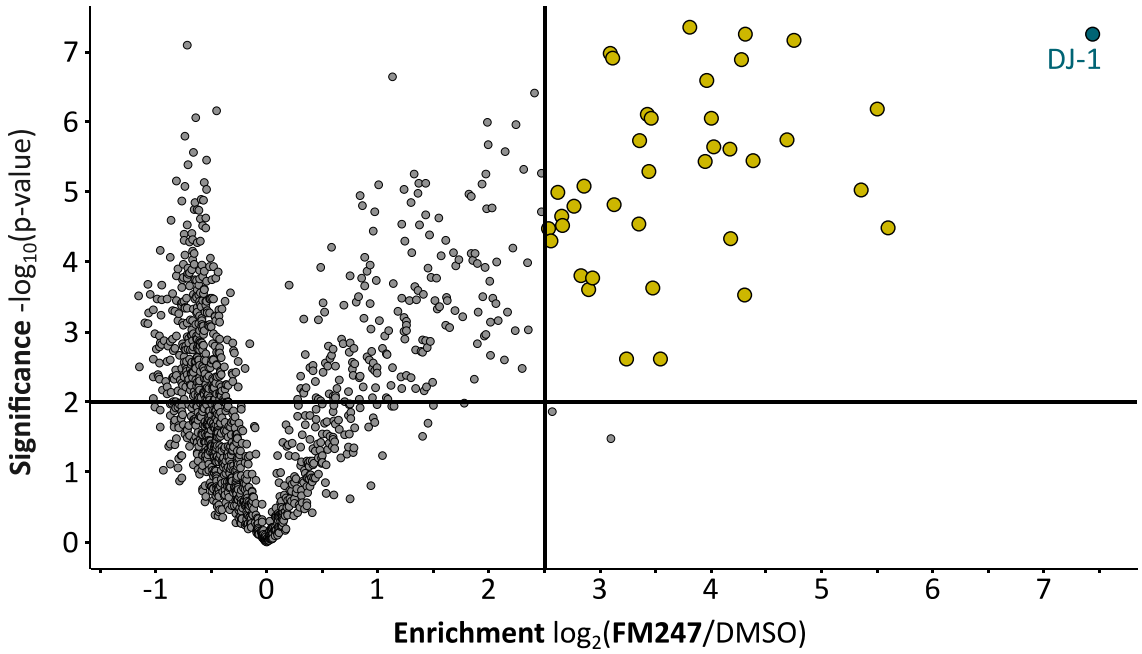

Figure 20: Results of the quantitative SILAC experiments using 10 µM **FM247** in the human cancer cell line HeLa. The volcano plot displays the statistical significance of protein enrichment levels as a function of protein enrichment ratios from probe-treated to control cells. Cut offs are at a $-\log_{10}$(p-value) of 2 and a t-test difference of 2.5.

most enriched target, demonstrating the desired high specificity for DJ-1 in complex proteomic samples. Additional, yet less enriched proteins, which are involved in diverse cellular functions such as cell redox homeostasis and protein folding, were detected as well (Table 1).

Table 1: Strongest enriched proteins using **FM247** in the human cancer cell line HeLa.

Protein name	Enrichment	Significance
	$\log_2$(**FM247**/DMSO)	-$\log_{10}$(p-value)
Protein deglycase DJ-1	7.41	7.21
Heme oxygenase 2	5.57	4.44
Protein disulfide-isomerase	5.47	6.14
Hydroxymethylglutaryl-CoA synthase, cytoplasmic	5.32	4.98
Voltage-dependent anion-selective channel protein 3	4.72	7.12
ERO1-like protein alpha	4.66	5.70
Thymidylate synthase	4.35	5.40
Thioredoxin domain-containing protein 5	4.28	7.21
OCIA domain-containing protein 1	4.28	3.48
Voltage-dependent anion-selective channel protein 2	4.25	6.85

2.7. Oxidative-stress Labelling – LFQ

As early onset Parkinsonism is associated with elevated ROS levels, the key to a successful diagnostic probe would be to differentiate between the redox states of DJ-1, as the protein in its cellular role is among the first to detect oxidative stress. Selectively targeting either thiol or sulfinic acid cysteine would allow to monitor changes of the cellular redox environment. With the proven selectivity for DJ-1 in complex proteomic samples, the final experiment was to test whether **FM247** is also able to detect different oxidation states of the enzyme *in situ*. For this, HeLa cells were treated with H_2O_2 at two concentrations and the extent of DJ-1 labelling by **FM247** was subsequently monitored via LC-MS/MS proteomic analysis and label-free quantification (Figure 21,A3). Satisfyingly, the

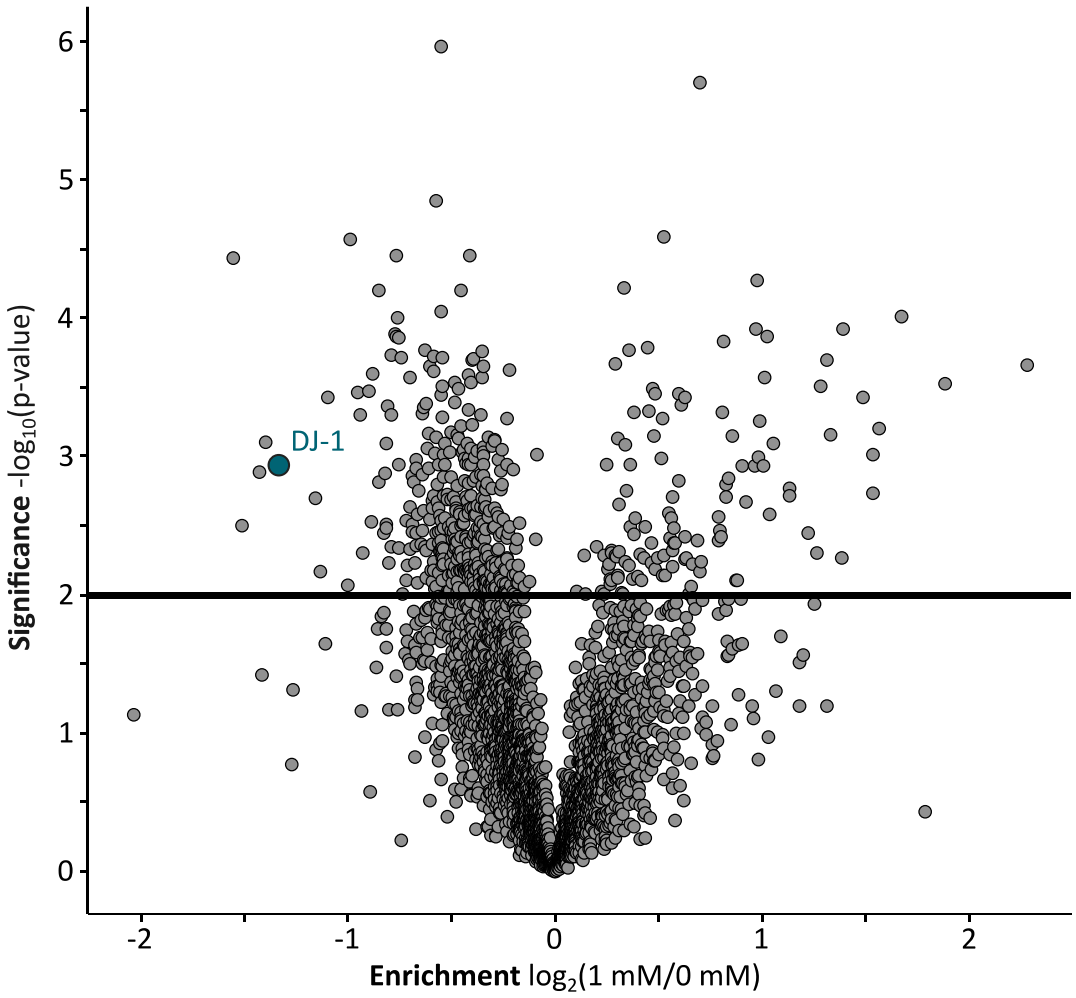

Figure 21: Results of the quantitative LFQ experiment showing the decrease of the DJ-1 labelling intensity after pre-incubation with 1 mM H_2O_2 using **FM247** in the human cancer cell line HeLa.

enrichment of DJ-1 strongly decreased upon these oxidative conditions by about 60%, speaking for a higher share of oxidized protein within the cell, which escapes detection.

3. Summary and Outlook

With increasing life expectancy, age-related ailments like Parkinson's disease (PD) are becoming a growing threat not only for the people directly affected, but also for the whole society as they represent a high burden for health care systems. As an early diagnosis often strongly benefits treatment or in some cases even prevents full outbreak of said diseases, great effort is put in the development of new diagnostic tools.

In the course of finding selective biomarkers, DJ-1 gained attention due to its link to early-onset PD and oxidative stress regulation. Although the function of the cysteine sensor is still enigmatic, probes that monitor its oxidation state might help to identify the disease in an early stage. Recently, several aminoepoxycyclohexenones (AECHs) were found to bind to bacterial members of the DJ-1 protein family. In this work, applying these results to a human cell setting enabled *in situ* profiling of DJ-1 and therefore opens new perspectives for selective studies of this protein. **FM247** not only binds and inhibits DJ-1 in protein assays, but also detects DJ-1 in complex proteomic samples while retaining its selectivity towards the reduced state of the enzyme. One could now think of using **FM247** in combination with a global oxidation probe to directly determine ratios of reduced vs. oxidized DJ-1. Such combined studies might be of particular importance for PD biomarker analysis. Furthermore, **FM247** and tools derived thereof are promising for imaging of DJ-1 in live cells to obtain direct information on cellular localization. Given the fact that siRNA-induced knockdown of DJ-1 showed promising results in combination with N-(4-hydroxyphenyl)retinamide for the treatment of cervical cancer, a thiol-selective DJ-1 inhibitor might also be of great interest in the field of chemosensitizers.[*88*] This study thus provides starting points for diagnostic applications as well as further medicinal developments.[*89*]

4. Experimental

4.1. Buffers

Table 2: Buffers for protein purification.

Buffer	Content
His Lysis Buffer	20 mM Tris/HCl 10 mM Imidazole 150 mM NaCl 2 mM β-Mercaptoethanol 0.2% (v/v) NP-40 pH 8.0 in ddH_2O
Washing Buffer 1 (WB1)	20 mM Tris/HCl 10 mM Imidazole 150 mM NaCl 2 mM β-Mercaptoethanol pH 8.0 in ddH_2O
Washing Buffer 2 (WB2)	20 mM Tris/HCl 10 mM Imidazole 1 M NaCl 2 mM β-Mercaptoethanol pH 8.0 in ddH_2O
Washing Buffer 3 (WB3)	20 mM Tris/HCl 40 mM Imidazole 150 mM NaCl 2 mM β-Mercaptoethanol pH 8.0 in ddH_2O
Elution Buffer (EB)	20 mM Tris/HCl 500 mM Imidazole 150 mM NaCl

	2 mM β-Mercaptoethanol (if used for esterase assay) or 2 mM DTT (if used for IP-MS) pH 8.0 in ddH_2O
DJ-1 storage buffer	PBS (pH 7.4) 1 mM DTT

Table 3: Proteomics buffers.

Buffer	Content
Lysis buffer	PBS (pH 7.4) 1% (v/v) NP40 1% (w/v) sodium deoxycholate
Gel loading buffer (2x)	126 mM Tris/HCl 20% (v/v) Glycerin 4% (w/v) SDS 0.005% (w/v) Bromophenol blue 10% (v/v) β-Mercaptoethanol in ddH_2O

4.2. Cell Culture

All cell lines and their respective media are shown in Table 4:

Table 4: Information on the used cell lines.

Cell line	Species	Cell type	Medium
HeLa	Homo Sapiens	Lung adenocarcinoma	DMEM
A549	Homo Sapiens	Cervix carcinoma	DMEM
SH-SY5Y	Homo Sapiens	Neuroblastoma	DMEM/F12

If not depicted otherwise, all media were supplemented with 10% (v/v) fetal bovine serum (FBS) and 2 mM glutamine.

For splitting and passaging, the medium was removed, and cells were washed with 10 mL of PBS. Afterwards the cells were incubated with 1 mL of Accutase® for 10 min at 37 °C until full detachment. Then, 10 mL of the respective medium were added, mixed thoroughly and 1 mL of this cell-solution was transferred into a new flask. The cell-solution was diluted with medium until a volume of 10 mL.

For preparation of isotopically labelled cells, cells were grown in the respective SILAC-medium (medium ≙ Lys-4, Arg-6; heavy ≙ Lys-8, Arg-10) and splitted at least eight times in advance of the experiment to ensure complete incorporation of labelled amino acids.

4.3. Protein Overexpression and Purification

DJ-1 wild type

For the recombinant expression of DJ-1, the Invitrogen™ Gateway™ cloning system (Thermo Scientific) was used. The following primers containing the required attB recombination sites and a TEV protease cleavage site were designed (for = forward, rev = reverse):

Table 5: Primers used in the recombinant expression of DJ-1.

Name	Design
For_attB1_TEV_DJ-1	5'-g ggg aca agt ttg tac aaa aaa gca ggc ttt gag aat ctt tat ttt cag ggc gct tcc aaa aga gct c-3'
Rev_attB2_DJ-1	5'-ggg gac cac ttt gta caa gaa agc tgg gtg cta gtc ttt aag aac aag t-3'

The polymerase chain reaction (PCR) was carried out in a CFX96 TM Real-time System in combination with a C1000 TM Thermal Cycler (BioRad). As template a human HeLa cell cDNA library (Bio Academia) was used. The reaction mixture contained 10 µL GC buffer (NEB), 1 µL dNTP (10 mM), 1.25 µL primer (fwd.), 1.25 µL primer (rev.), 1 µL cDNA (4 ng/ µL), 0.5 µL Phusion® High Fidelity DNA polymerase (NEB) and 35 µL ddH_2O. The

temperature program used for the PCR is shown in Table 6. The PCR products were purified by the MicroElute® Cycle-Pure Kit (OMEGA bio-tek) and finally the DNA concentration was measured on an Infinite M200 Pro NanoQuant multiplate reader (Tecan).

Table 6: Temperature program used in the PCR used for the expression of wild type DJ-1.

	Temperature [°C]	Time [min]
Initial denaturation	98	00:30
35 Cycles	98	00:10
	47	00:30
	72	00:10
Final elongation	72	07:00
	4	hold

In the BP-reaction the PCR-product is incorporated in the destination vector of choice. For this, 3 µL of the PCR-product (8-13 ng/µL), 3 µL of the vector pDONR™201 (50 ng/µL), 2 µL TE-buffer and 2 µL Gateway® BP Clonase® II enzyme mix (Invitrogen) were mixed and incubated for 20 h at RT. For transformation, the BP-solution was added to 200 µL of chemically competent *E. coli* TOP10 cells (Invitrogen) and incubated for 15 min on ice. After a 40 sec heat shock at 42 °C the cells were put on ice for another 5 min. Afterwards, the cells were grown for 1.5 h in 500 µL SOC-medium at 37 °C, plated on kanamycin LB agar plates and incubated at 37 °C overnight. Single colonies were picked and grown in 5 mL LB medium containing 5 µL kanamycin (25 mg/mL) for 15 h at 37 °C. The plasmid DNA from 2 mL of the cells was isolated using the E.Z.N.A.® Plasmid DNA Mini Kit I (OMEGA Bio-Tek) according to the manufacturer's protocol and the final DNA concentration was measured on an Infinite M200 Pro NanoQuant multiplate reader (Tecan). The success of the BP-reaction was verified by DNA sequencing done by GATC Biotech AG.

For the following LR-reaction 1 µL plasmid DNA (179 ng/µl), 1 µL expression vector pET300 (77 ng/µl), 6 µL TE-buffer and 2 µL Gateway® LR Clonase® II enzyme mix (Invitrogen) were mixed and incubated for 6 h at RT. The transformation in chemically competent *E. coli* Rosetta2 cells was done as already described in the BP-reaction. The cells were plated on

kanamycin-chloramphenicol LB agar plates and incubated at 37 °C overnight. Single colonies were picked and grown in 5 mL LB medium containing 5 µL kanamycin (25 mg/mL) and 5 µL chloramphenicol (34 mg/mL) for 15 h at 37 °C. The plasmid DNA from 2 mL of the cells was isolated using the E.Z.N.A.® Plasmid DNA Mini Kit I (OMEGA Bio-Tek) according to the manufacturer's protocol and the final DNA concentration was measured on an Infinite M200 Pro NanoQuant multiplate reader (Tecan). The success of the LR-reaction was verified by DNA sequencing done by the GATC Biotech AG.

To overexpress DJ-1 pET300-Rosetta2 cells were grown at 37 °C overnight in 20 mL LB medium containing 20 µL ampicillin (100 mg/mL). The next day, 10 mL of the overnight culture were transferred in 1 L LB medium containing 1 mL ampicillin (100 mg/mL) and grown at 37 °C to an OD_{600} of 0.6. Then, the gene expression was induced by the addition of 250 µL IPTG and the cells were grown for another 4 h at 37 °C. Afterwards the cells were harvested (6000 g, 4 °C, 30 min) and washed with PBS. Cells were then resuspended in 20 mL His-lysis buffer and lysed by sonication using the following protocol twice: 7 min at 30% intensity, 3 min at 80% intensity. Soluble and insoluble fractions were separated by centrifugation (18000 rpm, 4 °C, 30 min). For protein purification the soluble fraction was loaded on a 50 mL Superloop (GE Healthcare) and injected into an Äkta Purifier 10 System equipped with UV-detector (UPC900, P900, Box900, Frac950, GE Healthcare). The affinity chromatography was done using a His-Trap HP 5 mL column (GE Healthcare) which was equilibrated with WB1 (5 CV). After loading the proteins onto the column they were washed with WB1, WB2 and WB3 (8 CV each) and eluted with EB. The protein-containing fractions were pooled and dialysed in 2 L DJ-1 storage buffer overnight, aliquoted and stored at -80 °C.

DJ-1 C106A point mutation

The PCR for obtaining the DJ-1 C106A point mutation was carried out as shown above using 10 µL GC buffer (NEB), 1 µL dNTP (10 mM), 1 µL cDNA (50 ng/ µL, DJ-1 expression strain Rosetta2), 0.5 µL Phusion® High Fidelity DNA polymerase (NEB), 31.5 µL ddH2O, 0.5 µL DMSO, 1.25 µL primer (FW DJ-1 C106A) and 1.25 µL primer (REV DJ-1 C106A). Primers are detailed in Table 7.

Table 7: Primers used in the recombinant expression of DJ-1 C106A.

Name	Design
FW DJ-1 C106A	5’-ctg ata gcc gcc atc gct gca ggt cct act gc-3’
REV DJ-1 C106A	5’-gc agt agg acc tgc agc gat ggc ggc tat cag-3’

The temperature program used for the PCR is shown in Table 8

Table 8: Temperature program used in the PCR used for the expression of DJ-1 C106A.

	Temperature [°C]	Time [min]
Initial denaturation	98	03:00
35 Cycles	98	00:45
	65	00:30
	72	03:00
Final elongation	72	07:00
	4	hold

4.4. Esterase Assay

Inhibition assay

The enzyme-catalysed hydrolysis reaction of *p*-nitrophenyl acetate (pNPA) to acetic acid and *p*-nitrophenol (pNP) was photometrically determined at 410 nm. Due to the instability of pNPA in aqueous solution, the auto-hydrolysis of the substrate in PBS without enzyme was additionally monitored as control. DJ-1 (1 µM) was pre-incubated for 30 min at 25 °C with either DMSO or probe (1 - 20 µM, DMSO stock, final DMSO concentration per well ≤ 1%) in PBS. The enzyme mixture was then transferred into a 96-well plate (200 µL per well) after which the substrate (pNPA, 6 mM in DMSO, 40 µL) was added via an on-board injector. The reaction was monitored at 410 nm and 25 °C using an Infinite M200 Pro multiplate reader (Tecan). Calculations were performed using Graphpad Prism 6.

Kinetic assay

The substrate (pNPA, 6 mM in DMSO, 40 µL) and varying concentrations of inhibitor (2.4 µL of a 100x stock in DMSO) were dissolved in 187.6 µL of PBS. 10 µL of DJ-1 (final concentration 1 µM) was added and the increase in fluorescence was followed as described above. For control samples, pure DMSO was used. Evaluation of the recorded curves and fitting was carried out with Graphpad Prism 6. Kinetic constants were obtained from fitting the curves to

$$F(t) = F_0 + A(1 - e^{-K_{obs}t})$$

wherein F(t) denotes the fluorescence time course, F_0 denotes the initial fluorescence, A denotes the slope of the uninhibited control samples and K_{obs} denotes the rate constants. This model implies the reactions to follow pseudo-first-order kinetics as the concentration of the inhibitor was generally larger than five times the enzyme concentration. K_{obs}/I-values were obtained from linear regression of the rate constants plotted over the inhibitor concentration for the linear interval to enable comparison of inhibitors with different potencies.

4.5. Intact Protein Mass Spectrometry

DJ-1 was incubated with 10 eq. of the respective probe at RT for 30 min. For kinetic studies the samples were measured at various time points after addition of probe. For measurements of the oxidized DJ-1-SO_2H the protein was treated with 2 mM H_2O_2 for 30 min on ice before adding the probe. Samples were analyzed on a LTQ FT Ultra™ mass spectrometer (Thermo Scientific) equipped with electro spray ionization (ESI) source operated in positive ionization mode, coupled to a Dionex Ultimate 3000 HPLC system (Thermo Scientific). 1 µL of protein solution (1 µM) was applied to a protein desalting column, eluted with an acetonitrile gradient and passed to the MS unit. Intact protein spectra were analyzed and deconvoluted using the Thermo Xcalibur software (Thermo Scientific).

4.6. Thermal Shift Assay

Thermal denaturation temperatures of DJ-1 were measured via thermal shift assay, performed with a CFX96 Real-time System in combination with a C1000 Thermal Cycler (BioRad). SYPRO Orange (Sigma) was added to the PBS (1:1000) containing DJ-1 at a concentration of 5 µM. In case any inhibitor was added in various concentrations, the total amount of DMSO per well was at most 1%. A control containing the protein and DMSO was included. After vortexing, 50 µL of each sample were pipetted in a 96-well PCR plate. Measurements were performed in triplicates.

4.7. Gel-based ABPP

Analytical labelling in A549

A549 cells were seeded in 6 well plates and allowed to grow to 80 - 90% confluence. After removing the growth medium, 1 mL PBS containing 1 µL of the respective compound (DMSO stock in various concentrations) was added. The cells were incubated for 1 h at 37 °C in a 5% CO_2 atmosphere, afterwards scraped of the dish, pelletized (800 g, 3 min, 4 °C), subsequently washed with 1 mL PBS and pelletized again (800 g, 3 min, 4 °C). For lysis, cells were resuspended in 100 µL lysis buffer, incubated for 15 min on ice and insoluble fragments were separated by centrifugation (max. rpm, 45 min, 4 °C). The supernatant was subjected to click reaction by adding 2 µL rhodamine azide (10 mM in DMSO), 2 µL tris(2-carboxyethyl)phosphine (TCEP) (52 mM in ddH_2O), 6 µL tris(benzyltriazolylmethyl)amine (1 × TBTA) ligand and 2 µL $CuSO_4$ (50 mM in ddH_2O) and incubated for 1 h at RT. After adding 100 µL of gel loading buffer, the samples were stored at −20 °C or directly loaded on a SDS-gel.

Labelling of recombinant DJ-1 in A549 lysate

A549 cells were lysed as described above. The lysate was adjusted to a final protein concentration of 1 mg/mL with lysis buffer. Afterwards 1 µL of DJ-1 in various concentrations was added to 98 µL of lysate and each sample treated with 10 µM **FM247** for 1 h at RT. The samples were then subjected to click reaction as described above and stored at −20 °C or directly loaded on a SDS-gel.

Labelling in the expression strain Rosetta2

For analytical in situ labelling in the expression strain DJ-1-pET300-Rosetta2, 100 mL of LB media containing 100 µL ampicillin (100 mg/mL) were inoculated with 1 mL of an overnight culture and incubated at 37 °C and 200 rpm until an OD_{600} of 0.6. Then, protein expression was induced by the addition of 25 µL IPTG and the cells were grown for another 4 h at 37 °C. Afterwards, cells were harvested (6000 g, 4 °C, 30 min), washed with PBS and resuspended in PBS to a theoretical OD_{600} of 40. 200 µL of the bacterial suspension were then incubated with 2 µL of **FM247** in DMSO in varying concentrations for 1 h at room temperature. A DMSO control containing no probe was additionally added to each experiment. After centrifugation (10 min, 4 °C, 6000 rpm), the bacterial cells were washed with 800 µL PBS and lysed in 100 µL PBS by sonication (3 × 20 sec, 85% max. intensity, on ice). Insoluble fragments were separated by centrifugation (max. rpm, 45 min, 4 °C). The supernatant was subjected to click reaction by adding 2 µL rhodamine azide (10 mM in DMSO), 2 µL TCEP (52 mM in ddH_2O), 6 µL 1 × TBTA-ligand and 2 µL $CuSO_4$ (50 mM in ddH_2O) and incubated for 1 h at RT. After adding 100 µL of gel loading buffer, samples were stored at −20 °C or directly loaded on a SDS-gel.

Labelling of recombinant DJ-1

For labelling of recombinant DJ-1 (wt and C106A) 100 µL of the protein in PBS (1 µM) were incubated with 1 µL of probe in varying concentrations for 1 h at RT. The heat control (h.c.) was boiled at 95 °C for 5 min prior to addition of the probe. In the case of oxidation dependent labelling the protein was incubated with 2 mM H_2O_2 for 30 min on ice before adding the probe. Afterwards the samples were subjected to click reaction by adding 2 µL rhodamine azide (10 mM in DMSO), 2 µL TCEP (52 mM in ddH_2O), 6 µL 1 × TBTA-ligand and 2 µL $CuSO_4$ (50 mM in ddH_2O) and incubated for 1 h at RT. After adding 100 µL of gel loading buffer, samples were stored at −20 °C or directly loaded on a SDS-gel.

4.8. Gel-free ABPP

SILAC

Cells were grown in the respective SILAC-medium and splitted at least eight times in advance of the experiment to ensure complete incorporation of heavy amino acids. Cells were plated on a 15 cm dish and grown to 80 - 90% confluence. After washing the cells with 10 mL PBS, 10 mL PBS containing either 100 µL of compound (DMSO-stock) or 100 µL DMSO as control were added to a pair of heavy and medium cells and *vice versa* for label-switch. The cells were incubated for 1 h at 37 °C in a 5% CO_2 atmosphere. Then, the cells were scraped of the dish, subsequently pelletized (800 g, 3 min, 4 °C), washed with 10 mL PBS and pelletized again (800 g, 3 min, 4 °C). For lysis, the cells were resuspended in 1 mL lysis buffer and incubated for 15 min on ice. After resuspending cell fragments by sonication, the protein concentration of each sample was determined by BCA assay and equal protein amounts of heavy or medium cells were pooled. The total volume was then adjusted to 1880 µL with PBS and the samples were further subjected to the following click reaction by adding 40 µL Biotin-PEG_3-N_3 (10 mM in DMSO), 20 µL TCEP (52 mM in ddH_2O), 60 µL 1 × TBTA ligand and 20 µL $CuSO_4$ (50 mM in ddH_2O). After incubation for 1 h at RT the proteins were precipitated by adding 8 mL of cold acetone and incubation overnight at -20 °C. After centrifugation (≥13000 rpm, 15 min, 4 °C) the pellet was washed twice with 200 µL cold methanol (-80 °C) and the proteins were resuspended in 500 µL PBS + 0.4% SDS (v/v) by sonication at RT. For enrichment the protein solution was added to 50 µL pre-washed avidin-agarose beads suspension (1.1 mg/mL in glycerol, washed three times with 1 mL PBS + 0.4% SDS) and incubated for 1 h under continuous gentle mixing. To remove unbound proteins, the beads were washed three times with 1 mL PBS + 0.4% SDS, two times with urea (6 M in ddH_2O) and three times with 1 mL PBS. Afterwards, the beads were carefully resuspended in 200 µL capping-buffer (7 M urea, 2 M thiourea in 20 mM HEPES). Reduction was performed by adding 0.2 µL dithiothreitol (DTT) (1 M in ddH_2O) and shaking the reaction mixture (450 rpm) for 45 min at RT. On addition of 2 µL iodoacetamide (IAA) (550 mM in ddH_2O) the proteins were alkylated for 30 min under continuous shaking (450 rpm) at RT and exclusion of light. The reaction was stopped by adding 0.8 µL DTT (1 M in ddH_2O) and incubation for 30 min at RT. To digest

the proteins 1 µL endoproteinase Lys-C (LysC) (1 M in ddH_2O) was added to each sample and incubated for 2.5 h at RT under continuous shaking (450 rpm) and exclusion of light. Afterwards 600 µL, tetraethylammonium bromide (TEAB) (50 mM in ddH_2O) and 1.5 µL trypsin (0.5 µg/µL in ddH_2O) were added and the samples were incubated overnight at 37 °C under continuous shaking (450 rpm). The digestion was stopped by adding 8 µL formic acid (FA) and the suspension was then centrifuged (13000 rpm, 3 min, RT) to pelletize the beads. The supernatant was loaded on 50 mg SepPak C 18 columns (Waters) equilibrated with 0.1% trifluoroacetic acid (TFA). The peptides were washed three times with 1 mL 0.1% TFA and 250 µL 0.5% FA. Afterwards, the peptides were eluted three times with 250 µL elution buffer (80% acetonitrile (ACN), 0.5% FA), lyophilized and stored at -80 °C until further usage.

LFQ

HeLa cells were plated on a 15 cm dish and grown to 80-90% confluence. After washing the cells with 10 mL PBS, 10 mL DMEM containing various concentrations H_2O_2 (final concentrations: 0/1/2 mM) were added and the cells were incubated for 1 h at 37 °C in a 5% CO2 atmosphere. Afterwards the cells were washed again with 10 mL PBS, treated with 10 mL PBS containing **FM247** (final concentration 10 µM) and incubated for 1 h at 37 °C in a 5% CO_2 atmosphere. Then, the cells were scraped of the dish, subsequently pelletized (800 g, 3 min, 4 °C), washed with 10 mL PBS and pelletized again (800 g, 3 min, 4 °C). For lysis, the cells were resuspended in 1 mL lysis buffer and incubated for 15 min on ice. After resuspending cell fragments by sonication, the protein concentration of each sample was determined by BCA assay and the samples were adjusted to the same protein concentration using PBS. Further sample handling was performed as described for SILAC experiments.

Site-ID

For site identification experiments, 4.5 µg DJ-1 were incubated with three-fold molar excess of **FM247** for 1.5 h at RT. Afterwards, free probe was removed by centrifugal filters (vivaspin, 10 kDa, 15000 g, 10 min) and the protein washed twice with capping buffer (7 M

urea, 2 M thiourea in 20 mM HEPES). Reduction and alkylation was performed as described above. Excess DTT and IAA were removed by centrifugal filters (vivaspin, 10 kDa, 15000 g, 10 min) and the protein washed twice with NH_4HCO_3 buffer (25 mM). Subsequently, $CaCl_2$ (final concentration 10 mM) and 1 µL chymotrypsin (0.5 µg/µL) were added and proteins incubated at 25 °C and 450 rpm over night. Further sample handling was performed as described under for SILAC experiments.

LC-MS/MS

Before MS measurements the lyophilized peptides were resolved in 30 µL 1% FA and filtered through centrifugal filters (0.45 µm, VWR), which were equilibrated with 300 µL 1% FA. The filtrate was transferred into MS-vials and stored at -20 °C until the measurements were performed.

LTQ Orbitrap XL (A549)

Samples were analysed on a LTQ Orbitrap XL™ mass spectrometer (Thermo Scientific) equipped with electro spray ionization (ESI) source operated in positive ionization mode coupled to a Dionex Ultimate 3000 HPLC system (Thermo Scientific). The samples were loaded on an Acclaim C18 PepMap100 (75 µm ID × 2 cm) trap column at a flow rate of 5 µL/min for 10 min in 0.1% FA and separated on an Acclaim C18 PepMap RSLC (75 µm ID × 30 cm) separation column. Eluent A consisted of water with 0.1% (v/v) FA and 5% (v/v) DMSO in water (LC/MS grade), eluent B consisted of 0.1% (v/v) FA and 5% (v/v) DMSO in acetonitrile (LC/MS grade). Peptides were separated by applying a gradient ranging from 4% B to 35% B over 102 min at a flow of 200 nL/min. The mass spectrometer was operated in data dependent mode. Full scans were acquired in the orbitrap at R = 60000 from m/z = 350 - 1400. The five most intense peaks were selected for collision induced fragmentation (CID) and analysed in the ion trap at normal scan rate (isolation width: 2 ppm; activation time: 30 ms; normalized collision energy: 35; minimum signal threshold: 1000 counts; dynamic exclusion duration: 120 s).

Q Exactive Plus (HeLa)

Samples were analysed with an UltiMate 3000 nano HPLC system (Dionex) using an Acclaim C18 PepMap100 (75 µm ID × 2 cm) trap column and an Acclaim PepMap RSLC C18 (75 µm ID × 50 cm) separation column coupled to a Q Exactive Plus (Thermo Fisher) in EASY-spray setting. Samples were loaded on the trap column and washed with 0.1% TFA, then transferred to the analytical column (buffer A: H_2O with 0.1% FA, buffer B: ACN with 0.1% FA, flow 300 nL/min, gradient 5 to 22% buffer B in 115 min, then to 32% buffer B in 10 min, then to 90% buffer B in 10 min and hold 90% buffer B for 10 min, then to 5% buffer B in 0.1 min and hold 5% buffer B for 9.9 min). Q Exactive Plus was operated in a TOP12 data dependent mode. Full scan acquisition was performed in the orbitrap at a resolution of 70000 and an AGC target of $3e^6$ in a scan range of 300−1500 m/z. Monoisotopic precursor selection as well as dynamic exclusion (exclusion duration: 60 s) was enabled. Precursors with charge states of >1 and intensities greater than $1e^5$ were selected for fragmentation. Isolation was performed in the quadrupole using a window of 1.6 m/z. Precursors were collected to an AGC target of $5e^4$ for a maximum injection time of 50 ms. Fragments were generated using higher-energy collisional dissociation (HCD, normalized collision energy: 27%) and detected in the orbitrap.

Orbitrap Fusion (SH-SY5Y)

Nanoflow LC-MS/MS analysis was performed with an UltiMate 3000 Nano HPLC system (Thermo Scientific) coupled to an Orbitrap Fusion (Thermo Scientific). Peptides were loaded on a trap column (Acclaim C18 PepMap100 75 µm ID × 2 cm) and washed for 10 min with 0.1% FA and 5% DMSO (10 µL/min flow rate), then transferred to an analytical column (Acclaim C18 PepMap RSLC, 75 µM ID × 15 cm) and separated using a 125 min gradient from 3% to 40% (120 min from 3% to 25% and 5 min to 40%) ACN in 0.1% FA and 5% DMSO at a flow rate of 200 nL/min. Peptides were ionized using a nanospray source at 1.9 kV and a capillary temperature of 275 °C. Orbitrap Fusion was operated in a top speed data dependent mode with a cycle time of 3 s. Full scan acquisition (scan range of 300 – 1700 m/z) was performed in the orbitrap at a resolution of 120000 (at m/z 200) and with an automatic gain control ion target value of $4e^5$. Monoisotopic precursor selection

as well as dynamic exclusion of 60 s were enabled. Internal calibration was performed using the ion signal of fluoranthene cations (EASY-ETD/IC source). Most intense precursors with charge states of 2 - 7 and intensities greater than $5e^3$ were selected for fragmentation. Isolation was performed in the quadrupole using a window of 1.6 m/z. Ions were collected to a target of $1e^2$ for a maximum injection time of 250 ms with "inject ions for all available parallelizable time" enabled. Fragments were generated using higher-energy collisional dissociation (HCD) and detected in the ion trap at a rapid scan rate.

Data evaluation

MS data analysis

Raw files were analysed using MaxQuant software (version 1.5.3.8 or higher) with the Andromeda search engine.[30] The following settings were applied: fixed modification: carbamidomethylation (cysteine); variable modification: oxidation (methionine), acetylation (N-terminus), NH (aspartate) and in the case of Side-ID experiments **FM247** (cysteine); proteolytic enzyme: trypsin/P; missed cleavages: 2; main search tolerance: 4.5 ppm; MS/MS tolerance: 0.5 Da; false discovery rates: 0.01. The options "requantification", "second peptide identification" and "match between runs" (0.7 min match and 20 min alignment time windows) were enabled. Quantification of SILAC pairs was carried out based on unique peptides only using "Arg6" and "Lys4" as "light" and "Arg10" and "Lys8" as "heavy" isotope identifiers requiring a minimum ratio count of 2. For raw files resulting from label switched experiments, the isotope identifiers were defined in reverse order resulting in the ratios of probe vs. DMSO. For label-free quantification the corresponding parameter was set to "LFQ". Searches were performed against the Uniprot database for Homo sapiens. Statistical analysis of the data was performed using Perseus (version 1.5.3.2. or higher).[90] SILAC ratios were $\log_2$ -transformed and $-\log_{10}$ (p-values) were obtained by a two-sided one sample Student's t-test. LFQ intensities were $\log_2$-transformed and $-\log_{10}$ (p-values) were obtained by a two-sided two sample Student's t-test.

GO-analysis

GO term enrichment analysis for the "biological process" branch was performed using the BiNGO plugin for Cytoscape.[91,92] Proteins that were at least significantly 2-fold up- or down-regulated were subjected to a hypergeometric test to decipher overrepresented GO categories. In order to construct a reference set, all GO annotations of Homo sapiens were collected using QuickGO (https://www.ebi.ac.uk/QuickGO/, 29th November 2017). The ontology go.obo was downloaded from http://geneontology.org (29th November 2017). The derived p-values were corrected for multiple testing by the method of Benjamini and Hochberg with a significance level of $p = 0.05$.

III. Tranylcypromine Specificity for Monoamine Oxidase is Limited by Promiscuous Protein Labelling and Lysosomal Trapping

1. Introduction

Mental and behavioural disorders had the second biggest share of Germanys total costs of illness in 2017 with 44.4 billion euro, which indicates the great desire for improved diagnostics and treatments in this field.[93] However, medicinal research on these conditions has proven to be particularly frustrating, as diagnosis can be ambiguous.[94] A classic, and still effective, treatment of a variety of mental illnesses, such as depression or anxiety disorders, is to modulate the patient's neurotransmitter and neuromodulator levels using psychoactive drugs. One way of achieving this, is to inhibit a family of proteins called monoamine oxidases (MAOs), which includes two types: MAOA and MAOB.

The main cellular function of these enzymes is to oxidize neurotransmitters that bear a primary amine e.g. dopamine or serotonin into the corresponding aldehyde (Figure 22). For this reaction, MAO uses FAD as cofactor, which is covalently bound through a histidine residue. By limiting natural metabolism, MAO inhibitors (MAOIs) are used to artificially elevate neurotransmitter levels.[95,96] MAOIs come in different forms of selectivity towards MAOA or MAOB but can also be pigeonholed by their binding mode as being either reversible or irreversible (Figure 23). First introduced in the 1950s, were inhibitors like tranylcypromine, pargyline and phenelzine, which bind covalently to the FAD-cofactor of MAO.[97–100] These drugs showed to be highly effective in the treatment of depression, but their severe side effects and interactions with other drugs led to them nearly vanishing from the marked and being replaced by reversible MAOIs with better overall tolerance. Only tranylcypromine experienced a revival in prescription rates for its good results in severe cases of anxiety disorders, when other treatments fail, and because recent studies showed its potential use in the therapy of Parkinson's disease and cancer.[101–104]

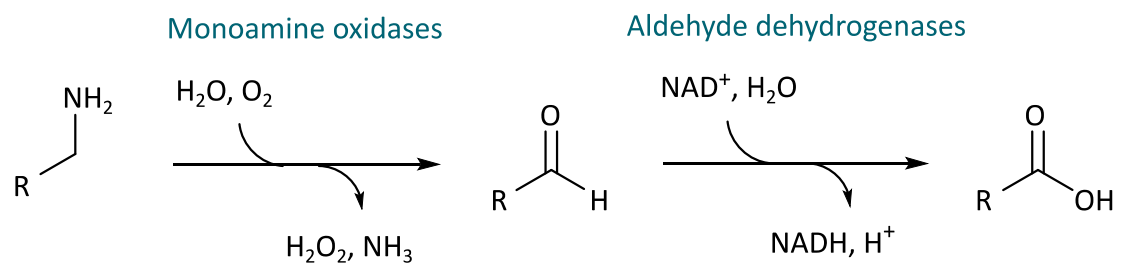

Figure 22: General depiction of intra cellular metabolism of primary amines. Monoamine oxidases catalyse the conversion to the corresponding aldehyde, followed by aldehyde dehydrogenase mediated carboxylic acid generation.

Irreversible

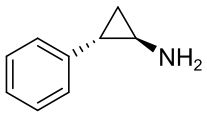

Tranylcypromine
Condition: Depression

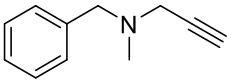

Pargyline
Condition: Hypertension

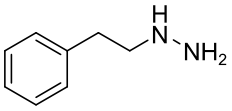

Phenelzine
Condition: Depression

Reversible

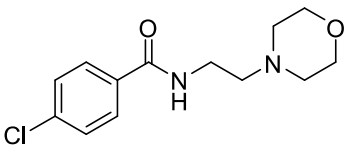

Chlorgiline
Condition: Depression

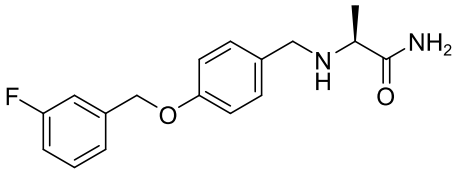

Safinamide
Condition: Parkinson's Disease

Figure 23: Structures of irreversible and reversible MAO inhibitors and their primary field of use.

Despite being marketed for so long, global proteomic studies on the cellular targets of tranylcypromine were still missing, so the aim of this work was to synthesize suitable probes to elucidate the off-target profiles as well as their cellular localization. The results were to be compared to a previously established probe based on pargyline, another covalent MAOI.[*105*]

2. Results and Discussion

2.1. Probe Synthesis

When designing an ABPP probe, certain aspects need to be considered. The probe has to show the same binding profile as the parent molecule, so functional groups responsible for target specificity cannot be altered. The probe should also show a comparable cellular uptake and distribution and should not be metabolized within the experiment's timeframe. A functional group that has proven to fulfil these requirements is the terminal alkyne. It is small, biorthogonal and allows efficient detection *via* click chemistry. In the case of a small molecule like tranylcypromine, one is not left with many design options. The cyclopropylamine is crucial for binding and therefore best left untouched in a first approach, leaving the phenyl ring as the only reasonable modification point. Previous work showed that derivatives at the *para*-position of cyclopropylamine can even increase the potency of the inhibitor.[106] As the probe was to be compared to an established pargyline probe **FBP1,** an analogous probe design was used. The synthesis was initiated

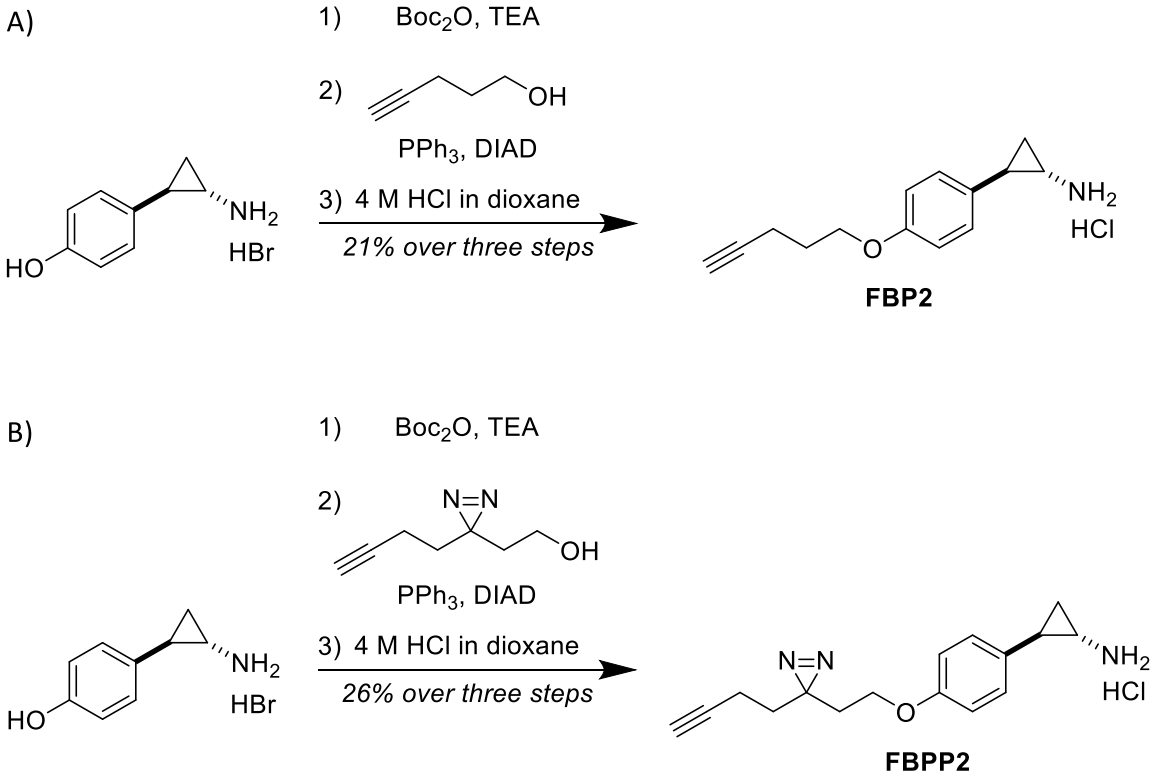

Scheme 1: Synthesis of tranylcypromine-derived flavin binding probe (**FBP2**) and flavin binding photo-probe (**FBPP2**).

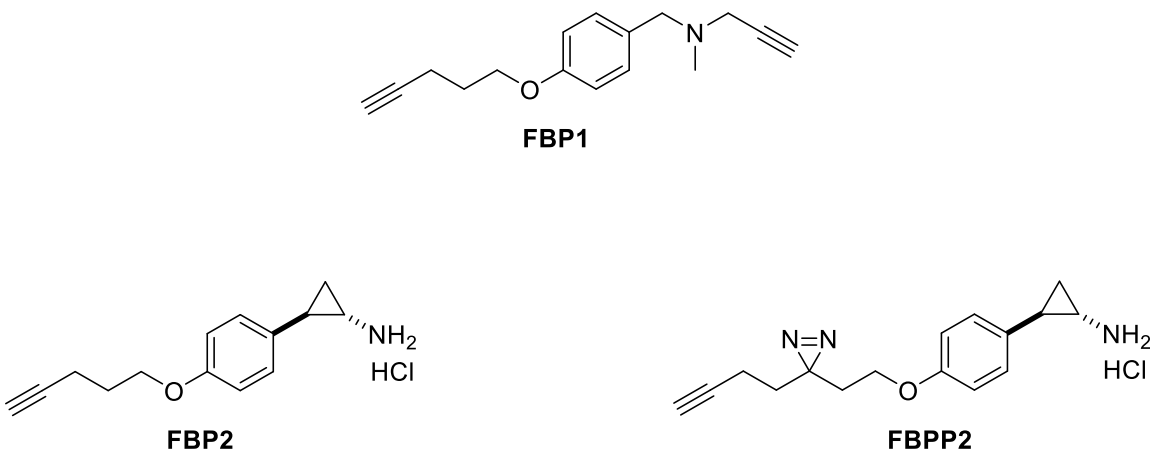

Figure 24: Compounds used for proteomic studies on pargyline (**FBP1**) and tranylcypromine (**FBP2** and **FBPP2**).

by amine protection of (*trans*)-2-(4-hydroxyphenyl)cyclopropanamine followed by *Mitsunobu* reaction and acidic deprotection to give **FBP2** with an overall yield of 21%. To complement the analysis with the detection of putative reversible binders, probe **FBPP2** was synthesized bearing a diazirine photocrosslinker moiety *via* a similar synthetic strategy.[*105*]

2.2. Target Identification - LFQ

After the successful syntheses, an ABPP approach was used to determine the covalent protein targets of both **FBP1** and **FBP2** in human cancer cells. In order to get a broad overview, two cell lines were selected - SH-SY5Y due to its widespread use as a model cell

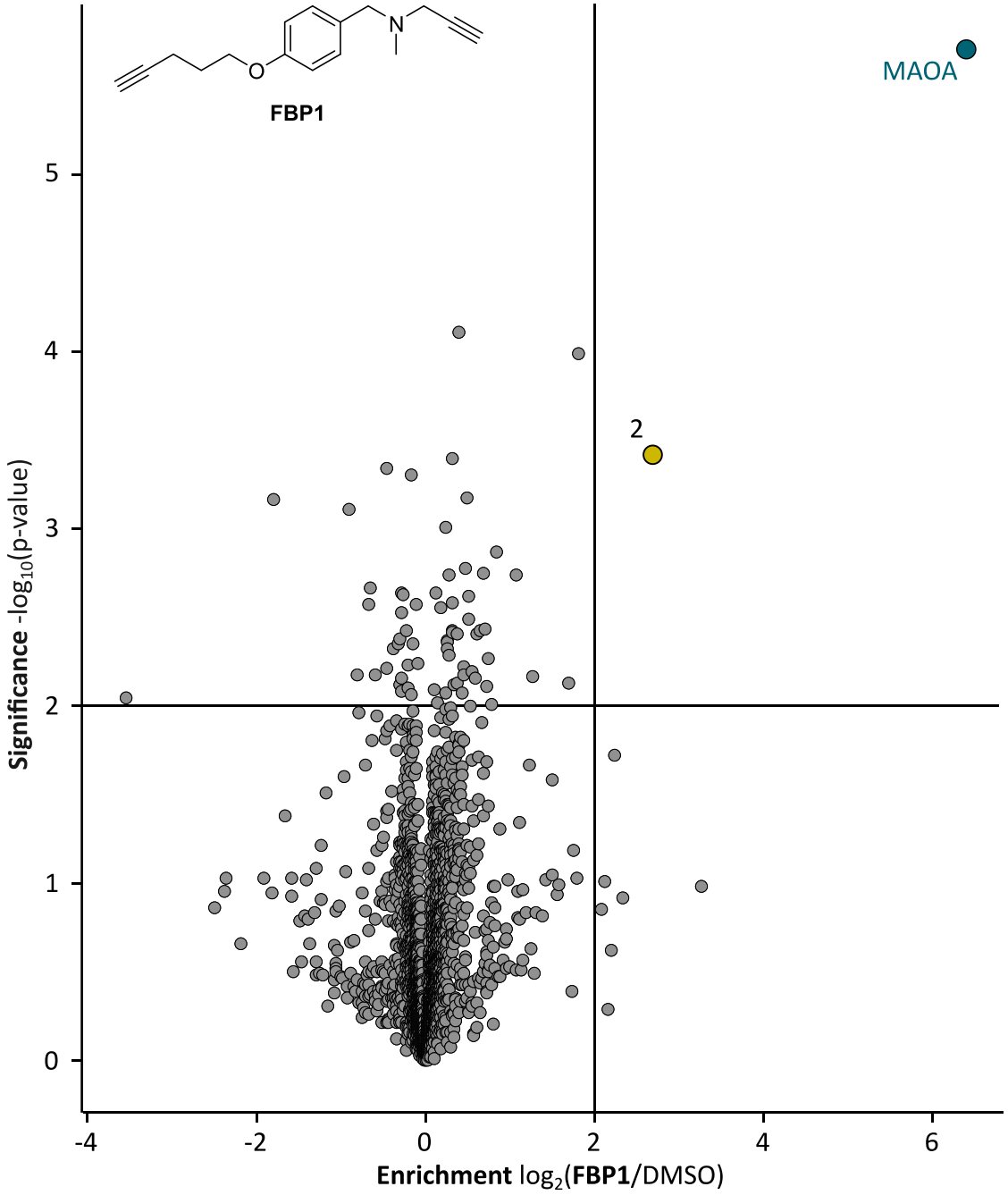

Figure 25: Result of target enrichment experiment using **FBP1** in the human cancer cell line SH-SY5Y with 100 µM probe concentration. The scatter plot shows statistical significance of protein enrichment levels over protein enrichment ratios from probe treated to control cells. Cut offs are at a p-value < 0.01 and 4-fold enrichment over DMSO (indicated by solid lines). Proteins within these set criteria are highlighted in yellow and described in more detail in the corresponding Table 9. MAOA is highlighted in turquoise.

line for studying neuronal function and neurodegenerative disorders like Parkinson's disease, and HeLa as being the best characterized cell line overall.[107] Cells were treated

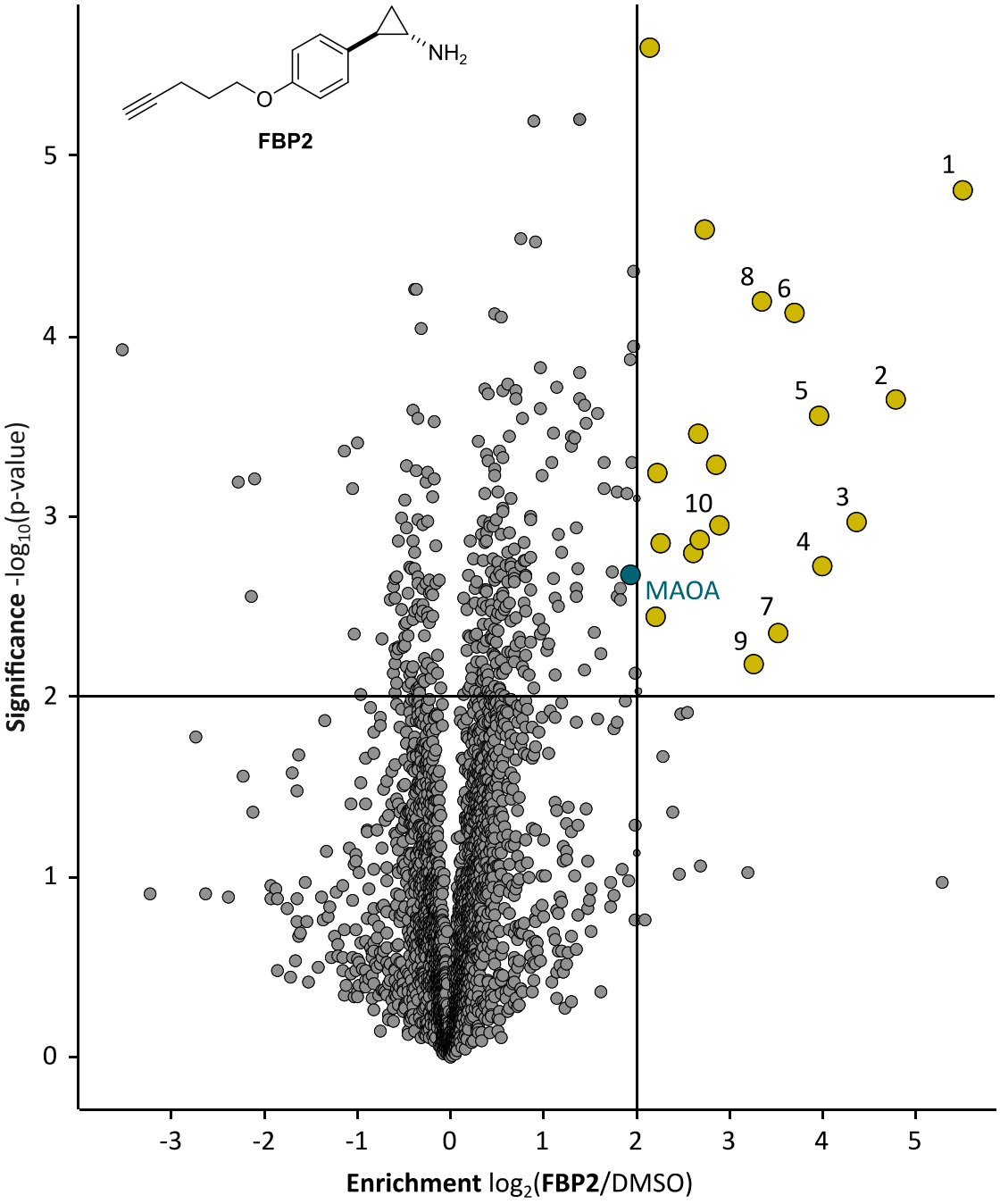

Figure 26: Result of target enrichment experiment using **FBP2** in the human cancer cell line SH-SY5Y with 100 µM probe concentration. The scatter plot shows statistical significance of protein enrichment levels over protein enrichment ratios from probe treated to control cells. Cut offs are at a p-value < 0.01 and 4-fold enrichment over DMSO (indicated by solid lines). Proteins within these set criteria are highlighted in yellow and described in more detail in the corresponding Table 10. MAOA is highlighted in turquoise

Table 9: Covalent protein targets of **FBP1**

Nr.	Gene name	Enrichment $\log_2$(**FBP1**/DMSO)	Significance $-\log_{10}$(p-value)
1	MAOA	6.34	5.69
2	ALDH1B1	2.63	3.39

with 100 µM of either probe for 1 h, followed by biotin-avidin-enrichment and further processing for quantitative LC-MS/MS analysis. In SH-SY5Y cells, pargyline probe **FBP1** revealed MAOA as the major target with an 81 fold enrichment over DMSO treated cells, followed by only one other significantly enriched protein, ALDH1B1, within the set criteria (Figure 25). Comparable results were seen in HeLa cells, with MAOA also being the major target followed by few off-targets including ALDH1B1 (Figure A4, Table 9). When labelling with the tranylcypromine derived probe FBP2, the resulting volcano plot demonstrated MAOA with a comparatively low 3.6 fold enrichment in SH-SY5Y cells (Figure 26). Additionally, the probe revealed rather promiscuous labelling to multiple off-targets, including ALDHs, heme oxygenase 2 and cathepsin L1, in both tested cell lines (Figure A5, Table 10). Strikingly, while the known target MAOB was among the top hits of **FBP1** in HeLa cells, no enrichment could be observed in SH-SY5Y. **FBP2** in contrast did not reveal any MAOB enrichment in either cell line.

To demonstrate that the targets found by an ABPP-probe reflect the binding of a parent molecule, competitive labelling experiments are used in which cells are pre-treated with the respective drug followed by probe incubation. As the target proteins are already blocked for probe binding, this should lead to significantly lower enrichment. So in order to validate drug targets, one needs to look for proteins enriched when labelling with just the probe, but absent in competition experiments. Following this strategy for both tranylcypromine and pargyline, MAOA and several off-targets including ALDHs and cathepsin L1 were outcompeted in either cell line, validating them as true off-targets

Table 10: Covalent protein targets of **FBP2**.

Nr.	Gene name	Enrichment log_2(**FBP2**/DMSO)	Significance $-log_{10}$(p-value)
1	HMOX2	5.41	4.77
2	PTGES2	4.70	3.61
3	CYB5B	4.27	2.92
4	PNPLA4	3.91	2.69
5	ALDH1A3	3.88	3.52
6	CALM3	3.62	4.09
7	C16orf58	3.44	2.31
8	ALDH1B1	3.27	4.15
9	ABHD6	3.18	2.14
10	BANF1	2.80	2.91
…	…	…	…
30	MAOA	1.83	2.60

(Figure A6-9). Again, **FBP2** revealed binding to more proteins than **FBP1**, proving its higher promiscuity throughout the cell lines.

With a panel of putative off-targets in hand, recombinant HMOX2 and ALDH2, two representative proteins, were overexpressed. In a gel-based approach, probe binding to

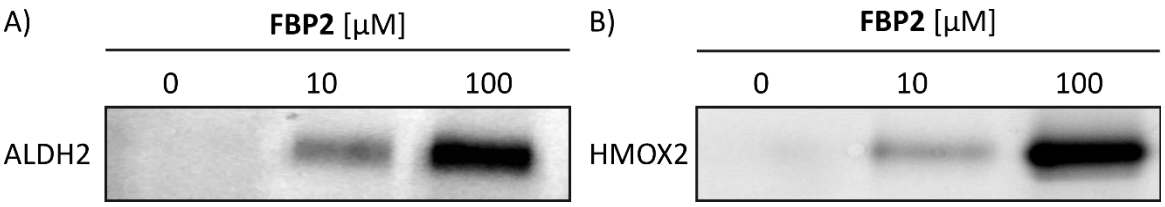

Figure 27: A) Labelling recombinant ALDH2 with various equivalents of **FBP2** led to concentration dependent modification of the protein. B) Labelling recombinant HMOX2 with various equivalents of **FBP2** led to concentration dependent modification of the protein.

the proteins was confirmed in a concentration dependent manner (Figure 27); however, no reduction of their activity upon compound treatment was observed. This suggests that at least for these proteins, inhibition seems not to be the main consequence of drug binding. Nevertheless, it cannot be excluded that alteration of protein pathways by impaired protein-protein interactions contribute to a global cellular dysregulation. To further stress this point, non-covalent targets were included into the scope of this project by performing affinity-based protein profiling (AfBPP) experiments using the photoprobe **FBPP2**.

2.3. Affinity-based Protein Profiling

The use of photo-reactive crosslinkers, allows covalent binding of a probe to its non-covalent target proteins. In the case of **FBPP2**, irradiation of the diazirine moiety with UV-light generates a reactive carbene, which subsequently inserts into protein C-H groups in close proximity.[108] As covalent target identification results couldn't completely explain the known side-effect profile of tranylcypromine, labelling of SH-SY5Y cell with **FBPP2** was performed to gain further insight (Figure 28). After incubation with 10 µM probe for 1 h,

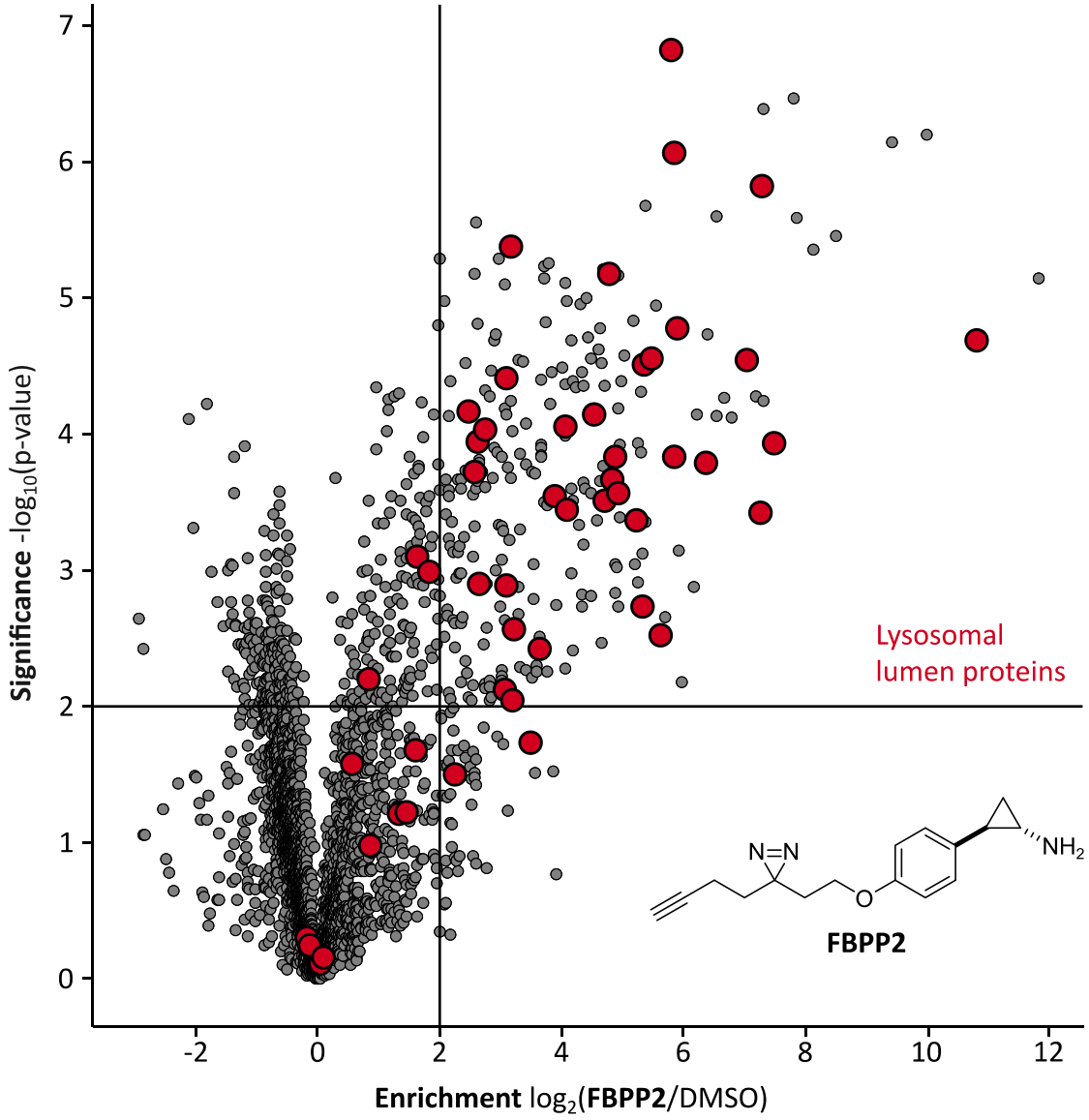

Figure 28: Results of the photo-affinity labelling experiment in SH-SY5Y cells using **FBPP2**. The scatter plot shows statistical significance of protein enrichment levels over protein enrichment ratios from probe treated to control cells. Cut offs are at a p-value < 0.01 and 4-fold enrichment over DMSO (indicated by solid lines). Proteins annotated to be located in the lysosomal lumen (GO:0043202) are highlighted in red.

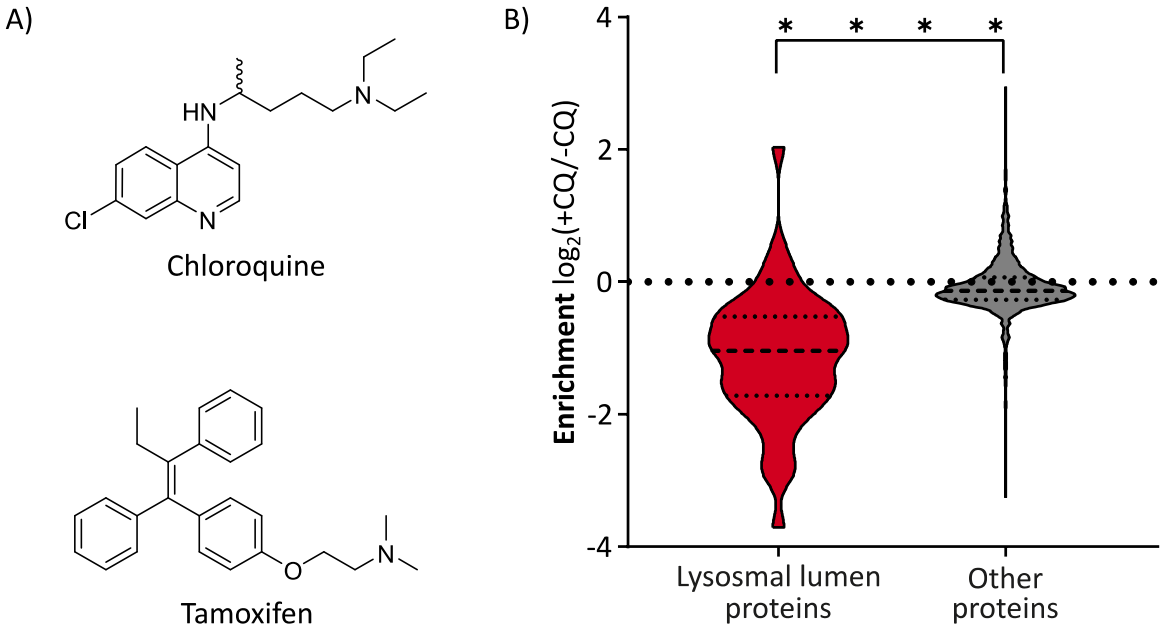

Figure 29: A) Structures of the two lysosomotropic compounds chloroquine (CQ) and tamoxifen. B) Violin plot demonstrating the significant decrease of lysosomal lumen protein enrichment when incubating the cells with chloroquine (CQ) prior to **FBPP2** treatment (****P<0.0001, two-tailed unpaired *t*-test).

cells were irradiated for 10 min, followed by the enrichment workflow performed for covalent target identification. Sample analysis by LC-MS/MS revealed even more putative hit proteins for **FBPP2** compared to **FBP2,** with a strong prevalence of lysosomal targets. This indicates that, in line with the primary amino functionality, the compound is trapped in acidic organelles and physically interacts with binding partners in this compartment.[*109,110*] In the cytosol, tranylcypromine is mostly in its neutral amine form, allowing it to freely pass through membranes. Upon entering the lysosomes, the pH changes to 4-5 shifting the equilibrium towards the ammonium cation. This charged form is repelled by the organelle membrane, leading to high accumulation in lysosomes. As the therapeutic MAO targets are located in mitochondria, lysosomal trapping for tranylcypromine lowers the effective dose at the cellular compartment of interest.

Lysosomotropic agents, such as chloroquine (CQ) and tamoxifen, are known to increase lysosomal pH and can therefore be used to release compounds from acidic organelles (Figure 29A).[*111*] To explore the possibility of manipulating trapping of **FBPP2**, photo-affinity labelling was repeated with cells that were either pre-treated with CQ or DMSO. This effect should allow a higher fraction of tranylcypromine to remain unprotonated and thereby untrapped. The results of this experiment nicely showed a very significant

decrease of **FBPP2** binding to proteins annotated to be located in the lysosomal lumen (Figure 29B). As the mean enrichment of all other proteins remained nearly unaltered, it emphasised the strong interaction of tranylcypromine with lysosomal proteins.

In conclusion, a combination of activity and affinity-based proteomic workflows was able to demonstrate the off-target reactivity of tranylcypromine. This is largely due to lysosomal trapping of the drug.

2.4. Fluorescence Imaging

Following up on the results obtained by MS-based proteomics, visualization of these findings was performed using fluorescence microscopy. For this, SH-SY5Y cells were treated with **FBP2** at 100 µM and subsequently fixed, permeabilized and clicked to rhodamine-azide. When detecting the fluorophores emission in comparison to an organelle specific marker, it allows the identification of possible co-localization. In accordance to the previous results, **FBP2** showed predominant localization in the

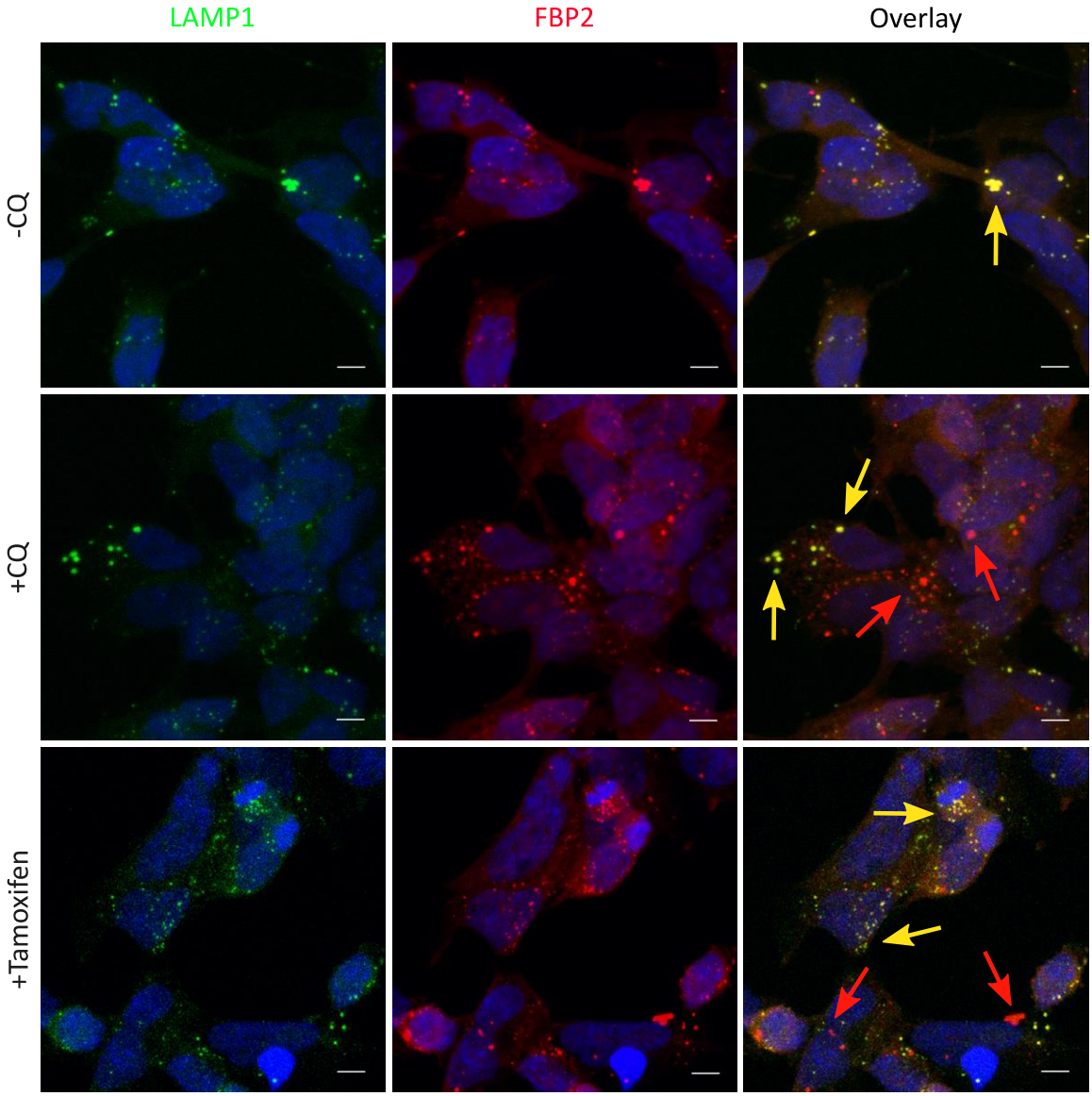

Figure 30: Fluorescence imaging with LAMP1 (green) and **FBP2** clicked to rhodamine-azide (red) in fixed SH-SY5Y cells. The top panel shows strong colocalization (yellow) between lysosomes and probe. The middle panel displays release of the probe from lysosomes by pre-treatment of cells with chloroquine (CQ). The colocalization between lysosomes and probe is also diminished by pre-treatment of cells with tamoxifen as seen in the bottom panel. (scale bar: 5 µm).

lysosome (Figure 30). Again, the next step was to visualise the release of the probe by lysosomotropic compounds. Satisfyingly, when pre-treating the cells with either chloroquine or tamoxifen, a clear release of the tranylcypromine probe from the lysosomes was detectable.

3. Summary and Outlook

Due to its unique binding mechanism to monoamine oxidases and use in various diseases, tranylcypromine has been subject to extensive scientific research, yet many aspects of this compound, like side effects or drug-drug-interactions remain hitherto unknown. The aim of this study, was to utilize modern LC MS/MS technology, in order to find reversible and irreversible protein targets of tranylcypromine. Synthesis of a novel ABPP-probe, allowed for quantitative proteomic experiments, which showed tranylcypromine, in contrast to pargyline, irreversibly binds to many off-target proteins. Additionally, by using a photoprobe as well as fluorescence imaging, strong lysosomal trapping of the compound was proven. A release of the drug was accomplished by addition of the lysosomotropic compounds chloroquine and tamoxifen.

Co-administration of therapeutic doses of chloroquine and tranylcypromine is known to cause severe side effects and research in this direction was therefore brought to a halt. As these new results show a release of tranylcypromine from the lysosome, it could become a starting point for new studies, looking into the possible use of lysosomotropic drugs to decrease tranylcypromine dosage.

4. Experimental

4.1. Probe Synthesis

General remarks

All air- or water-sensitive reactions were carried out under argon atmosphere in oven-dried glassware. Chemicals and solvents were purchased from Labseeker, Kumidas SA, Sigma-Aldrich, Alfa Aesar, Acros Organics, TCI Europe and Merck, were of reagent grade or higher and were used without further purification. In all reactions, temperatures were measured externally. Solvents removed under reduced pressure were evaporated at 40 °C. Flash column chromatography was performed on silica gel (40-63 µm) by VWR, elution solvents were distilled prior to use. Analytical thin-layer chromatography was carried out on aluminium-baked TLC Silica gel plates by Merck. Components were visualized by UV detection (254 nm, 312 nm) or stained *via* aqueous $KMnO_4$ or aqueous cerium molybdate (Hanessian's stain). ^{1}H-NMR and ^{13}C spectra of small molecules were recorded on Bruker instruments (300 MHz, 400 MHz or 500 MHz) and referenced to the residual proton signal of the deuterated solvent. ($CDCl_3$, DMSO-d6). Multiplets are described using following abbreviations: s - singlet, d - doublet, t - triplet, q - quartet, and m - multiplet. HR-MS-ESI spectra were recorded with a Thermo Scientific LTQ FT Ultra.

tert-Butyl (trans-2-(4-hydroxyphenyl)cyclopropyl)carbamate (1)

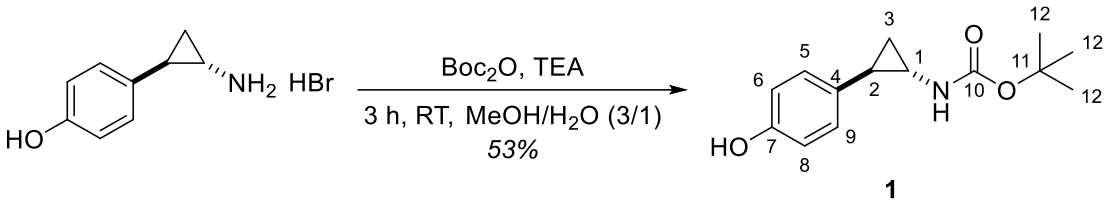

1

To a solution of 100 mg of *trans*-2-(4-hydroxyphenyl)cyclopropanamine hydrobromide (435 µmol, 1.0 eq.) and 150 µL of di-*tert*-butyl dicarbonate (142 mg, 652 µmol, 1.5 eq.) in 8 mL of MeOH/H_2O (3:1) were added 181 µL of Et_3N (132 mg, 1.30 mmol, 3.0 eq.) and stirred for 3 h at RT. The reaction mixture was diluted with EtOAc and extracted with H_2O. The organic layer was dried over Na_2SO_4 and the solvent removed under reduced pressure. The crude product was purified by flash chromatography to yield 57.0 mg of **1** (229 µmol, 53%) as a yellow oil.

HRMS (ESI): m/z calcd. for $C_{14}H_{19}NO_3$+H^+: 250.1443 $[M+H]^+$; found 250.1438.

^{1}H-NMR (300 MHz, $CDCl_3$) δ [ppm] = 6.90 (d, ^3J = 8.1 Hz, 2H, H5/9), 6.69 (d, ^3J = 8.1 Hz, 2H, H6/8), 4.97 (s, 1H, NH), 2.72 – 2.57 (m, 1H, H1), 1.96 (ddd, ^3J = 9.5, 6.6, 3.2 Hz, 1H, H2), 1.46 (s, 9H, H12), 1.11 – 0.99 (m, 2H, H3).

^{13}C-NMR (75 MHz, $CDCl_3$) δ [ppm] = 157.1, 154.8, 131.9, 127.7, 115.4, 80.3, 32.3, 28.6, 25.3, 15.8.

The analytical data obtained match those reported in the literature.[*112*]

tert-Butyl (trans-2-(4-(pent-4-yn-1-yloxy)phenyl)cyclopropyl)carbamate (2)

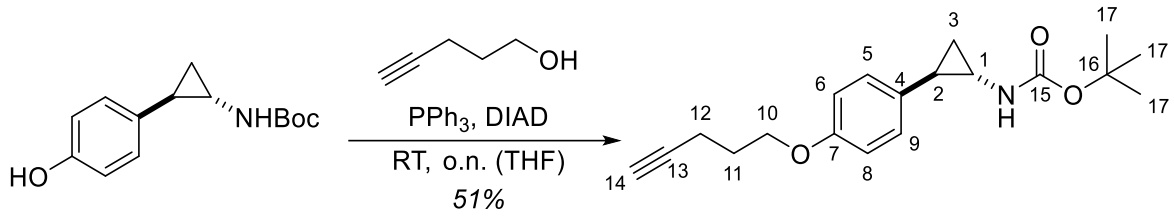

1 **2**

To a solution of 55.0 mg of **1** (221 µmol, 1.0 eq.) in 1.5 mL of dry THF were added 69.5 mg of triphenylphosphane (265 µmol, 1.2 eq.), 52.0 µL of diisopropyl azodicarboxylate (DIAD) (53.6 mg, 265 µmol, 1.2 eq.) and 24.7 µL of 4-pentyn-1-ol (22.3 mg, 265 µmol, 1.2 eq.). The reaction was stirred over night at RT. Afterwards, the solvent was removed under reduced pressure. The crude product was purified by flash chromatography to yield 35.8 mg of **2** (114 µmol, 51%) as a light yellow solid.

HRMS (ESI): m/z calcd. for $C_{38}H_{50}N_2O_6+H^+$: 631.3747 $[2M+H]^+$; found 631.3738.

^{1}H-NMR (500 MHz, $CDCl_3$) δ [ppm] = 7.06 (d, ^3J = 8.1 Hz, 2H, H5/9), 6.80 (d, ^3J = 8.1 Hz, 2H, H6/8), 4.86 (s, 1H, NH), 4.02 (t, ^3J = 6.1 Hz, 2H, H10), 2.69 – 2.56 (m, 1H, H1), 2.39 (td, ^3J = 7.0 Hz, ^4J = 2.7 Hz, 2H, H12), 2.02 – 1.91 (m, 4H, H2/11/14), 1.45 (s, 9H, H17), 1.12 – 1.01 (m, 2H, H3).

^{13}C-NMR (101 MHz, $CDCl_3$) δ [ppm] = 157.4, 132.9, 127.9, 114.6, 83.6, 68.9, 66.4, 60.5, 28.5, 28.3, 21.2, 16.0, 15.3, 14.3.

trans-2-(4-(Pent-4-yn-1-yloxy)phenyl)cyclopropan-1-amine hydrochloride (FBP2)

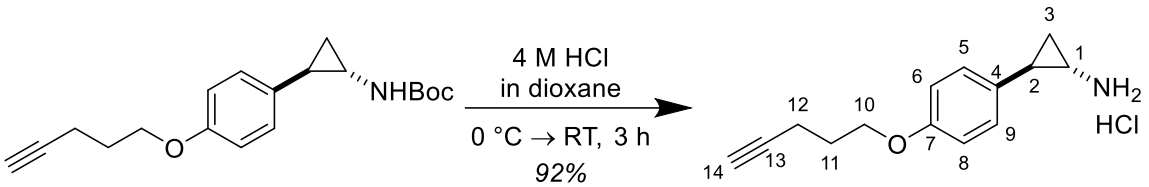

2 **FBP2**

35.8 mg of **2** (114 µmol, 1.0 eq.) were cooled to 0 °C. Then, 1.0 mL of 4 M HCl in dioxane was added. The reaction was stirred for 2.5 h at 0 °C followed by another 30 min at RT. The solvent was removed under reduced pressure to give 26.4 mg of **FBP2** (105 µmol, 92%) as a white solid.

HRMS (ESI): m/z calcd. for $C_{14}H_{17}NO+H^+$: 216.1388 $[M+H]^+$; found 216.1382.

^{1}H-NMR (500 MHz, MeOD) δ [ppm] = 7.09 (d, ^3J = 8.5 Hz, 2H, H5/9), 6.86 (d, ^3J = 8.5 Hz, 2H, H6/8), 4.03 (t, ^3J = 6.1 Hz, 2H, H10), 2.78 – 2.73 (m, 1H, H1), 2.39 – 2.30 (m, 3H, H2/12), 2.24 (t, ^4J = 2.7 Hz, 1H, H14), 1.94 (tt, ^3J = 6.6, 6.6 Hz, 2H, H11), 1.37 (ddd, ^2J = 10.4 Hz, ^3J = 6.5, 4.2 Hz, 1H, H3'), 1.26 – 1.22 (m, 1H, H3'').

^{13}C-NMR (101 MHz, MeOD) δ [ppm] = 159.4, 131.7, 128.6, 115.7, 84.1, 70.0, 67.4, 31.8, 29.5, 21.9, 15.7, 13.4.

trans-2-(4-(2-(3-(But-3-yn-1-yl)-3H-diazirin-3-yl)ethoxy)phenyl)cyclopropan-1-amine hydrochloride (FBPP2)

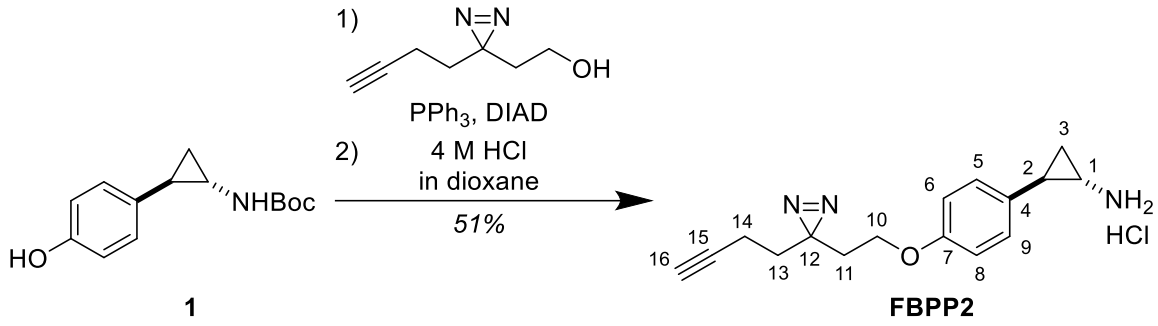

To a solution of 57.0 mg of **1** (229 µmol, 1.0 eq.) in 2.0 mL of dry THF were added 72.0 mg of triphenylphosphane (274 µmol, 1.2 eq.), 53.9 µL of DIAD (55.5 mg, 274 µmol, 1.2 eq.) and 37.9 mg of 2-(3-but-3-ynyl-3*H*-diazirin-3-yl)-ethanol (274 µmol, 1.2 eq.). The reaction was stirred for 4 h at RT. Afterwards, the solvent was removed under reduced pressure. The residue was purified by flash chromatography, intermediate containing fractions were pooled, the solvent evaporated under reduced pressure, and the residue taken up in 1.0 mL 4 M HCl in 1,4-dioxane. The resulting precipitate was filtered and dried in high vacuum to yield 33.0 mg of **FBPP2** (108 µmol, 47%) as an orange solid.

HRMS (ESI): m/z calcd. for $C_{16}H_{19}N_3O+H^+$: 270.1606 $[M+H]^+$; found 270.1603.

^{1}H-NMR (300 MHz, MeOD) δ [ppm] = 7.10 (d, ^3J = 8.6 Hz, 2H, H5/9), 6.86 (d, ^3J = 8.6 Hz, 2H, H6/8), 3.82 (t, ^3J = 6.1 Hz, 2H, H10), 3.35 (s, 1H, NH), 2.76 (dt, ^3J = 7.8, 4.0 Hz, 1H, H1), 2.33 (ddd, ^3J = 10.2, 6.6, 3.5 Hz, 1H, H2), 2.26 (t, ^4J = 2.6 Hz, 1H, H16), 2.06 (td, $^{3/4}J$ = 7.4, 2.6 Hz, 2H, H14), 1.85 (t, ^3J = 6.1 Hz, 2H, H11), 1.67 (t, ^3J = 7.4 Hz, 2H, H13), 1.41 – 1.22 (m, 2H, H3).

^{13}C-NMR (75 MHz, MeOD) δ [ppm] = 159.0, 131.9, 128.7, 115.8, 83.7, 70.3, 63.9, 33.9, 33.8, 31.8, 27.8, 22.0, 13.8, 13.4.

4.2. Cell Culture

SH-SY5Y cells were grown in DMEM/F12 medium, HeLa cells in DMEM medium. All media were supplemented with 10% (v/v) FBS and 2 mM glutamine. For splitting, the medium was removed, and cells were washed with 10 mL of PBS. Afterwards, the cells were incubated with 1 mL of Accutase® for 10 min at 37 °C until full detachment. Then, 10 mL of the respective medium were added, mixed thoroughly and 1 mL of this cell-solution was transferred into a new flask. The cell-solution was diluted with medium to a volume of 10 mL.

4.3. Labelling of Recombinant Proteins

ALDH2 and HMOX2(1-264) were purified as described previously.[113,114] For labelling of recombinant proteins 100 µL protein solution in PBS (1 µM) were incubated with 1 µL of **FBP2** (10 and 100 eq., DMSO-stock) for 1 h at RT. Afterwards, the samples were subjected to click reaction by adding 2 µL rhodamine azide (10 mM in DMSO), 2 µL tris(2-carboxyethyl)phosphine (TCEP) (52 mM in ddH_2O), 6 µL tris(benzyltriazolyl-methyl)amine (1 × TBTA) ligand (1.67 mM) and 2 µL $CuSO_4$ (50 mM in ddH_2O) and incubating for 1 h at RT. After adding 100 µL of gel loading buffer, the samples were stored at −20 °C or directly loaded on a SDS-gel.

4.4. Gel-Free ABPP

Target Identification

SH-SY5Y or HeLa cells were plated on a 15 cm dish and grown to 80-90% confluence. The cells were washed with 10 mL PBS and treated with 10 mL PBS containing the respective probe **FBP1/2** (final concentration 100 µM) and incubated for 1 h at 37 °C in a 5% CO_2 atmosphere. For control experiments, cells were treated with DMSO. Then, the cells were scraped off the dish, subsequently pelletized (800 g, 3 min, 4 °C), washed with 10 mL PBS and pelletized again (800 g, 3 min, 4 °C). For lysis, the cells were resuspended in 1 mL lysis buffer (1% NP40 (v/v), 1% sodium deoxycholate (w/v) in PBS) and incubated for 15 min on ice, followed by mild sonication (10% intensity, 15 sec on ice). Protein concentration of each sample was determined by BCA assay and samples were adjusted to the same

protein concentration using PBS. The total volume was then adjusted to 1880 µL with PBS and the samples were further subjected to the following click reaction by adding 40 µL Biotin-PEG3-N_3 (10 mM in DMSO), 20 µL TCEP (52 mM in ddH_2O), 60 µL 1 × TBTA ligand (1.67 mM) and 20 µL $CuSO_4$ (50 mM in ddH_2O). After incubation for 1 h at RT, the proteins were precipitated by adding 8 mL of cold acetone and incubation overnight at -20 °C. After centrifugation (≥13000 rpm, 15 min, 4 °C) the pellet was washed twice with 200 µL cold methanol (-80 °C) and the proteins were resuspended in 500 µL PBS + 0.4% SDS (v/v) by sonication at RT. For enrichment, the protein solution was added to 50 µL pre-washed avidin-agarose bead suspension (1.1 mg/mL in glycerol, washed three times with 1 mL PBS + 0.4% SDS) and incubated for 1 h under continuous gentle mixing. To remove unbound proteins, the beads were washed three times with 1 mL PBS + 0.4% SDS, two times with urea (6 M in ddH_2O) and three times with 1 mL PBS. Afterwards, the beads were carefully resuspended in 200 µL capping buffer (7 M urea, 2 M thiourea in 20 mM HEPES). Reduction was performed by adding 0.2 µL dithiothreitol (DTT) (1 M in ddH_2O) and shaking the reaction mixture (450 rpm) for 45 min at RT. On addition of 2 µL iodoacetamide (IAA) (550 mM in ddH_2O) the proteins were alkylated for 30 min under continuous shaking (450 rpm) at RT and exclusion of light. The reaction was stopped by adding 0.8 µL DTT (1 M in ddH_2O) and incubation for 30 min at RT. To digest the proteins, 1 µL of endoproteinase Lys-C (LysC) (1 M in ddH_2O) was added to each sample and incubated for 2 h at RT under continuous shaking (450 rpm) and exclusion of light. Afterwards, 600 µL of tetraethylammonium bromide (TEAB) (50 mM in ddH_2O) and 1.5 µL of Trypsin (0.5 µg/µL in ddH_2O) were added and the samples were incubated overnight at 37 °C under continuous shaking (450 rpm). The digestion was stopped by adding 8 µL formic acid (FA) and the suspension was then centrifuged (13000 rpm, 3 min, RT) to pelletize the beads. The supernatant was loaded on 50 mg SepPak C 18 columns (Waters) equilibrated with 0.1% trifluoroacetic acid (TFA). The peptides were washed three times with 1 mL 0.1% TFA and 250 µL 0.5% FA. Afterwards, the peptides were eluted three times with 250 µL elution buffer (80% acetonitrile (ACN), 0.5% FA), lyophilized and stored at -80 °C until further usage.

Competition Experiments

For competition experiments, cells were pre-treated with tenfold excess of parent drug (pargyline in case of **FBP1,** tranylcypromine in case of **FBP2)** for 1 h prior to probe treatment. Further sample handling was done as described for target identification.

Photo-Affinity Labelling

SH-SY5Y cells were plated on a 15 cm dish and grown to 80-90% confluence. The cells were washed with 10 mL PBS and treated with 10 mL PBS containing **FBPP2** (final concentration 10 µM) and incubated for 1 h at 37 °C in a 5% CO_2 atmosphere. For control experiments, cells were treated with DMSO. In case of chloroquine pre-treatment, cells were treated with twofold excess of drug for 1 h prior to adding the probe. Afterwards, cells were irradiated with UV light (365 nm, 2 × 5 min at 0 °C, *Philips* TL-DBLB18W) to induce photo-crosslinking. Further sample handling was done as described for target identification.

LC-MS/MS

Before MS measurements, the lyophilized peptides were resolved in 30 µL 1% FA and filtered through centrifugal filters (0.45 µm, VWR), which were equilibrated with 300 µL 1% FA. The filtrate was transferred into MS-vials and stored at -20 °C until the measurements were performed.

Samples were analysed with an UltiMate 3000 nano HPLC system (Dionex) using an Acclaim C18 PepMap100 (75 µm ID × 2 cm) trap and an Aurora Series Emitter Column with Gen2 nanoZero fitting (75 µm ID × 25 cm, 1.6 µm FSC C18) separation columns (both heated to 40 °C) in an EASY-spray setting coupled to a Q Exactive Plus mass spectrometer (ThermoFisher). 1-10 µL of peptide samples were loaded on the trap and washed with 0.1% TFA, then transferred to the analytical column (buffer A: H_2O with 0.1% FA, buffer B: MeCN with 0.1% FA, flow 0.4 µL/min, gradient: 5% buffer B for 7 min, from 5% to 22% buffer B in 105 min, then to 32% buffer B in 10 min, to 90% buffer B in 10 min and hold at 90% buffer B for 10 min, then to 5% buffer B in 0.1 min and hold 5% buffer B for 9.9 min) and ionized at spray voltage of 2.0 kV and a capillary temperature of 275 °C. The Q Exactive Plus mass spectrometer was operated in a TOP12 data dependent mode with

full scan acquisition in the orbitrap at a resolution of R = 140,000 and an AGC target of $3e^6$ in a scan range of 300 – 1500 m/z with a maximum injection time of 80 ms. Monoisotopic precursor selection as well as dynamic exclusion (dynamic exclusion duration: 60 s) was enabled. Precursors with charge states >1 and intensities greater than $1e^4$ were selected for fragmentation. Isolation was performed in the quadrupole using a window of 1.6 m/z. Precursors were analysed in a scan range of 200 – 2000 m/z to an AGC target of $1e^5$ and a maximum injection time of 100 ms. Peptide fragments were generated by higher-energy collisional dissociation (HCD) with a normalized collision energy of 27% and detected in the orbitrap.

Data Evaluation

Raw files were analysed using MaxQuant software (version 1.6.2.10).[30] The following settings were applied: fixed modification: carbamidomethylation (cysteine); variable modification: oxidation (methionine), acetylation (N-terminus), NH (aspartate); proteolytic enzyme: trypsin/P; missed cleavages: 2; main search tolerance: 4.5 ppm; MS/MS tolerance: 0.5 Da; false discovery rates: 0.01. The options "LFQ" and "match between runs" (0.7 min match and 20 min alignment time windows) were enabled.[38] Searches were performed against the Uniprot database for Homo sapiens. Statistical analysis of the data was performed using Perseus (version 1.6.2.3.).[90] Putative contaminants, reverse peptides and peptides only identified by site were deleted. Data was filtered for three valid values in at least one group and a missing value imputation was performed over the total matrix. LFQ intensities were $\log_2$-transformed and $-\log_{10}$ (p-values) were obtained by a two-sided two sample Student's t-test.

4.5. Immunofluorescence Imaging

SH-SY5Y cells were cultured on glass coverslips and treated at 80% confluency with **FBP2** directly or following treatment with chloroquine or tamoxifen. In detail, cells were treated for 1 h with culture medium (DMEM/F12GlutaMAX supplemented with 10% FBS and 1:100 Antibiotic-Antimycotic) containing 20 µM of chloroquine or tamoxifen at 37 °C and 5% CO_2. Then, fresh medium was added to the cells containing 100 µM **FBP2** and cells

were incubated for additional 1 h at 37 °C and 5% CO_2. For control experiments, cells were treated with DMSO. For click chemistry and immunofluorescence, cells were fixed with 4% PFA at 4 °C and were permeabilized using 0.3% Triton X100 in 1x PBS for 5 min at RT. Cells were then incubated with click-chemistry staining mix (10 µM rhodamine-azide, 1 mM $CuSO_4$, 10 mM freshly prepared sodium ascorbate in 1x PBS) at RT for 2 h in the dark, followed by three washes with 1x PBS. Cells were subsequently blocked with 0.1% TWEEN, 10% Normal Goat Serum and 3% BSA diluted in 1x PBS.[115] Primary and secondary antibodies were diluted in blocking solution. Nuclei were visualized using 0.5 µg/mL 4,6-diamidino-2-phenylindole (DAPI, Sigma Aldrich). The antibodies used were mouse anti-LAMP1 1:50 (abcam ab25630) and goat anti-mouse Alexa Fluor 488 1:1000 (ThermoFisher Scientific, A28175). Immunostained cells were analysed using Leica SP8 confocal microscope. Different fields were taken using 63x objectives. Digital images were processed using Image J and Adobe Photoshop software.

4.6. NMR-Spectra

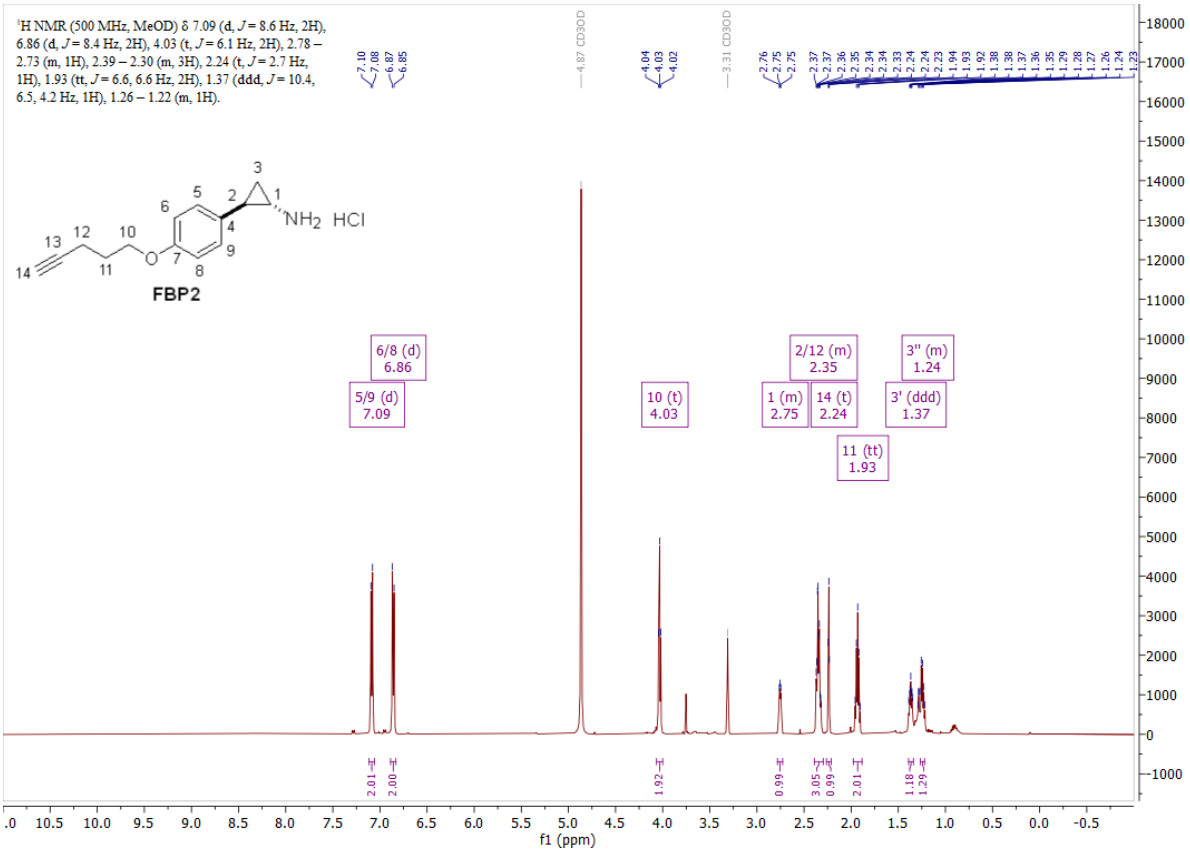

Figure S 1: ^{1}H-NMR of **FBP2**.

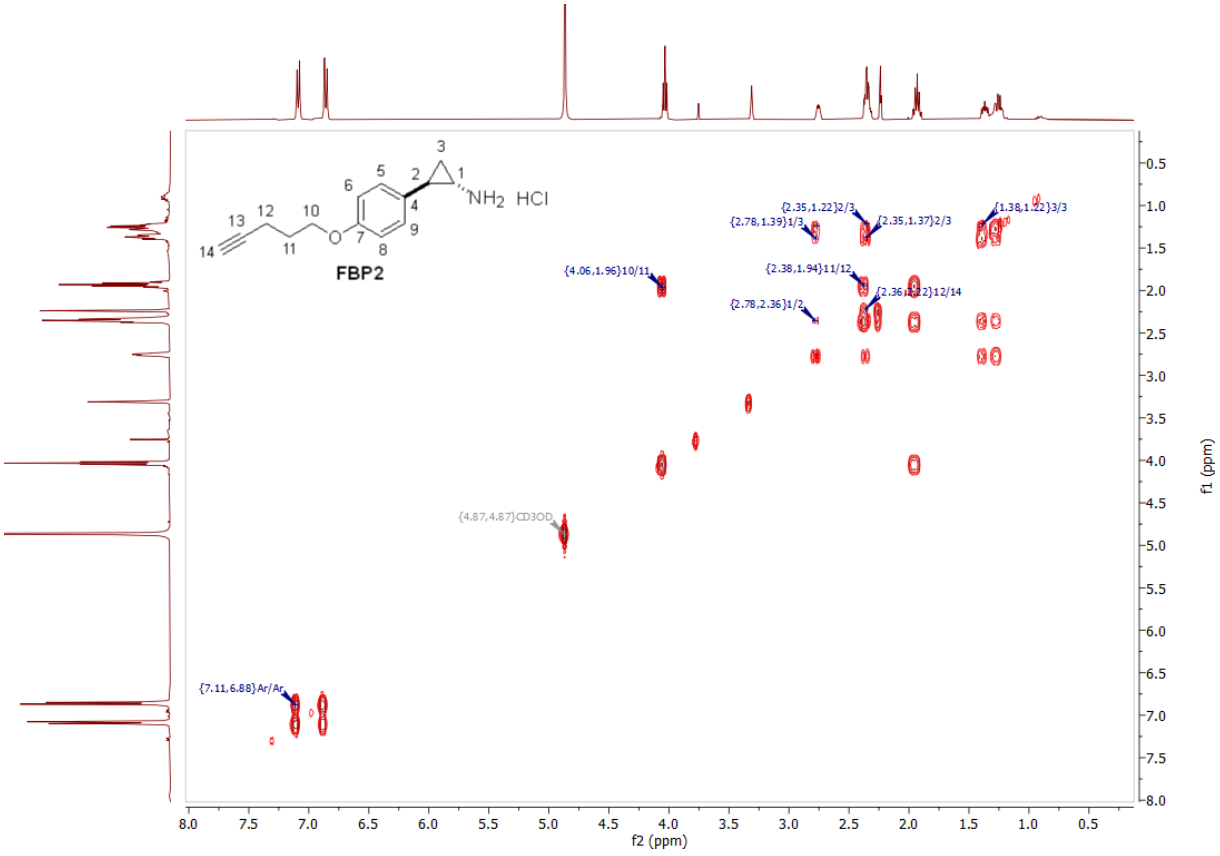

Figure S 2: COSY of **FBP2**.

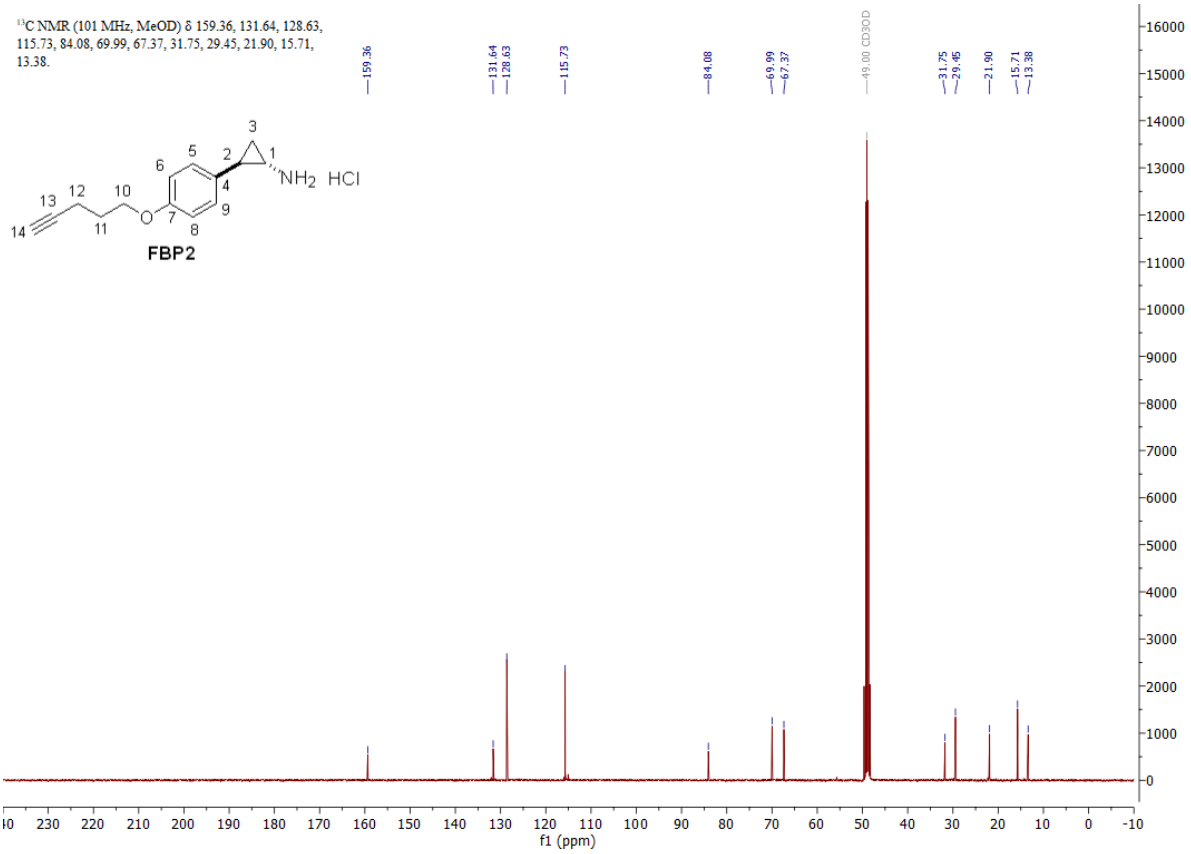

Figure S 3: ^{13}C-NMR of **FBP2**.

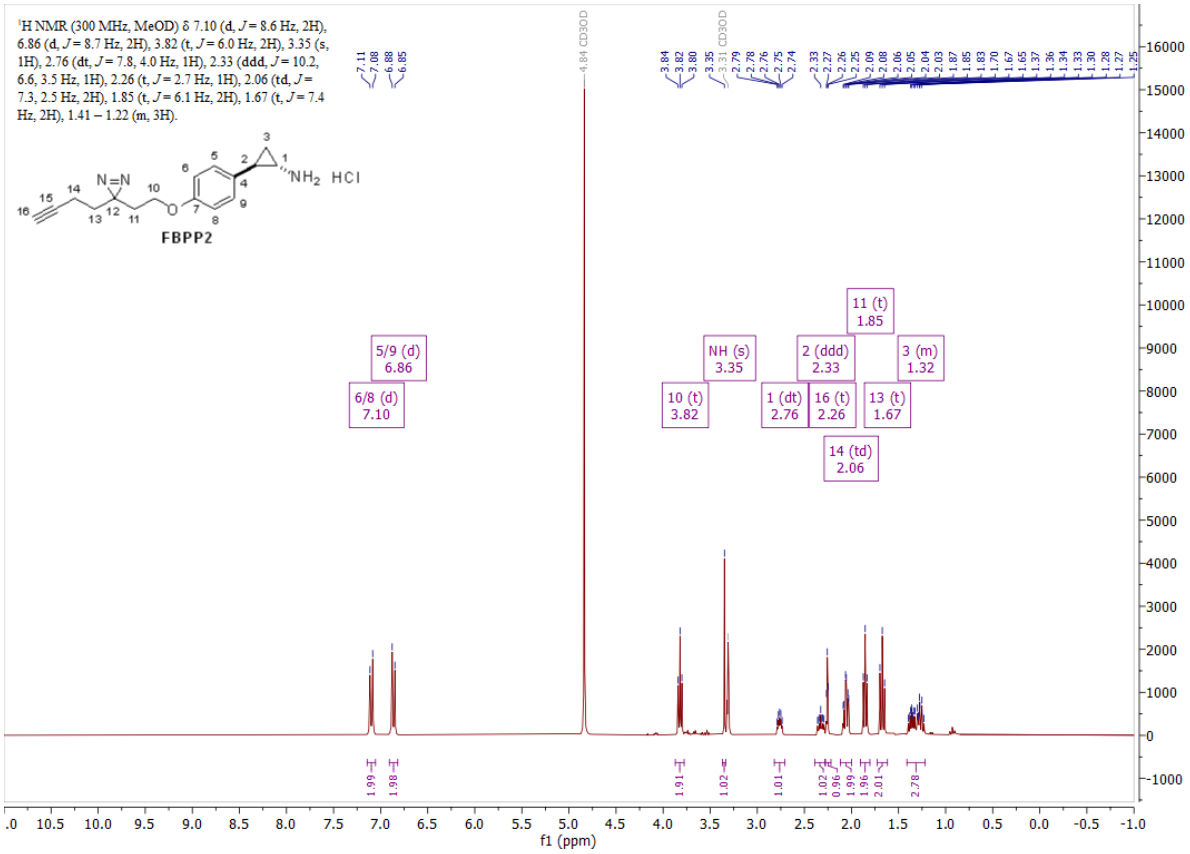

Figure S 4: ¹H-NMR of **FBPP2**.

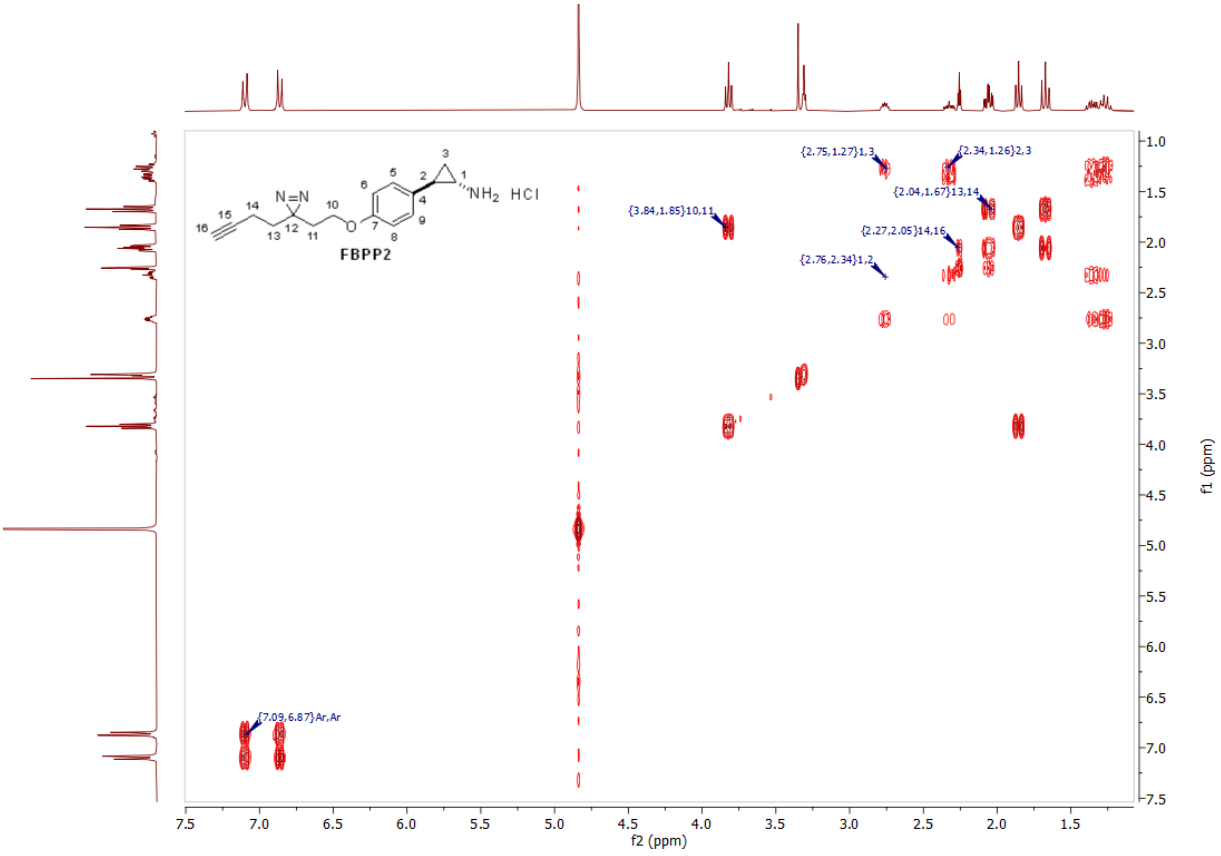

Figure S 5: COSY of **FBPP2**.

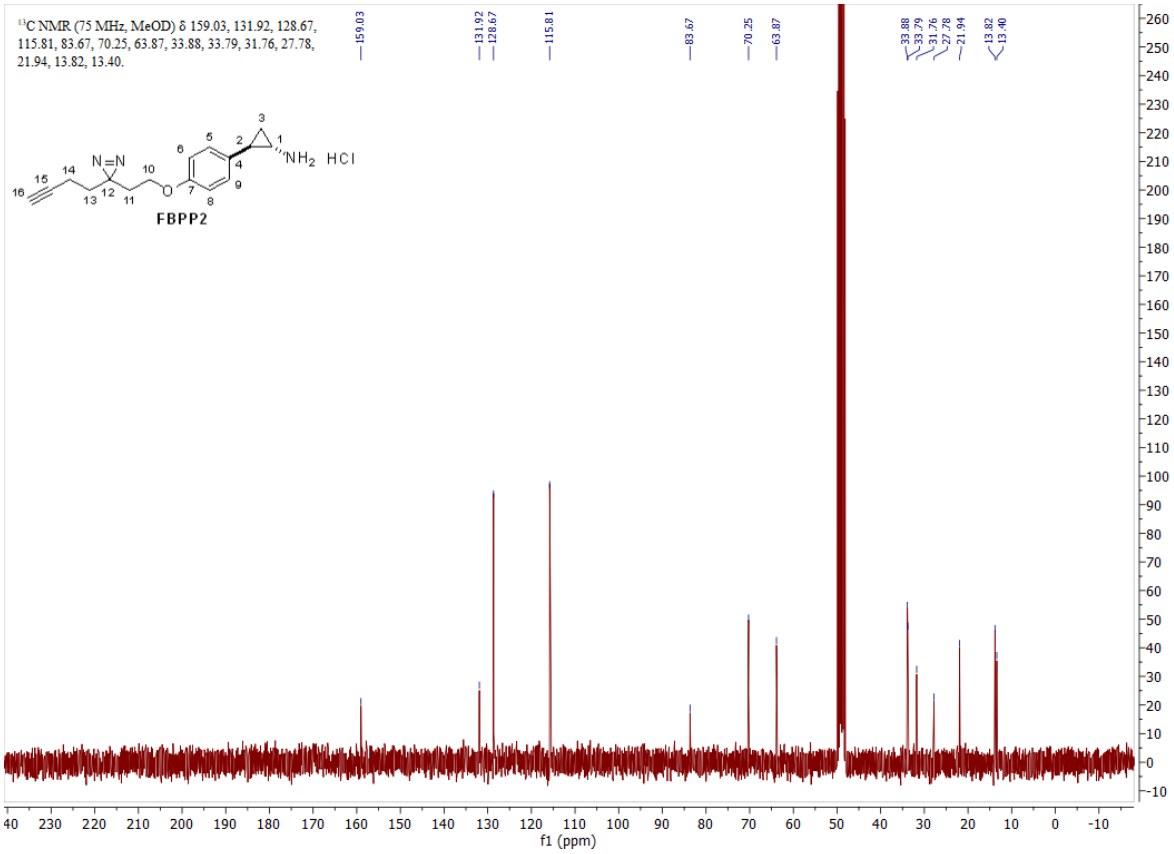

Figure S 6: ^{13}C-NMR of **FBPP2**.

IV. Abbreviations

ABPP Activity-based protein profiling

ACN Acetonitrile

AECH Aminoepoxycyclohexenone

AfBPP Affinity-based protein profiling

ALDH Aldehyde dehydrogenase

calcd Calculated

CQ Chloroquine

d Doublet

DAPI 4,6-Diamidino-2-phenylindole

DIAD Diisopropyl azodicarboxylate

DMEM Dulbecco's modified Eagle's medium

DML Dimethyl labelling

DMSO Dimethyl sulfoxide

DTT Dithiothreitol

eq Equivalent/s

ESI Electrospray ionization

Et_3N Triethylamine

EtOAc Ethyl acetate

FA Formic acid

FAD Flavin adenine dinucleotide

FBS Fetal bovine serum

FDA US food and drug administration

HEPES 4-(2-Hydroxyethyl)-1-piperazineethanesulfonic acid

HMOX Heme oxigenase

HPLC High-performance liquid chromatography

HR-MS High resolution mass spectrometry

IAA Iodoacetamide

IP-MS Intact protein mass spectrometry

iTRAQ Isobaric tags for relative and absolute quantitation

LC Liquid chromatography

LFQ Label-free quantification

m Multiplet

MAO Monoamine oxidase

MAOI Monoamine oxidase inhibitor

MeOH Methanol

MS Mass spectrometry

MS/MS Tandem mass spectrometry

NMR Nuclear magnetic resonance

PBS Phosphate buffered saline

PD Parkinson's disease

PFA Paraformaldehyde

pNP *p*-Nitrophenol

pNPA *p*-Nitrophenyl acetate

PTM Post-translational modification

q Quartet

RhN_3 Rhodamine azide

ROS Reactive oxygen species

RT Room temperature

s Singlet

SCRP-27A Sigma cross-reacting protein 27A

SDS-PAGE Sodium dodecyl sulfate-polyacrylamide gel electrophoresis

SILAC Stable isotope labelling by amino acids in cell culture

t Triplet

TBTA Tris(benzyltriazolylmethyl)amine

TCEP Tris(2-carboxyethyl)phosphine

TEAB Tetraethylammonium bromide

TFA Trifluoroacetic acid

THF Tetrahydrofuran

TMT Tandem mass tag

V. References

[1] Santos, R.; Ursu, O.; Gaulton, A.; Bento, A. P.; Donadi, R. S.; Bologa, C. G.; Karlsson, A.; Al-Lazikani, B.; Hersey, A.; Oprea, T. I.; Overington, J. P. A comprehensive map of molecular drug targets. *Nat. Rev. Drug Discov.* **2017,** *16* (1), 19–34.

[2] Schenone, M.; Dančík, V.; Wagner, B. K.; Clemons, P. A. Target identification and mechanism of action in chemical biology and drug discovery. *Nat. Chem. Biol.* **2013,** *9* (4), 232–240.

[3] Boutros, M.; Ahringer, J. The art and design of genetic screens: RNA interference. *Nat. Rev. Genet.* **2008,** *9* (7), 554–566.

[4] Ioerger, T. R.; O'Malley, T.; Liao, R.; Guinn, K. M.; Hickey, M. J.; Mohaideen, N.; Murphy, K. C.; Boshoff, H. I. M.; Mizrahi, V.; Rubin, E. J.; Sassetti, C. M.; Barry, C. E.; Sherman, D. R.; Parish, T.; Sacchettini, J. C. Identification of new drug targets and resistance mechanisms in Mycobacterium tuberculosis. *PLoS ONE* **2013,** *8* (9), e75245.

[5] Weinstein, J. N.; Myers, T. G.; O'Connor, P. M.; Friend, S. H.; Fornace, A. J.; Kohn, K. W.; Fojo, T.; Bates, S. E.; Rubinstein, L. V.; Anderson, N. L.; Buolamwini, J. K.; van Osdol, W. W.; Monks, A. P.; Scudiero, D. A.; Sausville, E. A.; Zaharevitz, D. W.; Bunow, B.; Viswanadhan, V. N.; Johnson, G. S.; Wittes, R. E.; Paull, K. D. An information-intensive approach to the molecular pharmacology of cancer. *Science* **1997,** *275* (5298), 343–349.

[6] Katsila, T.; Spyroulias, G. A.; Patrinos, G. P.; Matsoukas, M.-T. Computational approaches in target identification and drug discovery. *Comput. Struct. Biotechnol. J.* **2016,** *14*, 177–184.

[7] Liu, Y.; Patricelli, M. P.; Cravatt, B. F. Activity-based protein profiling: The serine hydrolases. *Proc. Natl. Acad. Sci.* **1999,** *96* (26), 14694–14699.

[8] Jessani, N.; Liu, Y.; Humphrey, M.; Cravatt, B. F. Enzyme activity profiles of the secreted and membrane proteome that depict cancer cell invasiveness. *Proc. Natl. Acad. Sci.* **2002,** *99* (16), 10335–10340.

[9] Speers, A. E.; Adam, G. C.; Cravatt, B. F. Activity-based protein profiling in vivo using a copper(I)-catalyzed azide-alkyne 3 + 2 cycloaddition. *J. Am. Chem. Soc.* **2003,** *125* (16), 4686–4687.

[10]Speers, A. E.; Cravatt, B. F. Chemical strategies for activity-based proteomics. *Chembiochem* **2004,** *5* (1), 41–47.

[11]Saghatelian, A.; Jessani, N.; Joseph, A.; Humphrey, M.; Cravatt, B. F. Activity-based probes for the proteomic profiling of metalloproteases. *Proc. Natl. Acad. Sci.* **2004,** *101* (27), 10000–10005.

[12]Evans, M. J.; Cravatt, B. F. Mechanism-based profiling of enzyme families. *Chem. Rev.* **2006,** *106* (8), 3279–3301.

[13]Greenbaum, D.; Medzihradszky, K. F.; Burlingame, A.; Bogyo, M. Epoxide electrophiles as activity-dependent cysteine protease profiling and discovery tools. *Chem. Biol.* **2000,** *7* (8), 569–581.

[14]Greenbaum, D.; Baruch, A.; Hayrapetian, L.; Darula, Z.; Burlingame, A.; Medzihradszky, K. F.; Bogyo, M. Chemical approaches for functionally probing the proteome. *Mol. Cell. Proteomics* **2002,** *1* (1), 60–68.

[15]Jeffery, D. A.; Bogyo, M. Chemical proteomics and its application to drug discovery. *Curr. Opin. Biotech.* **2003,** *14* (1), 87–95.

[16]Berger, A. B.; Vitorino, P. M.; Bogyo, M. Activity-based protein profiling: applications to biomarker discovery, in vivo imaging and drug discovery. *Am. J. Pharmacogenomics* **2004,** *4* (6), 371–381.

[17]Sieber, S. A.; Breinbauer, R. *Activity-based protein profiling*; Topics in current chemistry 324; Springer: Heidelberg, 2012.

[18]1,3-Dipolar cycloaddition chemistry. *J. Heterocycl. Chem.* **1986,** *23* (6), 1899.

[19]Kolb, H. C.; Finn, M. G.; Sharpless, K. B. Click Chemistry: Diverse Chemical Function from a Few Good Reactions. *Angew. Chem. Int. Ed.* **2001,** *40* (11), 2004–2021.

[20]Lewis, W. G.; Green, L. G.; Grynszpan, F.; Radić, Z.; Carlier, P. R.; Taylor, P.; Finn, M. G.; Sharpless, K. B. Click Chemistry In Situ: Acetylcholinesterase as a Reaction Vessel for the Selective Assembly of a Femtomolar Inhibitor from an Array of Building Blocks. *Angew. Chem. Int. Ed.* **2002,** *41* (6), 1053–1057.

[21]Rostovtsev, V. V.; Green, L. G.; Fokin, V. V.; Sharpless, K. B. A Stepwise Huisgen Cycloaddition Process: Copper(I)-Catalyzed Regioselective “Ligation” of Azides and Terminal Alkynes. *Angew. Chem. Int. Ed.* **2002,** *41* (14), 2596–2599.

[22]Hofmann, K.; Kiso, Y. An approach to the targeted attachment of peptides and proteins to solid supports. *Proc. Natl. Acad. Sci.* **1976,** *73* (10), 3516–3518.

[23]Chait, B. T. Chemistry. Mass spectrometry: bottom-up or top-down? *Science* **2006,** *314* (5796), 65–66.

[24]Toby, T. K.; Fornelli, L.; Srzentić, K.; DeHart, C. J.; Levitsky, J.; Friedewald, J.; Kelleher, N. L. A comprehensive pipeline for translational top-down proteomics from a single blood draw. *Nat. Protoc.* **2019,** *14* (1), 119–152.

[25]Catherman, A. D.; Skinner, O. S.; Kelleher, N. L. Top Down proteomics: facts and perspectives. *Biochem. Biophys. Res. Commun.* **2014,** *445* (4), 683–693.

[26]Aebersold, R.; Mann, M. Mass spectrometry-based proteomics. *Nature* **2003,** *422* (6928), 198–207.

[27]Aebersold, R.; Mann, M. Mass-spectrometric exploration of proteome structure and function. *Nature* **2016,** *537* (7620), 347–355.

[28]Pappireddi, N.; Martin, L.; Wühr, M. A Review on Quantitative Multiplexed Proteomics. *Chembiochem* **2019,** *20* (10), 1210–1224.

[29]Kong, A. T.; Leprevost, F. V.; Avtonomov, D. M.; Mellacheruvu, D.; Nesvizhskii, A. I. MSFragger: ultrafast and comprehensive peptide identification in mass spectrometry-based proteomics. *Nat. Methods* **2017,** *14* (5), 513–520.

[30]Cox, J.; Mann, M. MaxQuant enables high peptide identification rates, individualized p.p.b.-range mass accuracies and proteome-wide protein quantification. *Nat. Biotechnol.* **2008,** *26* (12), 1367–1372.

[31]MacLean, B.; Tomazela, D. M.; Shulman, N.; Chambers, M.; Finney, G. L.; Frewen, B.; Kern, R.; Tabb, D. L.; Liebler, D. C.; MacCoss, M. J. Skyline: an open source document editor for creating and analyzing targeted proteomics experiments. *Bioinformatics* **2010,** *26* (7), 966–968.

[32]Ong, S.-E.; Mann, M. A practical recipe for stable isotope labeling by amino acids in cell culture (SILAC). *Nat. Protoc.* **2006,** *1* (6), 2650–2660.

[33]Hogrebe, A.; Stechow, L. von; Bekker-Jensen, D. B.; Weinert, B. T.; Kelstrup, C. D.; Olsen, J. V. Benchmarking common quantification strategies for large-scale phosphoproteomics. *Nat. Commun.* **2018,** *9* (1), 1045.

[34]Hsu, J.-L.; Huang, S.-Y.; Chow, N.-H.; Chen, S.-H. Stable-isotope dimethyl labeling for quantitative proteomics. *Anal. Chem.* **2003,** *75* (24), 6843–6852.

[35]Boersema, P. J.; Raijmakers, R.; Lemeer, S.; Mohammed, S.; Heck, A. J. R. Multiplex peptide stable isotope dimethyl labeling for quantitative proteomics. *Nat. Protoc.* **2009,** *4* (4), 484–494.

[36]Mueller, L. N.; Brusniak, M.-Y.; Mani, D. R.; Aebersold, R. An assessment of software solutions for the analysis of mass spectrometry based quantitative proteomics data. *J. Proteome Res.* **2008,** *7* (1), 51–61.

[37]Liu, H.; Sadygov, R. G.; Yates, J. R. A model for random sampling and estimation of relative protein abundance in shotgun proteomics. *Anal. Chem.* **2004,** *76* (14), 4193–4201.

[38]Cox, J.; Hein, M. Y.; Luber, C. A.; Paron, I.; Nagaraj, N.; Mann, M. Accurate proteome-wide label-free quantification by delayed normalization and maximal peptide ratio extraction, termed MaxLFQ. *Mol. Cell. Proteomics* **2014,** *13* (9), 2513–2526.

[39]Ross, P. L.; Huang, Y. N.; Marchese, J. N.; Williamson, B.; Parker, K.; Hattan, S.; Khainovski, N.; Pillai, S.; Dey, S.; Daniels, S.; Purkayastha, S.; Juhasz, P.; Martin, S.; Bartlet-Jones, M.; He, F.; Jacobson, A.; Pappin, D. J. Multiplexed protein quantitation in Saccharomyces cerevisiae using amine-reactive isobaric tagging reagents. *Mol. Cell. Proteomics* **2004,** *3* (12), 1154–1169.

[40]Wiese, S.; Reidegeld, K. A.; Meyer, H. E.; Warscheid, B. Protein labeling by iTRAQ: a new tool for quantitative mass spectrometry in proteome research. *Proteomics* **2007,** *7* (3), 340–350.

[41]Unwin, R. D. Quantification of proteins by iTRAQ. *Methods Mol. Biol.* **2010,** *658*, 205–215.

[42]Thompson, A.; Schäfer, J.; Kuhn, K.; Kienle, S.; Schwarz, J.; Schmidt, G.; Neumann, T.; Johnstone, R.; Mohammed, A. K. A.; Hamon, C. Tandem mass tags: a novel quantification strategy for comparative analysis of complex protein mixtures by MS/MS. *Anal. Chem.* **2003,** *75* (8), 1895–1904.

[43]Zhang, L.; Elias, J. E. Relative Protein Quantification Using Tandem Mass Tag Mass Spectrometry. *Methods Mol. Biol.* **2017,** *1550*, 185–198.

[44]Ahrné, E.; Glatter, T.; Viganò, C.; Schubert, C. von; Nigg, E. A.; Schmidt, A. Evaluation and Improvement of Quantification Accuracy in Isobaric Mass Tag-Based Protein Quantification Experiments. *J. Proteome Res.* **2016,** *15* (8), 2537–2547.

[45]O'Brien, J. J.; O'Connell, J. D.; Paulo, J. A.; Thakurta, S.; Rose, C. M.; Weekes, M. P.; Huttlin, E. L.; Gygi, S. P. Compositional Proteomics: Effects of Spatial Constraints on Protein Quantification Utilizing Isobaric Tags. *J. Proteome Res.* **2018,** *17* (1), 590–599.

[46]Wenger, C. D.; Lee, M. V.; Hebert, A. S.; McAlister, G. C.; Phanstiel, D. H.; Westphall, M. S.; Coon, J. J. Gas-phase purification enables accurate, multiplexed proteome quantification with isobaric tagging. *Nat. Methods* **2011,** *8* (11), 933–935.

[47]Ting, L.; Rad, R.; Gygi, S. P.; Haas, W. MS3 eliminates ratio distortion in isobaric multiplexed quantitative proteomics. *Nat. Methods* **2011,** *8* (11), 937–940.

[48]Twelves, D.; Perkins, K. S. M.; Counsell, C. Systematic review of incidence studies of Parkinson's disease. *Mov. Disord.* **2003,** *18* (1), 19–31.

[49]van den Eeden, S. K.; Tanner, C. M.; Bernstein, A. L.; Fross, R. D.; Leimpeter, A.; Bloch, D. A.; Nelson, L. M. Incidence of Parkinson's disease: variation by age, gender, and race/ethnicity. *Am. J. Epidemiol.* **2003,** *157* (11), 1015–1022.

[50]Hirsch, L.; Jette, N.; Frolkis, A.; Steeves, T.; Pringsheim, T. The Incidence of Parkinson's Disease: A Systematic Review and Meta-Analysis. *Neuroepidemiology* **2016,** *46* (4), 292–300.

[51]Poewe, W.; Seppi, K.; Tanner, C. M.; Halliday, G. M.; Brundin, P.; Volkmann, J.; Schrag, A.-E.; Lang, A. E. Parkinson disease. *Nat. Rev. Dis. Primers* **2017,** *3*, 17013.

[52]Dickson, D. W.; Braak, H.; Duda, J. E.; Duyckaerts, C.; Gasser, T.; Halliday, G. M.; Hardy, J.; Leverenz, J. B.; Del Tredici, K.; Wszolek, Z. K.; Litvan, I. Neuropathological assessment of Parkinson's disease: refining the diagnostic criteria. *Lancet Neurol.* **2009,** *8* (12), 1150–1157.

[53]Savica, R.; Grossardt, B. R.; Bower, J. H.; Ahlskog, J. E.; Rocca, W. A. Incidence and pathology of synucleinopathies and tauopathies related to parkinsonism. *JAMA neurology* **2013,** *70* (7), 859–866.

[54]Armstrong, M. J.; Okun, M. S. Diagnosis and Treatment of Parkinson Disease: A Review. *JAMA* **2020,** *323* (6), 548–560.

[55]Dias, V.; Junn, E.; Mouradian, M. M. The role of oxidative stress in Parkinson's disease. *J. Parkinsons Dis.* **2013,** *3* (4), 461–491.

[56]Kahle, P. J.; Waak, J.; Gasser, T. DJ-1 and prevention of oxidative stress in Parkinson's disease and other age-related disorders. *Free Radic. Biol. Med.* **2009,** *47* (10), 1354–1361.

[57]Wilson, M. A. The role of cysteine oxidation in DJ-1 function and dysfunction. *Antioxid. Redox Signal.* **2011,** *15* (1), 111–122.

[58]Ariga, H.; Takahashi-Niki, K.; Kato, I.; Maita, H.; Niki, T.; Iguchi-Ariga, S. M. M. Neuroprotective function of DJ-1 in Parkinson's disease. *Oxid. Med. Cell. Longev.* **2013,** *2013*, 683920.

[59]Honbou, K.; Suzuki, N. N.; Horiuchi, M.; Niki, T.; Taira, T.; Ariga, H.; Inagaki, F. The crystal structure of DJ-1, a protein related to male fertility and Parkinson's disease. *J. Biol. Chem.* **2003,** *278* (33), 31380–31384.

[60]Lee, S.-J.; Kim, S. J.; Kim, I.-K.; Ko, J.; Jeong, C.-S.; Kim, G.-H.; Park, C.; Kang, S.-O.; Suh, P.-G.; Lee, H.-S.; Cha, S.-S. Crystal structures of human DJ-1 and Escherichia coli Hsp31, which share an evolutionarily conserved domain. *J. Biol. Chem.* **2003,** *278* (45), 44552–44559.

[61]Uhlén, M.; Fagerberg, L.; Hallström, B. M.; Lindskog, C.; Oksvold, P.; Mardinoglu, A.; Sivertsson, Å.; Kampf, C.; Sjöstedt, E.; Asplund, A.; Olsson, I.; Edlund, K.; Lundberg, E.; Navani, S.; Szigyarto, C. A.-K.; Odeberg, J.; Djureinovic, D.; Takanen, J. O.; Hober, S.; Alm, T.; Edqvist, P.-H.; Berling, H.; Tegel, H.; Mulder, J.; Rockberg, J.; Nilsson, P.; Schwenk, J. M.; Hamsten, M.; Feilitzen, K. von; Forsberg, M.; Persson, L.; Johansson, F.; Zwahlen, M.; Heijne, G. von; Nielsen, J.; Pontén, F. Proteomics. Tissue-based map of the human proteome. *Science* **2015,** *347* (6220), 1260419.

[62]Thul, P. J.; Åkesson, L.; Wiking, M.; Mahdessian, D.; Geladaki, A.; Ait Blal, H.; Alm, T.; Asplund, A.; Björk, L.; Breckels, L. M.; Bäckström, A.; Danielsson, F.; Fagerberg, L.; Fall, J.; Gatto, L.; Gnann, C.; Hober, S.; Hjelmare, M.; Johansson, F.; Lee, S.; Lindskog, C.; Mulder, J.; Mulvey, C. M.; Nilsson, P.; Oksvold, P.; Rockberg, J.; Schutten, R.; Schwenk, J. M.; Sivertsson, Å.; Sjöstedt, E.; Skogs, M.; Stadler, C.; Sullivan, D. P.; Tegel, H.; Winsnes, C.; Zhang, C.; Zwahlen, M.; Mardinoglu, A.; Pontén, F.; Feilitzen, K. von;

Lilley, K. S.; Uhlén, M.; Lundberg, E. A subcellular map of the human proteome. *Science* **2017,** *356* (6340). DOI: 10.1126/science.aal3321.

[63] Uhlen, M.; Zhang, C.; Lee, S.; Sjöstedt, E.; Fagerberg, L.; Bidkhori, G.; Benfeitas, R.; Arif, M.; Liu, Z.; Edfors, F.; Sanli, K.; Feilitzen, K. von; Oksvold, P.; Lundberg, E.; Hober, S.; Nilsson, P.; Mattsson, J.; Schwenk, J. M.; Brunnström, H.; Glimelius, B.; Sjöblom, T.; Edqvist, P.-H.; Djureinovic, D.; Micke, P.; Lindskog, C.; Mardinoglu, A.; Ponten, F. A pathology atlas of the human cancer transcriptome. *Science* **2017,** *357* (6352). DOI: 10.1126/science.aan2507.

[64] Bandopadhyay, R.; Kingsbury, A. E.; Cookson, M. R.; Reid, A. R.; Evans, I. M.; Hope, A. D.; Pittman, A. M.; Lashley, T.; Canet-Aviles, R.; Miller, D. W.; McLendon, C.; Strand, C.; Leonard, A. J.; Abou-Sleiman, P. M.; Healy, D. G.; Ariga, H.; Wood, N. W.; Silva, R. de; Revesz, T.; Hardy, J. A.; Lees, A. J. The expression of DJ-1 (PARK7) in normal human CNS and idiopathic Parkinson's disease. *Brain* **2004,** *127* (Pt 2), 420–430.

[65] Nagakubo, D.; Taira, T.; Kitaura, H.; Ikeda, M.; Tamai, K.; Iguchi-Ariga, S. M.; Ariga, H. DJ-1, a novel oncogene which transforms mouse NIH3T3 cells in cooperation with ras. *Biochem. Biophys. Res. Commun.* **1997,** *231* (2), 509–513.

[66] Junn, E.; Taniguchi, H.; Jeong, B. S.; Zhao, X.; Ichijo, H.; Mouradian, M. M. Interaction of DJ-1 with Daxx inhibits apoptosis signal-regulating kinase 1 activity and cell death. *Proc. Natl. Acad. Sci.* **2005,** *102* (27), 9691–9696.

[67] Zhou, W.; Zhu, M.; Wilson, M. A.; Petsko, G. A.; Fink, A. L. The oxidation state of DJ-1 regulates its chaperone activity toward alpha-synuclein. *J. Mol. Biol.* **2006,** *356* (4), 1036–1048.

[68] Zhang, Y.; Gong, X.-G.; Wang, Z.-Z.; Sun, H.-M.; Guo, Z.-Y.; Hu, J.-H.; Ma, L.; Li, P.; Chen, N.-H. Overexpression of DJ-1/PARK7, the Parkinson's disease-related protein, improves mitochondrial function via Akt phosphorylation on threonine 308 in dopaminergic neuron-like cells. *Eur. J. Neurosci.* **2016,** *43* (10), 1379–1388.

[69] Richarme, G.; Mihoub, M.; Dairou, J.; Bui, L. C.; Leger, T.; Lamouri, A. Parkinsonism-associated protein DJ-1/Park7 is a major protein deglycase that repairs methylglyoxal- and glyoxal-glycated cysteine, arginine, and lysine residues. *J. Biol. Chem.* **2015,** *290* (3), 1885–1897.

[70]Lee, J.-y.; Song, J.; Kwon, K.; Jang, S.; Kim, C.; Baek, K.; Kim, J.; Park, C. Human DJ-1 and its homologs are novel glyoxalases. *Hum. Mol. Genet.* **2012,** *21* (14), 3215–3225.

[71]Kinumi, T.; Kimata, J.; Taira, T.; Ariga, H.; Niki, E. Cysteine-106 of DJ-1 is the most sensitive cysteine residue to hydrogen peroxide-mediated oxidation in vivo in human umbilical vein endothelial cells. *Biochem. Biophys. Res. Commun.* **2004,** *317* (3), 722–728.

[72]Taira, T.; Saito, Y.; Niki, T.; Iguchi-Ariga, S. M. M.; Takahashi, K.; Ariga, H. DJ-1 has a role in antioxidative stress to prevent cell death. *EMBO Rep.* **2004,** *5* (2), 213–218.

[73]Wilson, M. A.; St Amour, C. V.; Collins, J. L.; Ringe, D.; Petsko, G. A. The 1.8-A resolution crystal structure of YDR533Cp from Saccharomyces cerevisiae: a member of the DJ-1/ThiJ/PfpI superfamily. *Proc. Natl. Acad. Sci.* **2004,** *101* (6), 1531–1536.

[74]Wilson, M. A.; Collins, J. L.; Hod, Y.; Ringe, D.; Petsko, G. A. The 1.1-A resolution crystal structure of DJ-1, the protein mutated in autosomal recessive early onset Parkinson's disease. *Proc. Natl. Acad. Sci.* **2003,** *100* (16), 9256–9261.

[75]Shendelman, S.; Jonason, A.; Martinat, C.; Leete, T.; Abeliovich, A. DJ-1 is a redox-dependent molecular chaperone that inhibits alpha-synuclein aggregate formation. *PLoS Biol.* **2004,** *2* (11), e362.

[76]Kim, R. H.; Peters, M.; Jang, Y.; Shi, W.; Pintilie, M.; Fletcher, G. C.; DeLuca, C.; Liepa, J.; Zhou, L.; Snow, B.; Binari, R. C.; Manoukian, A. S.; Bray, M. R.; Liu, F.-F.; Tsao, M.-S.; Mak, T. W. DJ-1, a novel regulator of the tumor suppressor PTEN. *Cancer Cell* **2005,** *7* (3), 263–273.

[77]Xu, J.; Zhong, N.; Wang, H.; Elias, J. E.; Kim, C. Y.; Woldman, I.; Pifl, C.; Gygi, S. P.; Geula, C.; Yankner, B. A. The Parkinson's disease-associated DJ-1 protein is a transcriptional co-activator that protects against neuronal apoptosis. *Hum. Mol. Genet.* **2005,** *14* (9), 1231–1241.

[78]Miyazaki, S.; Yanagida, T.; Nunome, K.; Ishikawa, S.; Inden, M.; Kitamura, Y.; Nakagawa, S.; Taira, T.; Hirota, K.; Niwa, M.; Iguchi-Ariga, S. M. M.; Ariga, H. DJ-1-binding compounds prevent oxidative stress-induced cell death and movement defect in Parkinson's disease model rats. *J. Neurochem.* **2008,** *105* (6), 2418–2434.

[79] McNally, R. S.; Davis, B. K.; Clements, C. M.; Accavitti-Loper, M. A.; Mak, T. W.; Ting, J. P.-Y. DJ-1 enhances cell survival through the binding of Cezanne, a negative regulator of NF-kappaB. *J. Biol. Chem.* **2011,** *286* (6), 4098–4106.

[80] Bonifati, V.; Rizzu, P.; van Baren, M. J.; Schaap, O.; Breedveld, G. J.; Krieger, E.; Dekker, M. C. J.; Squitieri, F.; Ibanez, P.; Joosse, M.; van Dongen, J. W.; Vanacore, N.; van Swieten, J. C.; Brice, A.; Meco, G.; van Duijn, C. M.; Oostra, B. A.; Heutink, P. Mutations in the DJ-1 gene associated with autosomal recessive early-onset parkinsonism. *Science* **2003,** *299* (5604), 256–259.

[81] Saito, Y. Oxidized DJ-1 as a possible biomarker of Parkinson's disease. *J. Clin. Biochem. Nutr.* **2014,** *54* (3), 138–144.

[82] Saito, Y. DJ-1 as a Biomarker of Parkinson's Disease. *Adv. Exp. Med. Biol.* **2017,** *1037*, 149–171.

[83] Mandl, F. A.; Kirsch, V. C.; Ugur, I.; Kunold, E.; Vomacka, J.; Fetzer, C.; Schneider, S.; Richter, K.; Fuchs, T. M.; Antes, I.; Sieber, S. A. Natural-Product-Inspired Aminoepoxybenzoquinones Kill Members of the Gram-Negative Pathogen Salmonella by Attenuating Cellular Stress Response. *Angew. Chem. Int. Ed.* **2016,** *55* (47), 14852–14857.

[84] Bandyopadhyay, S.; Cookson, M. R. Evolutionary and functional relationships within the DJ1 superfamily. *BMC Evol. Biol.* **2004,** *4*, 6.

[85] Vázquez-Mayorga, E.; Díaz-Sánchez, Á. G.; Dagda, R. K.; Domínguez-Solís, C. A.; Dagda, R. Y.; Coronado-Ramírez, C. K.; Martínez-Martínez, A. Novel Redox-Dependent Esterase Activity (EC 3.1.1.2) for DJ-1: Implications for Parkinson's Disease. *Int. J. Mol. Sci.* **2016,** *17* (8). DOI: 10.3390/ijms17081346.

[86] Lo, M.-C.; Aulabaugh, A.; Jin, G.; Cowling, R.; Bard, J.; Malamas, M.; Ellestad, G. Evaluation of fluorescence-based thermal shift assays for hit identification in drug discovery. *Anal. Biochem.* **2004,** *332* (1), 153–159.

[87] Canet-Avilés, R. M.; Wilson, M. A.; Miller, D. W.; Ahmad, R.; McLendon, C.; Bandyopadhyay, S.; Baptista, M. J.; Ringe, D.; Petsko, G. A.; Cookson, M. R. The Parkinson's disease protein DJ-1 is neuroprotective due to cysteine-sulfinic acid-driven mitochondrial localization. *Proc. Natl. Acad. Sci.* **2004,** *101* (24), 9103–9108.

[88]Cao, J.; Ying, M.; Xie, N.; Lin, G.; Dong, R.; Zhang, J.; Yan, H.; Yang, X.; He, Q.; Yang, B. The oxidation states of DJ-1 dictate the cell fate in response to oxidative stress triggered by 4-hpr: autophagy or apoptosis? *Antioxid. Redox Signal.* **2014,** *21* (10), 1443–1459.

[89]Drechsel, J.; Mandl, F. A.; Sieber, S. A. Chemical Probe To Monitor the Parkinsonism-Associated Protein DJ-1 in Live Cells. *ACS Chem. Biol.* **2018,** *13* (8), 2016–2019.

[90]Tyanova, S.; Temu, T.; Sinitcyn, P.; Carlson, A.; Hein, M. Y.; Geiger, T.; Mann, M.; Cox, J. The Perseus computational platform for comprehensive analysis of (prote)omics data. *Nat. Methods* **2016,** *13* (9), 731–740.

[91]Shannon, P.; Markiel, A.; Ozier, O.; Baliga, N. S.; Wang, J. T.; Ramage, D.; Amin, N.; Schwikowski, B.; Ideker, T. Cytoscape: a software environment for integrated models of biomolecular interaction networks. *Genome Res.* **2003,** *13* (11), 2498–2504.

[92]Maere, S.; Heymans, K.; Kuiper, M. BiNGO: a Cytoscape plugin to assess overrepresentation of gene ontology categories in biological networks. *Bioinformatics* **2005,** *21* (16), 3448–3449.

[93]Statistisches Bundesamt. *Herz-Kreislauf-Erkrankungen verursachen die höchsten Kosten*. *Pressemitteilung Nr. 347*, 2017.

[94]Clark, L. A.; Cuthbert, B.; Lewis-Fernández, R.; Narrow, W. E.; Reed, G. M. Three Approaches to Understanding and Classifying Mental Disorder: ICD-11, DSM-5, and the National Institute of Mental Health's Research Domain Criteria (RDoC). *Psychol. Sci. Public Interest.* **2017,** *18* (2), 72–145.

[95]Youdim, M. B. H.; Edmondson, D.; Tipton, K. F. The therapeutic potential of monoamine oxidase inhibitors. *Nat. Rev. Neurosci.* **2006,** *7* (4), 295–309.

[96]Bortolato, M.; Chen, K.; Shih, J. C. Monoamine oxidase inactivation: from pathophysiology to therapeutics. *Adv. Drug Deliv. Rev.* **2008,** *60* (13-14), 1527–1533.

[97]Mimasu, S.; Sengoku, T.; Fukuzawa, S.; Umehara, T.; Yokoyama, S. Crystal structure of histone demethylase LSD1 and tranylcypromine at 2.25 A. *Biochem. Biophys. Res. Commun.* **2008,** *366* (1), 15–22.

[98] Binda, C.; Li, M.; Hubalek, F.; Restelli, N.; Edmondson, D. E.; Mattevi, A. Insights into the mode of inhibition of human mitochondrial monoamine oxidase B from high-resolution crystal structures. *Proc. Natl. Acad. Sci.* **2003,** *100* (17), 9750–9755.

[99] Baker, G. B.; Urichuk, L. J.; McKenna, K. F.; Kennedy, S. H. Metabolism of monoamine oxidase inhibitors. *Cell Mol. Neurobiol.* **1999,** *19* (3), 411–426.

[100] Kumar, B.; Sheetal, S.; Mantha, A. K.; Kumar, V. Recent developments on the structure–activity relationship studies of MAO inhibitors and their role in different neurological disorders. *RSC Adv.* **2016,** *6* (48), 42660–42683.

[101] Ricken, R.; Ulrich, S.; Schlattmann, P.; Adli, M. Tranylcypromine in mind (Part II): Review of clinical pharmacology and meta-analysis of controlled studies in depression. *Eur. Neuropsychopharmacol.* **2017,** *27* (8), 714–731.

[102] Pollock, J. A.; Larrea, M. D.; Jasper, J. S.; McDonnell, D. P.; McCafferty, D. G. Lysine-specific histone demethylase 1 inhibitors control breast cancer proliferation in ERα-dependent and -independent manners. *ACS Chem. Biol.* **2012,** *7* (7), 1221–1231.

[103] Riederer, P.; Laux, G. MAO-inhibitors in Parkinson's Disease. *Exp. Neurobiol.* **2011,** *20* (1), 1–17.

[104] Al-Nuaimi, S. K.; Mackenzie, E. M.; Baker, G. B. Monoamine oxidase inhibitors and neuroprotection: a review. *Am. J. Ther.* **2012,** *19* (6), 436–448.

[105] Krysiak, J. M.; Kreuzer, J.; Macheroux, P.; Hermetter, A.; Sieber, S. A.; Breinbauer, R. Activity-based probes for studying the activity of flavin-dependent oxidases and for the protein target profiling of monoamine oxidase inhibitors. *Angew. Chem. Int. Ed.* **2012,** *51* (28), 7035–7040.

[106] Abdel-Aleem, H.; El-Ashmawy, M. B.; Belal, F.; El-Amam, A. A.; Brittain, H. G. Tranylcypromine Sulfate. In *Analytical profiles of drug substances and excipients*; Florey, K., Brittain, H. G., Eds.; Analytical Profiles of Drug Substances and Excipients; Academic: New York, 1972-2002; pp 501–533.

[107] Xicoy, H.; Wieringa, B.; Martens, G. J. M. The SH-SY5Y cell line in Parkinson's disease research: a systematic review. *Mol. Neurodegener.* **2017,** *12* (1), 10.

[108] Kleiner, P.; Heydenreuter, W.; Stahl, M.; Korotkov, V. S.; Sieber, S. A. A Whole Proteome Inventory of Background Photocrosslinker Binding. *Angew. Chem. Int. Ed.* **2017,** *56* (5), 1396–1401.

[109] Duve, C. de; Barsy, T. de; Poole, B.; Trouet, A.; Tulkens, P.; van Hoof, F. Lysosomotropic agents. *Biochem. Pharmacol.* **1974,** *23* (18), 2495–2531.

[110] Kazmi, F.; Hensley, T.; Pope, C.; Funk, R. S.; Loewen, G. J.; Buckley, D. B.; Parkinson, A. Lysosomal sequestration (trapping) of lipophilic amine (cationic amphiphilic) drugs in immortalized human hepatocytes (Fa2N-4 cells). *Drug Metab. Dispos.* **2013,** *41* (4), 897–905.

[111] Lu, S.; Sung, T.; Lin, N.; Abraham, R. T.; Jessen, B. A. Lysosomal adaptation: How cells respond to lysosomotropic compounds. *PLoS ONE* **2017,** *12* (3), e0173771.

[112] Ortega-Munoz A.; Castro-Palomino Laria J.; Fyfe M. C. T. Lysine-specific demethylase 1 inhibitors and their use. WO2011035941 (A1), 2011.

[113] Heydenreuter, W.; Kunold, E.; Sieber, S. A. Alkynol natural products target ALDH2 in cancer cells by irreversible binding to the active site. *Chem. Commun.* **2015,** *51* (87), 15784–15787.

[114] Bianchetti, C. M.; Yi, L.; Ragsdale, S. W.; Phillips, G. N. Comparison of apo- and heme-bound crystal structures of a truncated human heme oxygenase-2. *J. Biol. Chem.* **2007,** *282* (52), 37624–37631.

[115] Kielkowski, P.; Buchsbaum, I. Y.; Becker, T.; Bach, K.; Cappello, S.; Sieber, S. A. A Pronucleotide Probe for Live-Cell Imaging of Protein AMPylation. *Chembiochem* **2020**, [early view].

VI. Appendix

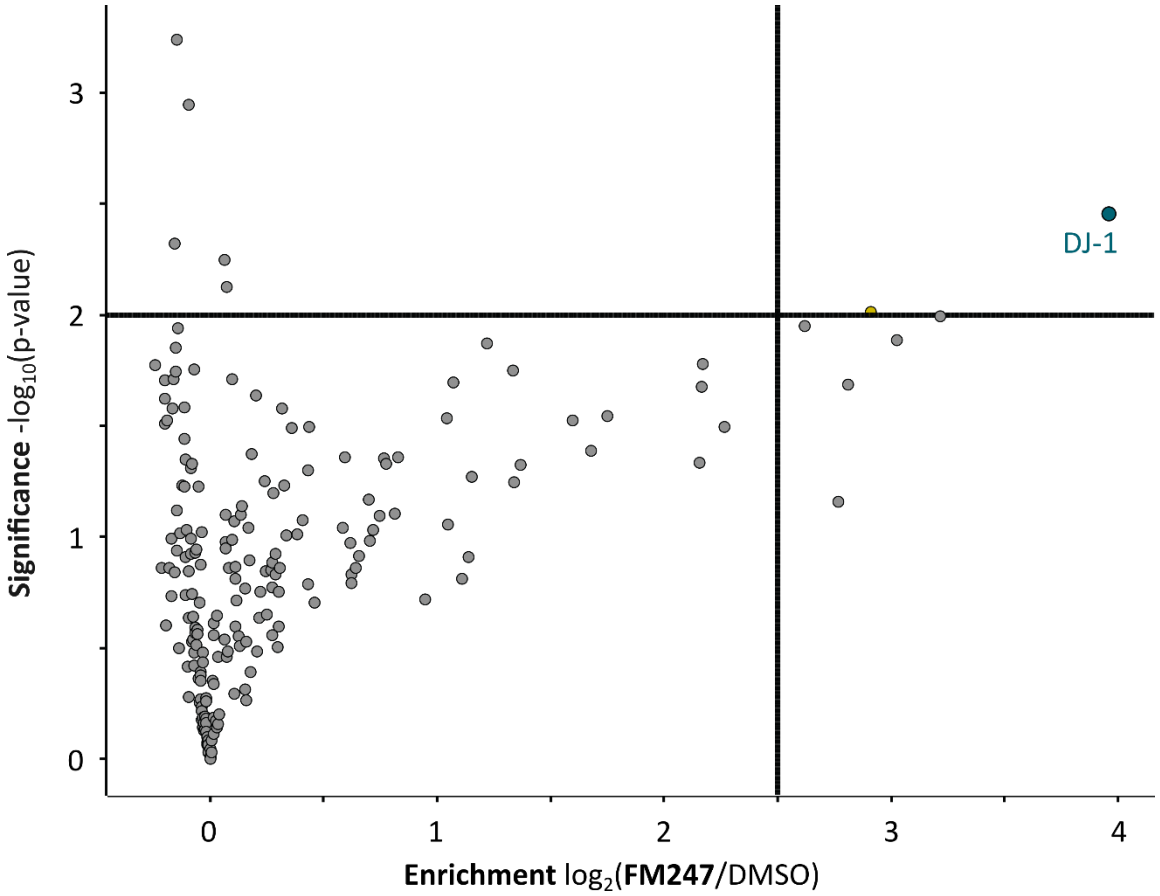

Figure A1: Result of the quantitative SILAC experiment using FM247 in the human cancer cell line A549. The volcano plot displays the statistical significance of protein enrichment levels as a function of protein enrichment ratios from probe treated to control cells, with a cut of at a -log10(p-value) of 2 and a t-test difference of 2.5.

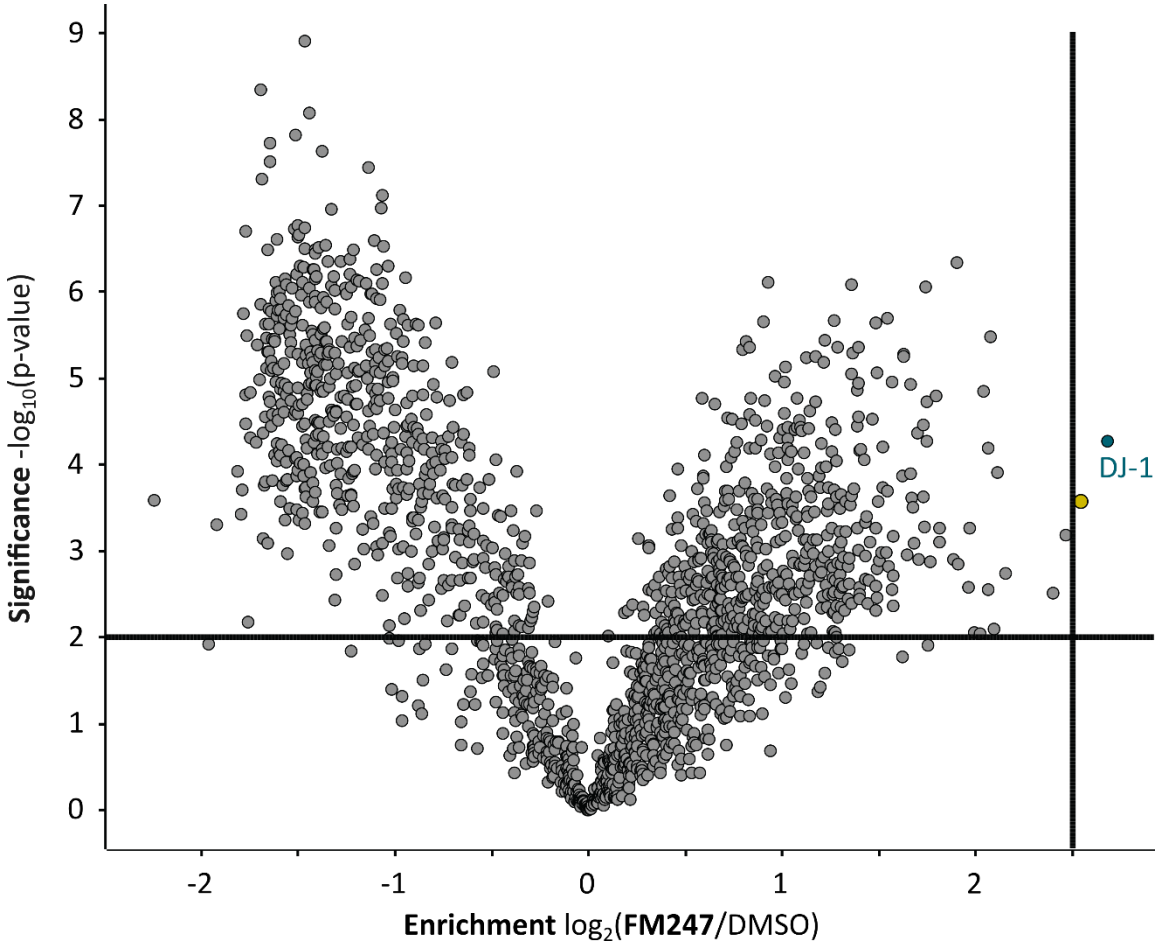

Figure A2: Result of the quantitative SILAC experiment using **FM247** in the human cancer cell line SH-SY5Y. The volcano plot displays the statistical significance of protein enrichment levels as a function of protein enrichment ratios from probe treated to control cells, with a cut of at a $-\log_{10}$(p-value) of 2 and a t-test difference of 2.5.

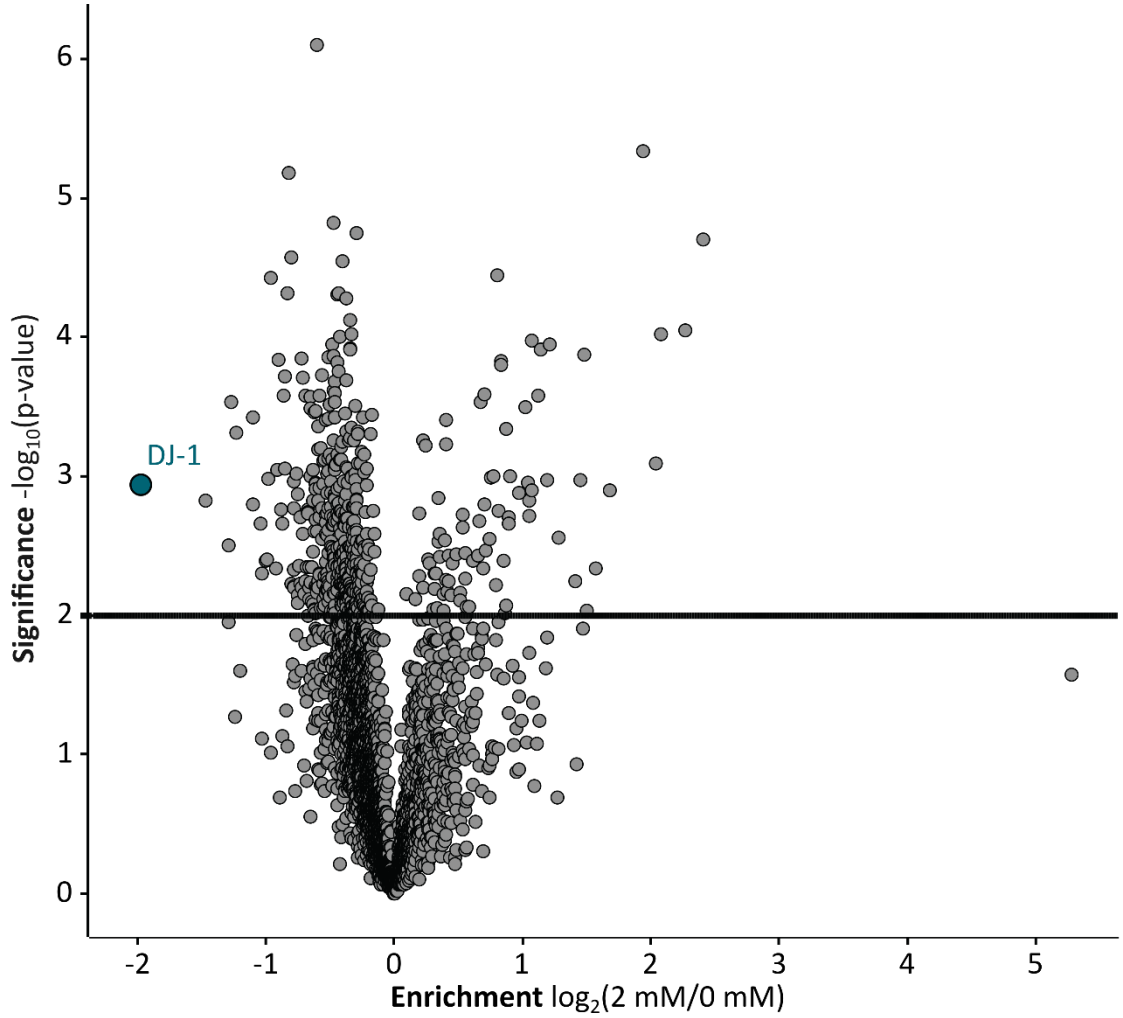

Figure A3: Results of the quantitative LFQ experiment showing the decrease of the DJ-1 labeling intensity after pre-incubation with 2 mM H_2O_2 using **FM247** in the human cancer cell line HeLa.

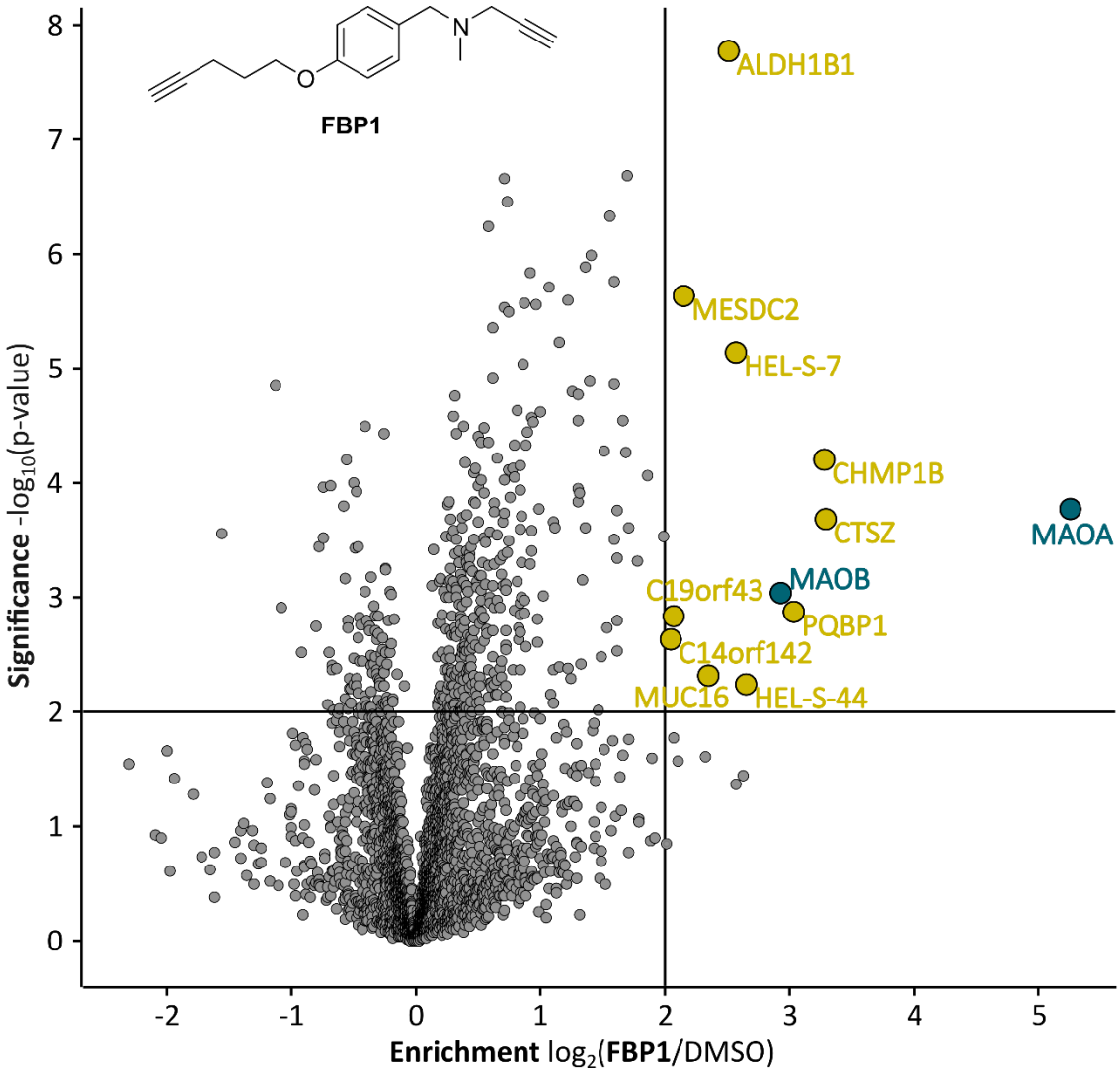

Figure A4: Result of target enrichment experiment using **FBP1** in the human cancer cell line HeLa with 100 µM probe concentration. The scatter plot shows statistical significance of protein enrichment levels over protein enrichment ratios from probe treated to control cells. Cut offs are at a p-value < 0.01 and 4-fold enrichment (indicated by solid lines). Proteins within these set criteria are highlighted in yellow; MAOA and MAOB are highlighted in turquoise.

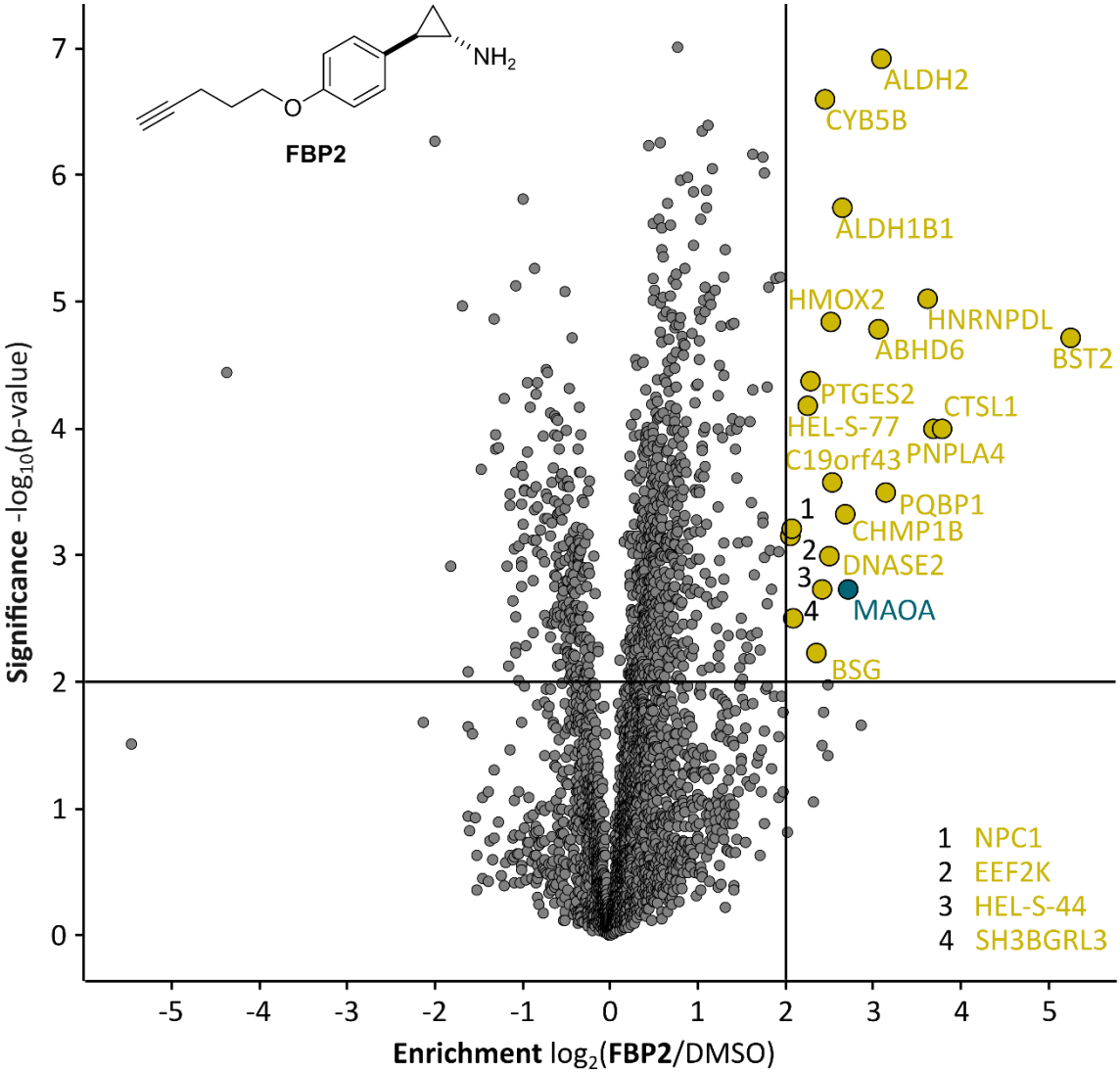

Figure A5: Result of target enrichment experiment using **FBP2** in the human cancer cell line HeLa with 100 µM probe concentration. The scatter plot shows statistical significance of protein enrichment levels over protein enrichment ratios from probe treated to control cells. Cut offs are at a p-value < 0.01 and 4-fold enrichment (indicated by solid lines). Proteins within these set criteria are highlighted in yellow; MAOA is highlighted in turquoise.

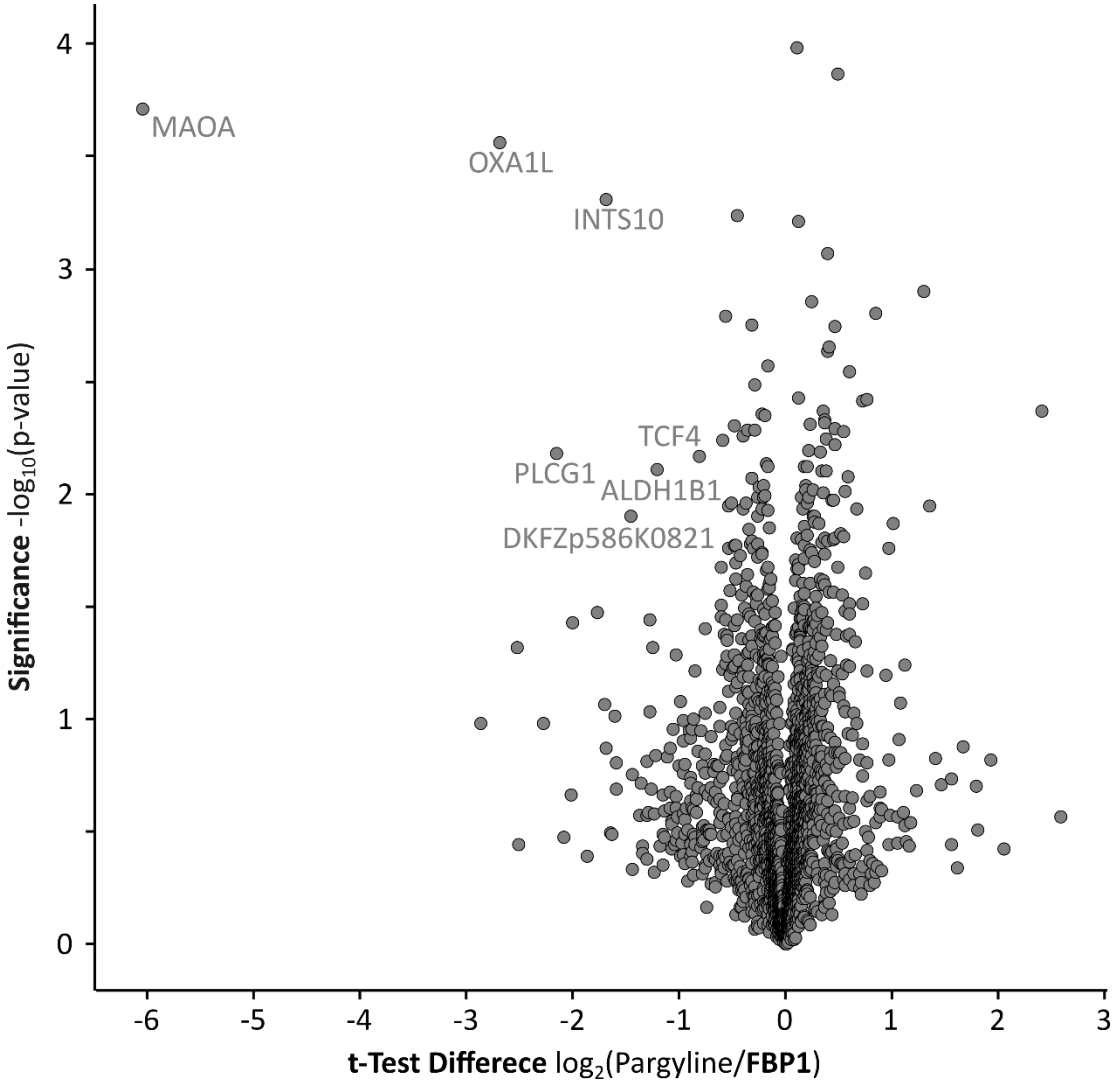

Figure A6: Result of competition experiment using **FBP1** in the human cancer cell line SH-SY5Y preincubated with pargyline. The scatter plot shows statistical significance of protein enrichment levels over protein enrichment ratios from drug treated to control cells.

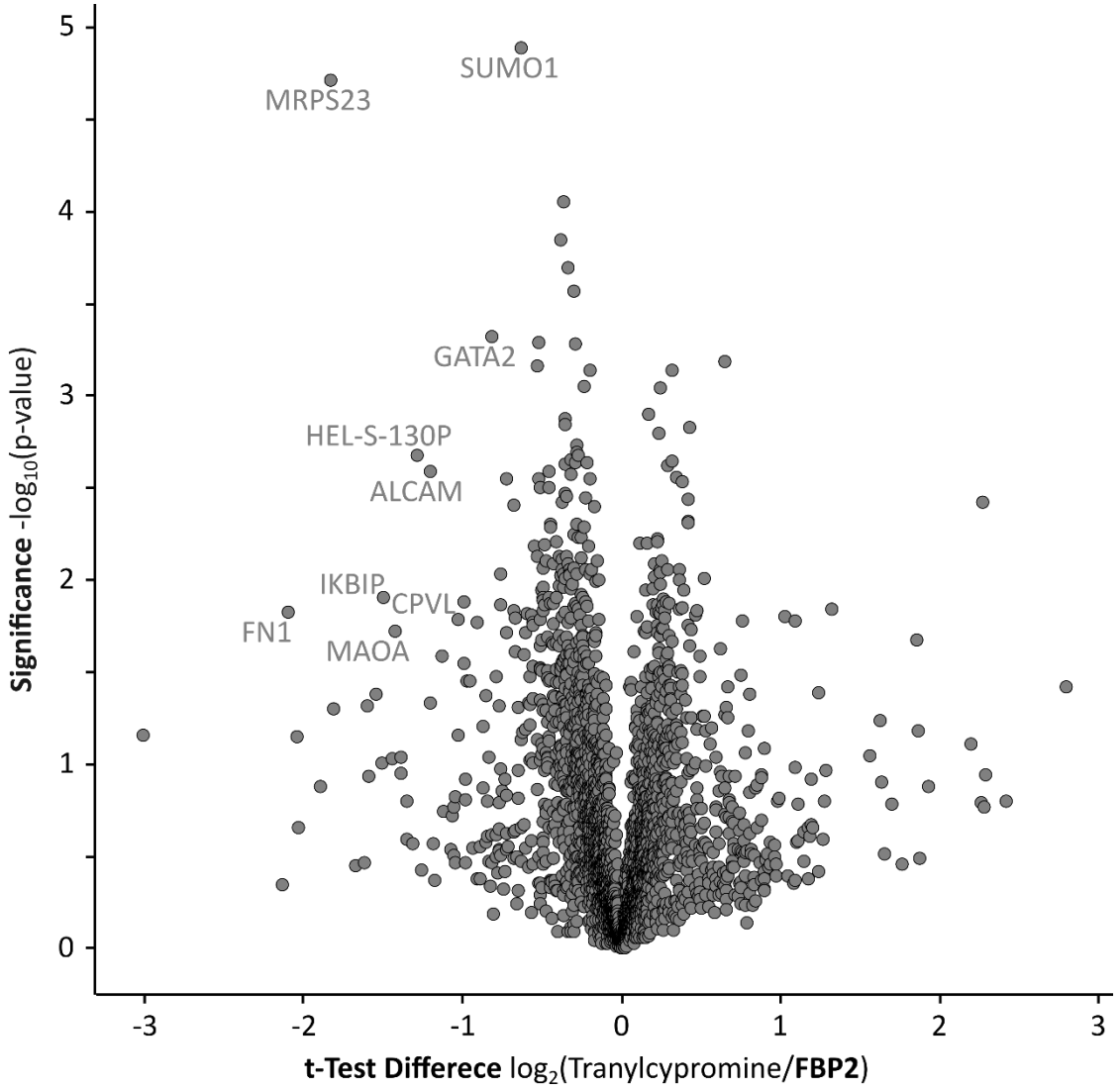

Figure A7: Result of competition experiment using **FBP2** in the human cancer cell line SH-SY5Y preincubated with tranylcypromine. The scatter plot shows statistical significance of protein enrichment levels over protein enrichment ratios from drug treated to control cells.

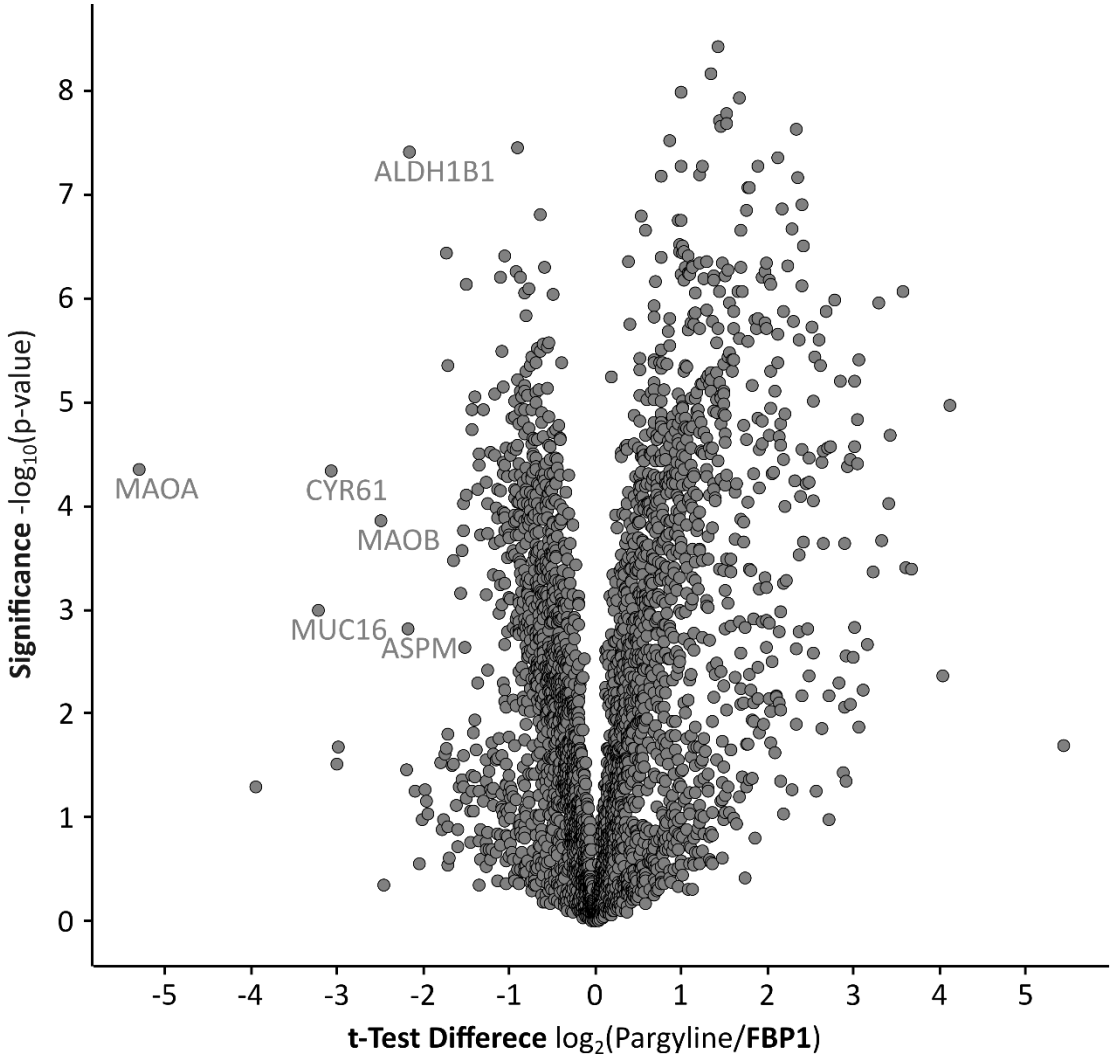

Figure A8: Result of competition experiment using **FBP1** in the human cancer cell line HeLa preincubated with pargyline. The scatter plot shows statistical significance of protein enrichment levels over protein enrichment ratios from drug treated to control cells.

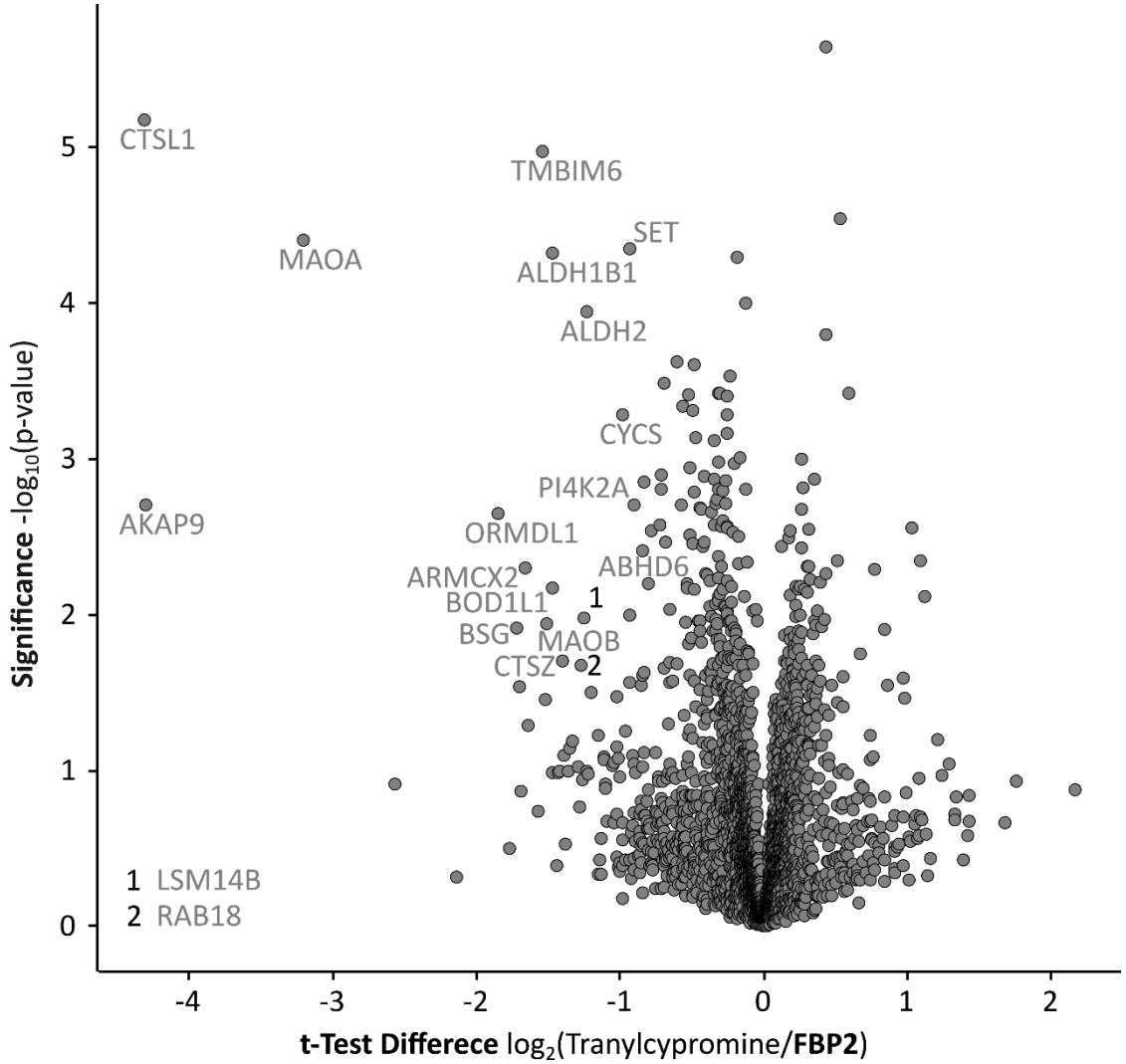

Figure A9: Result of competition experiment using **FBP2** in the human cancer cell line HeLa preincubated with tranylcypromine. The scatter plot shows statistical significance of protein enrichment levels over protein enrichment ratios from drug treated to control cells.